MONITORING FJORD CIRCULATION USING ICEBERG-MOUNTED GPS AS REAL-TIME DRIFTERS

by

GEORGE EDWARD ROTH

A THESIS

Presented to the Department of Geological Sciences
and the Graduate School of the University of Oregon
in partial fulfillment of the requirements
for the degree of
Master of Science

June 2014

THESIS APPROVAL PAGE

Student: George Edward Roth

Title: Monitoring Fjord Circulation Using Iceberg-Mounted GPS as Real-Time Drifters

This thesis has been accepted and approved in partial fulfillment of the requirements for the Master of Science degree in the Department of Geological Sciences by:

David Sutherland	Chairperson
Emilie Hooft	Member
Alan Rempel	Member

and

Kimberly Andrews Espy	Vice President for Research and Innovation; Dean of the Graduate School

Original approval signatures are on file with the University of Oregon Graduate School.

Degree awarded June 2014

THESIS ABSTRACT

George Edward Roth

Master of Science

Department of Geological Sciences

June 2014

Title: Monitoring Fjord Circulation Using Iceberg-Mounted GPS as Real-Time Drifters

Ocean circulation in Greenland's large glacial fjords is one mechanism that controls the rate of submarine melting at the termini of Greenland's outlet glaciers. Here we use hourly position data from GPS units deployed on ten large (>100 meter), deep-keeled icebergs in Sermilik Fjord, SE Greenland. We observe and quantify the motions of these icebergs moving through the mélange, fjord, and shelf regimes. In the mélange, icebergs move outward with glacier flow until pushed loose by large calving events. In the fjord, high frequency, low amplitude tidally-driven motions are superimposed on dominant 1-5 day events with net velocities exceeding 0.1 m/s. We interpret these events as two-layer, intermediary circulation driven by winds along the shelf, where icebergs travel southward in the East Greenland Coastal Current. These results showcase the potential of this novel instrumentation to link iceberg motion with circulation in any large glacial fjord.

CURRICULUM VITAE

NAME OF AUTHOR: George Edward Roth

GRADUATE AND UNDERGRADUATE SCHOOLS ATTENDED:

University of Oregon, Eugene
University of Washington, Seattle

DEGREES AWARDED:

Master of Science, Geological Sciences, 2014, University of Oregon
Bachelor of Science, Oceanography, 2012, University of Washington

AREAS OF SPECIAL INTEREST:

Oceanography
Glaciology

PROFESSIONAL EXPERIENCE:

Teaching assistant, Department of Geological Sciences, University of Oregon, Eugene, 2012-2014

Geospatial developer, Center for Environmental Genomics, School of Oceanography, University of Washington, Seattle, 2010-2011

GRANTS, AWARDS, AND HONORS:

Graduate Teaching Fellowship, Geological Sciences, 2012-2014
Mary Gates Research Scholarship, University of Washington, 2012

ACKNOWLEDGMENTS

I wish to express sincere appreciation to my primary thesis advisor, David Sutherland, for his wealth of ideas, enthusiasm, patience, and support throughout a process that was as new to him as it was to me. I thank my other committee members, Alan Rempel and Emilie Hooft, for their helpful comments and insights. Fellow oceanography graduate students Dustin Carroll and Molly O'Neill helped solve numerous mathematical and programming problems, and I thank them for sharing an office perfectly-equipped for both serious study and informal openness. Additionally, I thank the other graduate students in the Department of Geological Sciences for their support and friendship.

The following collaborators assisted with this project in numerous ways: Gordon Hamilton (University of Maine) and Leigh Stearns (Kansas University) for the original project idea and for deploying the GPS units, Fiamma Straneo and Rebecca Jackson (Woods Hole Oceanographic Institution) for providing ADCP data and helpful discussions on intermediary circulation, Marilena Oltmanns and Benjamin Harden (WHOI) for providing ECMWF-Interim wind data and discussions on barrier and katabatic winds, Sebastian Mernild (Los Alamos National Laboratory/Centro de Estudios Científicos, Chile) for weather station data, and Ellyn Enderlin (University of Maine) for discussions on iceberg melting in Sermilik Fjord.

This work was supported in part by a grant from the National Science Foundation, OCE-1130008, and by a grant from NASA, 11-IDS11-0033, to Dr. David Sutherland at the University of Oregon.

TABLE OF CONTENTS

Chapter Page

LIST OF FIGURES

Figure Page

Figure Page

LIST OF TABLES

Table Page

CHAPTER I

INTRODUCTION

The Greenland Ice Sheet (GrIS) is losing mass at an accelerating rate through an increase in ice calving and melting from its many tidewater outlet glaciers (Howat & Eddy, 2011; Howat, Joughin, & Scambos, 2007; Moon, Joughin, Smith, & Howat, 2012). In addition to atmospheric warming producing more surface melt, changes in the oceanic heat flux to the submerged glacier termini have been hypothesized to increase submarine melting and calving (Holland, Thomas, de Young, Ribergaard, & Lyberth, 2008; Joughin, Alley, & Holland, 2012; Rignot, Fenty, Menemenlis, & Xu, 2012; Rignot, Koppes, & Velicogna, 2010; Straneo, Sergienko, & Heimbach, 2012). Thus, understanding the structure and variability of the circulation in Greenland's glacial fjords is crucial to improving predictions of the GrIS's contribution to global sea level rise, which was estimated at 7.9 ± 2.7 mm between 1992 and 2011 (Shepherd et al., 2012) , and is predicted to range from 19-49 mm by the year 2200 (Nick et al., 2013).

Here, we explore the use of icebergs as a new tool to track fjord circulation at unprecedented spatial and temporal resolution. We also attempt to analyze and quantify several of the major forces responsible for the observed iceberg motion, including wind and ocean currents. Finally, we discuss the freshwater flux of icebergs into the fjord and how this freshwater may impact the stratification of water in the fjord.

Icebergs represent a tool for tracking fjord circulation that has been underutilized by the oceanographic community in attempts to constrain the processes that drive ocean variability in fjords. Tracking the movement of icebergs is advantageous, since 1) existing physical oceanographic instrumentation, such as CTDs or subsurface moorings, typically take Eulerian point measurements over a limited spatial domain to detect

changes in circulation and water properties over time, 2) ship-board or moored instrumentation requires an expensive ship presence and cannot safely be deployed in ice mélange or anywhere in the upper water column in these large glacial fjords due to the deep keels of the icebergs, and 3) Lagrangian instrumentation, such as drifters or autonomous gliders, are typically time-limited by the duration of their power source, and face the same safety risks in ice-choked environments.

Tracking and predicting the paths of icebergs is not a new field, and has long been of interest to the shipping industry, offshore installations, and national coast guards (Kubat, Sayed, Savage, Carrieres, & Crocker, 2007; McKenna, 2005; Newell, 1993) . Existing iceberg observation efforts, though, have been limited to the coarse spatial and temporal resolutions of remotely sensed imagery, aircraft flights, and ship-board observations (Canadian Ice Service, 2005). Current efforts to model iceberg motions use simulations of ocean currents combined with meteorological forcing, but have lacked enough direct observations to fully validate their results (Bigg et al., 2014; Bigg, Wadley, Stevens, & Johnson, 1996; Gladstone, Bigg, & Nicholls, 2001).

To address the movements of icebergs in fjords and coastal regions, we use novel instrumentation to track icebergs in the Helheim Glacier/Sermilik Fjord system in SE Greenland. The following subsidiary questions guide this analysis and discussion:

- What are the observed dynamics of iceberg motions in each of the three glacier-ocean regimes found in Sermilik Fjord – proglacial mélange, the main fjord, and on the continental shelf outside the mouth?
- What are the primary forces that dictate iceberg movement? Over which time and space scales are these forces significant?

- What are the relative magnitudes of these distinct physical forcing mechanisms, and how do they change over time?
- Do these new iceberg motion data provide insights into how the glacier/fjord system is coupled?

CHAPTER II

ICEBERG DYNAMICS IN SERMILIK FJORD, SOUTHEAST GREENLAND

2.1. Background

Helheim Glacier is a large tidewater outlet glacier in southeast Greenland, moving at a mean speed of approximately 8-11 km yr^{-1} (Moon et al., 2012). Helheim Glacier underwent a period of accelerated flow speed, calving, and thinning starting between 2000-2005 (Howat, Joughin, Tulaczyk, & Gogineni, 2005) and has had a net terminus retreat of up to 8 km since 2000. (Andresen, Straneo, Ribergaard, et al., 2011). This recent acceleration and retreat has resulted in a yearly net volume loss averaging 51 ± 8 km^3 yr^{-1} between 2001-2006 due to the combined effects of glacier thinning and retreat, with a contribution to global sea level of at least 0.1 ± 0.02 mm yr^{-1} (Stearns & Hamilton, 2007). Helheim Glacier, along with the smaller Fenris and Midgård glaciers, calves into Sermilik Fjord, which extends from the terminus of Helheim Glacier and the intersection of the 20 km Helheim Fjord out to the East Greenland continental shelf about 70 km away, where it enters the Irminger Sea (Figure 1). Sermilik Fjord has a mean depth ranging from 600 m near Helheim Glacier, deepening to 900 m at the mouth, and has no sill at its mouth (Sutherland, Straneo, & Pickart, 2014). These characteristics allow deep-keeled icebergs to easily exit the fjord (Andresen, Straneo, & Ribergaard, 2011).

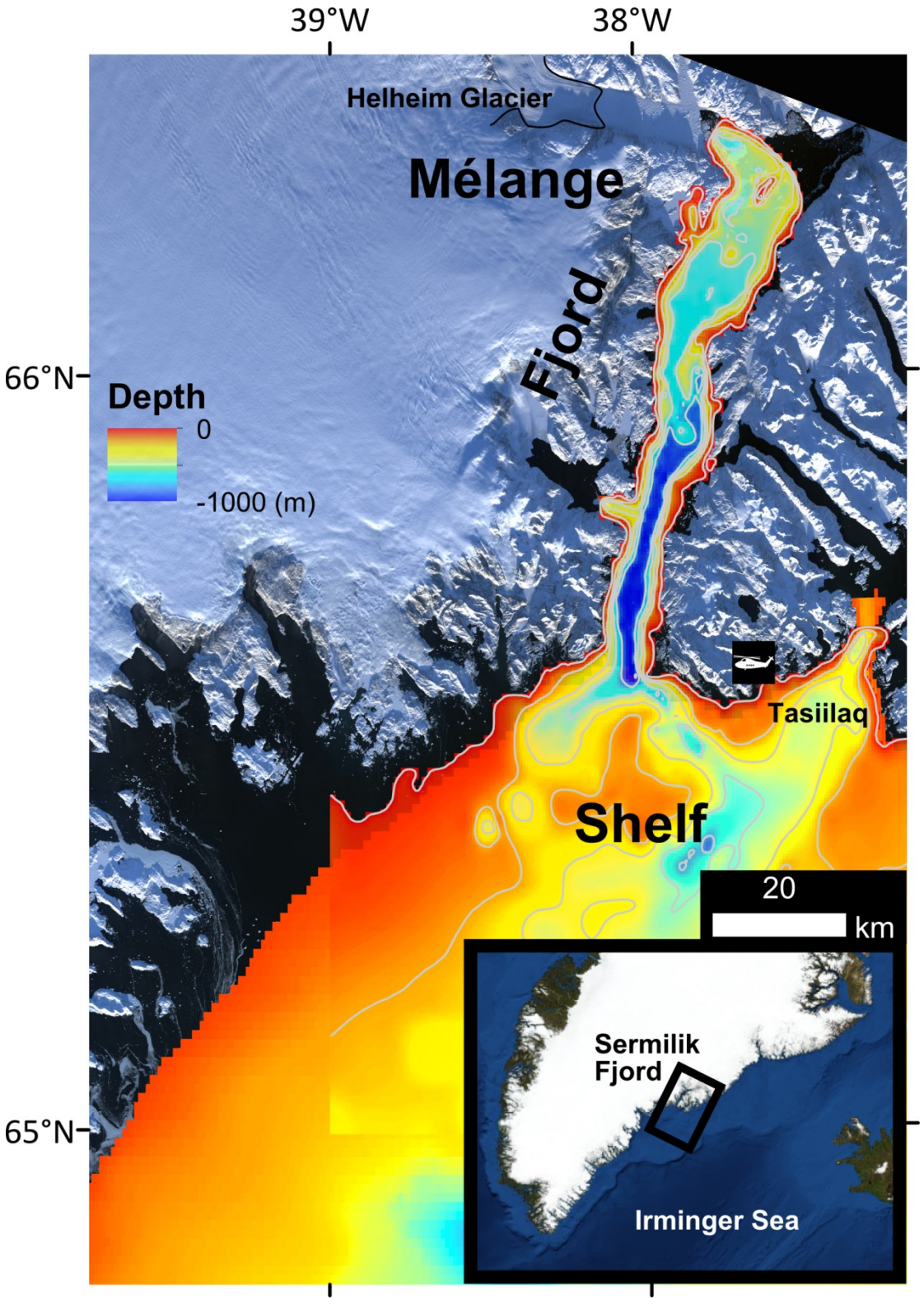

Figure 1. Location, map, and contoured bathymetry of Sermilik Fjord. Bathymetry data provided by a composite of GEBCO global bathymetry product, seal dive data on the shelf (Sutherland et al., 2013), and ship track data (Schjøth et al., 2012).

Outside Sermilik Fjord, the East Greenland Current (EGC) stretches from the Arctic Ocean at Fram Strait to the southern tip of Greenland, carrying a mean annual total flux of 21 Sv north of the Denmark Strait (Woodgate, Fahrbach, & Rohardt, 1999), much of which recirculates in the Greenland and Norwegian Seas, then combines with the southward-flowing branch of the Irminger Current (Pickart, Torres, & Fratantoni, 2005). The EGC is also responsible for a majority of the freshwater export from the Arctic Ocean through nearly equal parts liquid and sea ice (Serreze et al., 2006). On the southeast Greenland shelf, the EGC is joined by the Irminger Current (IC) that retroflects southward at Denmark Strait, bringing its relatively warmer and saltier, Atlantic-origin waters to the shelf break of the Greenland coast. These Atlantic-origin waters (AW) are denser than the EGC water, and are found typically underneath and seaward of the EGC. Thus in Sermilik Fjord, three main water masses are observed: Polar Water (PW, 0-200 m, -1-0 °C, 30-34 psu), Atlantic Water (AW, 200-800 m, 2-4 °C, 34.8-35 psu), and a thin surface layer that is modified by sea ice and seasonal glacier melt (Straneo et al., 2010; Sutherland & Pickart, 2008). The AW in Sermilik Fjord is warmer than that found to the north in East Greenland, as the IC is the main supply—farther north, AW comes from a more circuitous route that travels through the Arctic Ocean (Hansen & Østerhus, 2000).

A branch of the EGC, called the East Greenland Coastal Current (EGCC) is found in immediate proximity to the mouth of Sermilik Fjord (Bacon, Reverdin, Rigor, & Snaith, 2002; Sutherland & Pickart, 2008). The EGCC is hypothesized to form from a bifurcation of the EGC near the Denmark Strait and, enhanced by melting sea ice and freshwater export from the GrIS, flows along the shelf of southeast Greenland with an approximate width of 20 km and speeds up to 1 m s^{-1}. Its volume flux (~1 Sv) and

freshwater transport (~60-90 mSv) is the same order as in the thinner regions of the main EGC (Bacon, Marshall, Holliday, Aksenov, & Dye, 2014; Harden, Straneo, & Sutherland, 2014; Sutherland & Pickart, 2008). Despite this work, few *in-situ* observations of the EGCC outside the summer field season have been collected (Bacon et al., 2014). Changes in the speed and transport of the EGCC could have far-reaching effects on the export of Arctic sea ice and the ability of AW to reach East Greenland glaciers. This is essentially because the EGCC modulates the interface depth of the AW/PW transition outside the mouths of glacial fjords in SE Greenland and is sensitive to along-shelf wind forcing (Harden et al., 2014; Jackson, Straneo, & Sutherland, 2014).

Precise quantifications of the mechanisms that control circulation inside Sermilik Fjord, and in Greenland's other large outlet glacier fjords, remain murky at best. Better known are the water properties within these fjords (Azetsu-Scott & Tan, 1997; Christoffersen, O'Leary, Van Angelen, & Van Den Broeke, 2012; Mortensen, Lennert, Bendtsen, & Rysgaard, 2011; Murray et al., 2010; Rignot et al., 2010; Straneo et al., 2010; Straneo, Sutherland, et al., 2012; Sutherland et al., 2014). In Sermilik Fjord, as well as in other large Greenland fjords, the thin surface meltwater layer overlies a 100-200 m thick upper PW layer. This PW layer in turn overlies the relatively warm and saline AW layer that extends to the 600-900 m depth of the floor of the fjord (Straneo et al., 2010; Straneo, Sutherland, et al., 2012; Sutherland et al., 2014; Sutherland & Straneo, 2012).

Available observations from Sermilik Fjord and other fjords in Greenland are typically limited to summer, with a handful of records from moorings deployed through the winter (Jackson et al., 2014; Sutherland & Straneo, 2012). These data show a variable circulation that does not conform to a classic fjord estuarine-type circulation model with

a surface outflow and deep inflow. Indeed, many other processes may mask the buoyancy-driven estuarine flow, including intermediary circulation driven by changes in density structure on the shelf (Jackson et al., 2014; Stigebrandt, 2012), along-fjord winds (Moffat, 2014), or residual flow from tides (Cottier et al., 2010; Stigebrandt, 2012).

The driver behind the buoyancy-driven flow is typically assumed to be submarine discharge from the base of the glacier (Johnson, Münchow, Falkner, & Melling, 2011; Mortensen et al., 2013, 2011; Sciascia, Straneo, Cenedese, & Heimbach, 2013; Xu, Rignot, Fenty, Menemenlis, & Flexas, 2013). This discharge escapes the glacier bed in a buoyant, turbulent upwelling plume, whose mixing effects can further melt the glacier face, adding additional freshwater to the system. Analysis of satellite data has led to estimates that 33.9×10^9 m^3 yr^{-1}, or 85% of the total freshwater input into Sermilik Fjord, comes from ice discharge, with most of the remaining 6.5×10^9 m^3 yr^{-1} coming from surface melt and runoff (Mernild et al., 2010). However, so far there has been no quantification of the impact of icebergs melting in the fjord after they have calved, on the ambient stratification and freshwater transport in Greenland's large glacial fjords.

Intermediary circulation has been observed and quantified in a number of fjords, and it can be driven by local or remote winds blowing on the shelf that drive fluctuations in the density gradients between the fjord and shelf pycnoclines (Aure, Ert, & Stigebrandt, 1997; Klinck, O'Brien, & Svendsen, 1981; Stigebrandt, 1990, 2012; Straneo et al., 2010). This type of circulation has been observed in Sermilik Fjord, and is hypothesized to be the primary large-scale circulation mechanism, correlated strongly with high wind events on the shelf (Jackson, Straneo, & Sutherland, 2013; Jackson et al., 2014; Straneo et al., 2010). Strong, northeasterly "barrier winds" are common on the east

Greenland coast, where the cyclonic Icelandic Low is compressed and amplified by the steep topography. These wind events often exceed speeds of 20 m s^{-1} and occur as often as weekly during the winter months (Harden, Renfrew, & Petersen, 2011). Since northerly winds are downwelling-favorable on an eastern coast, the coastal sea surface rises and the pycnocline deepens, driving upfjord flow in the upper water layer and downfjord flow in the lower layer. This flow begins to increase the sea surface height and depress the pycnocline at the glacier terminus. As the coastal winds relax, the direction of the density gradient switches, reversing the vertical structure of the flow to downfjord at the surface and upfjord at depth. Jackson et al. (2014) show this mechanism causes a two-layer oscillatory flow in Sermilik Fjord with a zero-crossing of the along-fjord velocity that coincides with the AW/PW interface (typically at ~150-200 m depth).

Another potential wind-driven circulation mechanism in large Greenland fjords is the effect of strong alongfjord winds (known as "piteraqs" in east Greenland) generated by katabatic, downslope airflow from the Greenland Ice Sheet. In Sermilik Fjord, these winds are funneled through the Helheim Glacier trough, altering their heading to align with the fjord axis (Andersen et al., 2010). These wind events last between 20-30 h with speeds exceeding 20 m s^{-1}, and occur with a mean frequency of 7.8 +/- 3.1 times per year, predominantly in the winter (Oltmanns, Straneo, Moore, & Mernild, 2014). Other work suggests close linkages between katabatic wind events and large cyclones off the east Greenland coast, where the vigorous transport of cold downslope air serves to strengthen the vorticity of the cyclone near the shelf (Klein & Heinemann, 2002). Inside the fjord, katabatic winds are often responsible for flushing small icebergs and pancake sea ice out-

fjord, as well as potentially forming and maintaining small polynyas in otherwise ice-choked fjords (Christoffersen et al., 2012; Oltmanns et al., 2014).

Icebergs in the ocean act as drifters that sample not just the surface water, but the wind, with their above-water sails, and the portion of the water column extending to the depth of their keels. Predicting the paths of icebergs based on a combination of oceanic and atmospheric forcing has been the focus of several past efforts (Bigg et al., 2014, 1996; Gladstone et al., 2001). Large, deep-keeled icebergs, such as those examined in Sermilik Fjord, tend to move with the water, as opposed to much smaller (< 10 m width) bergy bits which tend to move with the wind. The predicted iceberg motion was used to model both the iceberg trajectories and when and where they melt in both the North Atlantic and Antarctic regions. Savage (2001) synthesized and updated this work, conceptualizing the force balance for iceberg movement as

$$m\left(\frac{d\boldsymbol{V}_i}{dt} + \boldsymbol{f} \times \boldsymbol{V}_i\right) = \boldsymbol{F}_a + \boldsymbol{F}_w + \boldsymbol{F}_\tau + \boldsymbol{F}_p + \boldsymbol{F}_{am} + \boldsymbol{F}_{si} \qquad (1)$$

Here, the total acceleration of an iceberg (LHS of Eqn. 1, including Coriolis force represented by Coriolis parameter *f*) of given mass *m* and velocity V_i at time *t* is calculated as the sum of forces on the RHS of Eqn. 1. These forces include the air drag F_a across the surface area of the iceberg above the water surface facing the wind, the water drag F_w integrated over the depth of the iceberg on the upstream submerged face, the wave radiation force F_τ, the horizontal pressure gradient force F_p, which is exerted on the iceberg by the water it displaces as it moves, the effective force F_{am} exerted by the added mass of water dragged along with the iceberg as it moves, and the drag due to sea-ice F_{si}.

In Sermilik Fjord we can generally disregard sea-ice drag, as the fjord itself normally remains too full of moving icebergs to enable successful formation of a sea ice layer. However, the east Greenland shelf is one of the main sites of both sea ice growth and export from the Arctic Ocean from winter months, and can become thick enough to slow or even stop iceberg motion and the exit of icebergs from the fjord.

The pressure gradient (F_p) term, is effectively the motion of the water column, such that the difference between the LHS of Eqn. 1 and F_p represents the expected difference between observed iceberg motion and observed water motion. This difference is thought to be dominated by the air and water drag terms and F_a and F_w respectively (Savage, 2001):

$$F_a = \frac{1}{2}\rho_a C_a A_a |u| u \qquad (2)$$

Where u is the difference between the iceberg drift velocity and the wind velocity, ρ_a is the air density, and A_a is the cross-sectional area of the iceberg above water and perpendicular to the relative velocity.

$$F_w = \frac{1}{2}\rho_w C_w \sum_i A_w(i) |v_r(i)| v_r(i) \qquad (3)$$

Where ρ_w is the water density, C_w is a drag coefficient ~1.0, $A_w(i)$ is the cross-sectional area of the iceberg vertical depth element, and $v_r(i)$ the relative velocity between the water and the submerged iceberg at that depth.

We calculate the air and water drag terms for an iceberg with a 90 m keel and a range of relative wind and water velocities (Figure 2) and find that for deep-keeled icebergs, $F_w >> F_a$ except at very high wind speeds. For example, a relative water velocity of 0.2 m s^{-1} exerts over 941 kN of drag force; to produce that same drag force, winds must exceed 19 m s^{-1}.

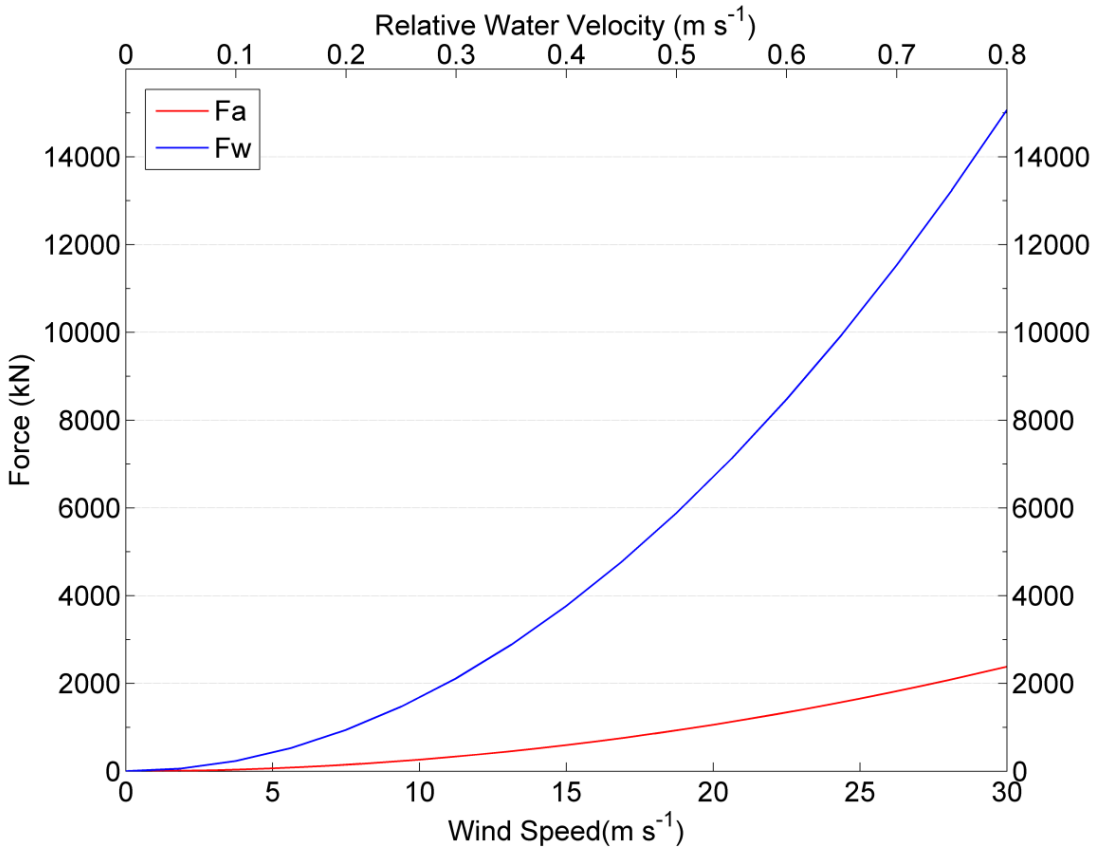

Figure 2. Forces contributed by F_w and F_a to an iceberg with a 90 m keel, from Eqns. 2 and 3.

However, little work has been done to ground truth these parameterizations that determine the iceberg trajectories. Morison and Goldberg (2012) tracked an Antarctic iceberg for several days with ship sonar and GPS, but mainly focused on the moving iceberg's interaction with local surface winds, wake dynamics, and internal wave effects on local water stratification. Dowdeswell et al. (1992) observed some qualitative variations in iceberg motion in the Scoresbysund fjord system, but were limited by the lack of available high-resolution satellite data during their field season.

Recently, a large amount of research has focused on the granular, semi-rigid proglacial ice mélange, including its rheology, stability, and the timing of movement

(Amundson et al., 2010), influence on fjord seiches and calving waves (MacAyeal, Freed-Brown, Zhang, & Amundson, 2012), and physical interactions between the mélange and the calving terminus (Joughin et al., 2008). In Sermilik Fjord, the mélange often consists of several large (>500 m diameter) icebergs with sea ice and smaller icebergs filling in the gaps. These previous studies have determined that the ice mélange is pushed forward with the advance of the glacier and suggest that back stress on the glacier is too small to slow or alter its flow speed, but may possibly be great enough to slow the frequency of large iceberg calving due to blocking the overturning and motion of otherwise calve-ready icebergs (Reeh, Thomsen, Higgins, & Weidick, 2001). However, these observations of the ice mélange have all depended on indirect methods, such as InSAR and visible satellite imagery, seismometers deployed near glaciers, or time-lapse photography of glacier termini. Attempts to directly measure the dynamics of the ice mélange have previously been deemed unfeasible and unsafe due to its inaccessibility. Here we present observations from new long-term, expendable, iceberg-resistant instrumentation was needed to examine the ice mélange in detail.

2.2. Methods

2.2.1. Iceberg Motion

We deployed Axonn AXTracker GPS tracking units (Figure 3) from a helicopter onto five large (>100 meter diameter) icebergs in Sermilik Fjord starting on 7 Sept 2012 (Table 1). An additional five trackers were deployed via helicopter the following year (called Year 2 here), starting on 18 Aug 2013. In 2013, we switched to using the

SmartOne GPS model. Each GPS tracker was set to report its position hourly via the Globalstar satellite network to a web portal, where the time- and position-stamped data were downloaded. A stationary GPS accuracy test done locally revealed GPS positioning errors of < 20 m for each hourly position fix, resulting in a velocity error of < 6 mm s^{-1} between two measurements.

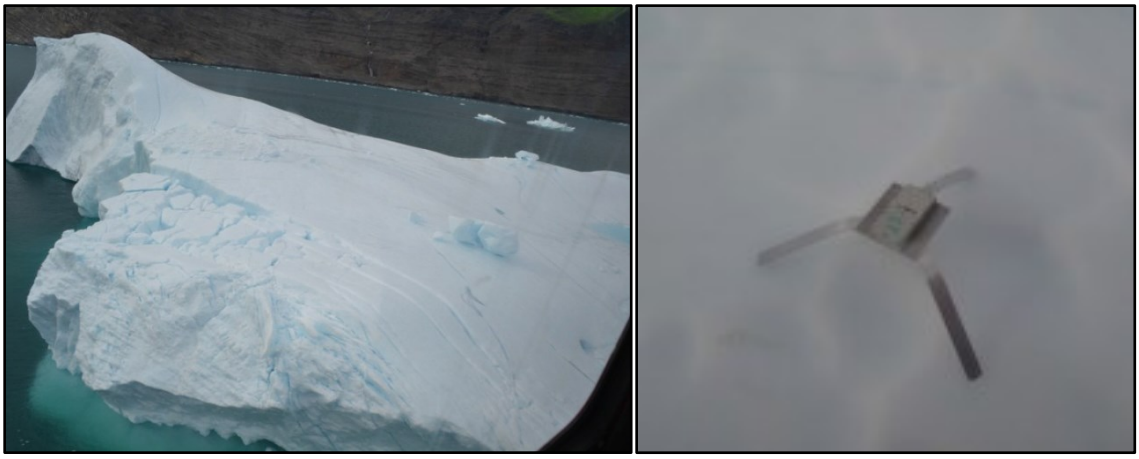

Figure 3. A typical deployment iceberg and an example of a deployed SmartOne GPS tracker on its metal tripod.

Table 1. GPS tracker deployment locations and dates (see Figure 7)

	Tracker	Location	Deployed
2012	UO1	Helheim-Sermilik intersection	7-Sep-12
	UO2	Helheim-Sermilik intersection	7-Sep-12
	UO3	Helheim-Sermilik intersection	7-Sep-12
	UO4	Helheim ice mélange	17-Sep-12
	UO5	Helheim ice mélange	17-Sep-12
2013	UO6	Helheim ice mélange	18-Aug-13
	UO8	Helheim-Sermilik intersection	18-Aug-13
	UO9	Helheim ice mélange	18-Aug-13
	UO10	Helheim ice mélange	18-Aug-13
	UO11	Helheim ice mélange	18-Aug-13

Though each tracker is set to transmit its position at an hourly interval, sparse satellite coverage in the high-latitudes, poor weather conditions, and the steep fjord walls occasionally reduced this interval. We used linear interpolation to fill in these data gaps, which were commonly on the order of several hours.

Battery life in each unit is estimated at over a year, but each GPS tracker eventually stops transmitting permanently due to other reasons. We assume this to be a result of the iceberg capsizing, overturning, or breaking up in such a way that the GPS unit falls into the water or a crack in the ice.

Zonal and meridional velocity components from the iceberg tracks were calculated from their positions and timestamps. Iceberg tracks were also separated into three regions – ice mélange, fjord, and shelf – based on their position. The defined mélange region extends approximately 25 km outward from the Helheim Glacier terminus, at the intersection of Helheim Fjord and the main branch of Sermilik Fjord (Figure 1). Though this region's extent is farther than the actual extent of the ice mélange, it provides enough space for seasonal variability in the size of the mélange, as well as the ability to examine the transition between mélange-bound and free-floating iceberg motion. The fjord region extends from the mélange region boundary to the mouth of Sermilik Fjord, defined here as 65.61°N, where the shelf region then begins. In the fjord region, the velocity data were then rotated into an alongfjord axis of 16 degrees east of north and filtered with a 24-24-25 hour Godin filter to remove the tidal components. In Sermilik Fjord, tides are semidiurnal, with peak amplitudes of 2 cm s^{-1} (Sutherland et al., 2014). Spurious data, such as configuration messages, GPS positions delayed during deployment, and other outlying position points were manually removed.

Gridded velocity fields for the fjord region were calculated by binning all available iceberg tracks into 1x1 km squares and averaging their velocities. Lack of spatial coverage in the ice mélange and shelf regions limited this gridding procedure to the fjord region only.

2.2.2. Atmospheric and Oceanic Forcing

Surface (10 m a.s.l.) wind field data for the analysis period 7-Sep-2012 to 28-Feb-2014 is provided by the ECMWF (European Centre for Medium-Range Weather Forecasts) Interim Reanalysis data product. This coarse-scale (0.75 degree grid size, 6 hr sampling interval) dataset captures the strong barrier wind events on the shelf (Harden et al., 2011) and is also capable of capturing downslope, katabatic wind events that flow along the fjord, originating from the GrIS (Oltmanns et al., 2014). Our timeseries of along-shelf wind was taken from a grid point 85 km SE of the mouth of Sermilik Fjord, at 64.91°N, 37.27°W, and was rotated to an axis 225 degrees from north to capture the greatest along-shelf velocity variability (Figure 4a).

A complementary wind dataset (Figure 4b) was obtained from a weather station established by the Danish Meteorological Institute (DMI). This station, “Station Coast,” lies at 25 m a.s.l., 7 km inside the fjord (Figure 7) on the eastern bank, along the Mittivakkat Glacier catchment (Mernild, Hansen, Jakobsen, & Hasholt, 2008). This weather station collected data every 10 minutes from 1 Jan 2012 to 30 Aug 2013, covering all of the 2012 iceberg analysis period and 12 days of the 2013 (Year 2) season.

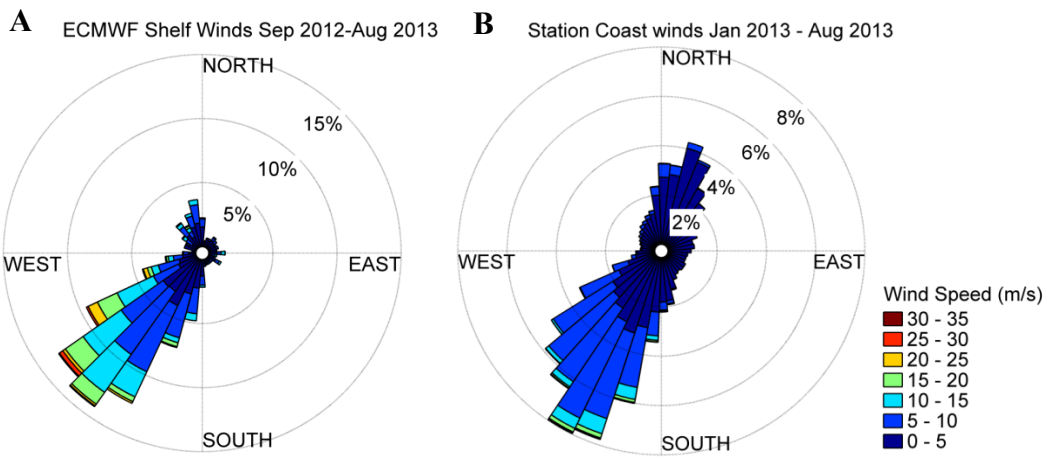

Figure 4. Wind direction/speed histograms taken from ECMWF-Interim data (A), at a single point outside the shelf and from DMI Station Coast (B) inside the fjord.

Time series of water velocity data in the fjord were obtained from an Acoustic Doppler Current Profiler (ADCP, Figure 7), moored at 65° 52.6' N, 37° 54.8' W on 19 Sept 2012 and retrieved on 19 Aug 2013 by Woods Hole Oceanographic Institution (Jackson et al., 2014). The ADCP sampled at 2 hr intervals, covering the water column from 54-384 m depth in 15 m depth bins. The top 54 m of the ADCP record was deleted in the quality-control process due to surface effects and instrument noise.

2.2.3. Bathymetry and Imagery

Fjord and shelf bathymetry were gridded by combining GEBCO global bathymetry data products with depths derived from tagged seals (Sutherland et al., 2013) on the shelf, and from compiled single-beam soundings in the fjord (Schjøth et al., 2012). Figure 1 and Figure 7 show this combined bathymetry. The GEBCO bathymetry inadequately resolved depths and bathymetric variation both within the fjord and particularly in the inner shelf region SW of Sermilik Fjord, where measured depths appeared to shoal to 0 m several km away from the coastline.

Within Sermilik Fjord, several crucial features are visible in the bathymetry. In the fjord basin north of 66°N, depths remain shallower than 500 m, and the fjord is relatively wide (>10 km). At the eastern bank of the fjord at 66°N, a shallow submarine ridge extends to the south, with depths shallower than 300 m, adding a horizontal barrier to the flow of both deeper water and deep-keeled icebergs. South of 66°N, the fjord narrows to less than 10 km and deepens, with depths frequently exceeding 900 m. At the fjord mouth, the deeper bathymetry branches in two directions, most visibly to the SE, but also to the SW. This SW branch, not visible in the GEBCO bathymetry product, represents an important physical pathway for deep-keeled icebergs to travel with the EGCC.

Two sources of satellite imagery aided inspection of ice and weather conditions in Sermilik Fjord. MODIS AQUA and TERRA imagery (Figure 5) were subsetted and provided by the Danish Meteorological Institute (DMI). (Data available at: http://ocean.dmi.dk/arctic/ammassalik.uk.php). 15 m resolution satellite imagery for the 2013 season, useful for examining conditions at the ice mélange, was provided by the Landsat 8 Operational Land Imager (Figure 6, Data available at: http://earthexplorer.usgs.gov/). The MODIS imagery aids inspection of synoptic weather, ice, and ocean conditions. In the September MODIS imagery, when the trackers were deployed, icebergs are at their peak concentration in the fjord after the July-September season of peak ice loss and terminus retreat (Schild & Hamilton, 2013). By November, calving has slowed and much of the smaller ice has left the fjord, and coastal storms increase in frequency and magnitude. In February, the mouth of the fjord appears almost entirely blocked by sea ice exported from the Arctic Ocean and carried along the coast by

the EGC/EGCC system. The Landsat imagery, at its higher resolution but lower acquisition frequency, better shows the spatial structure of the glacier-iceberg-ocean system within Sermilik Fjord. In Figure 6, this imagery displays the terminus of Helheim glacier, the extent and structure of the ice mélange and large icebergs entrained in the mélange, as well as the mélange edge, from which icebergs are able to flow into the fjord.

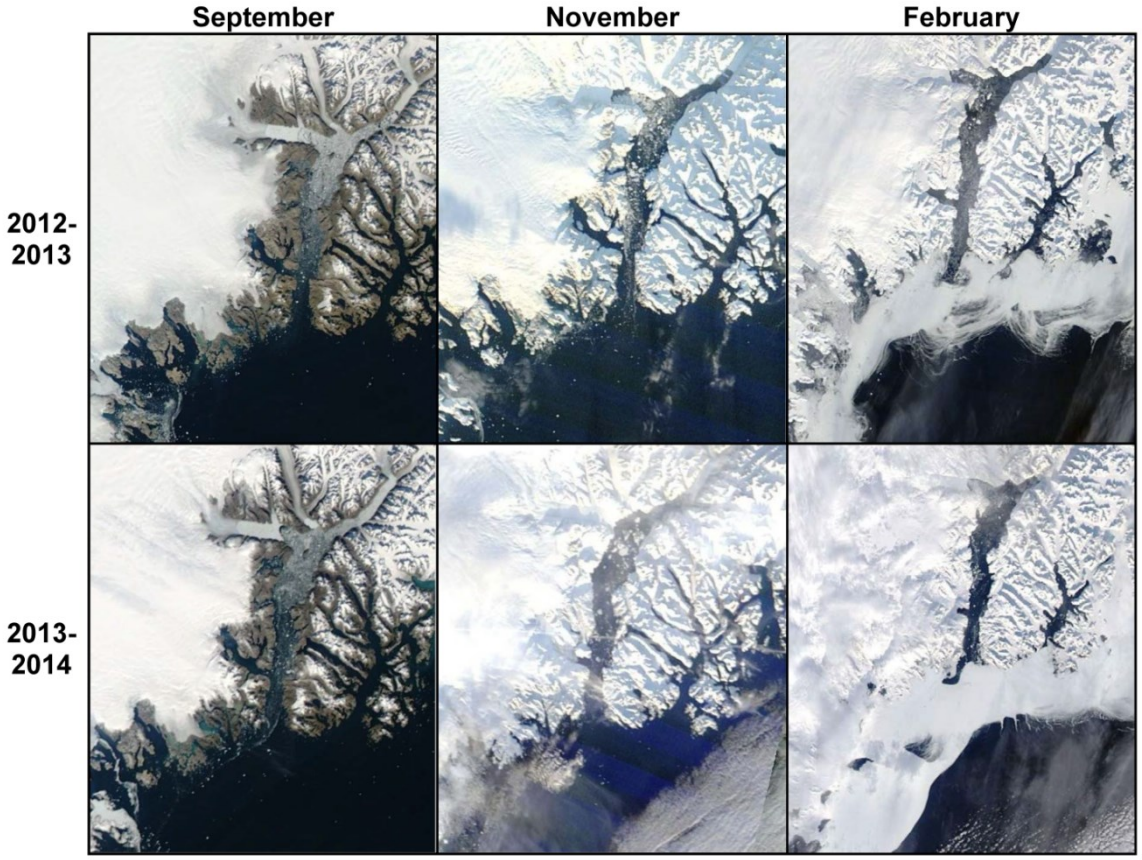

Figure 5. Compiled MODIS imagery showing conditions in Sermilik Fjord over the 2012 and 2013 drifter seasons.

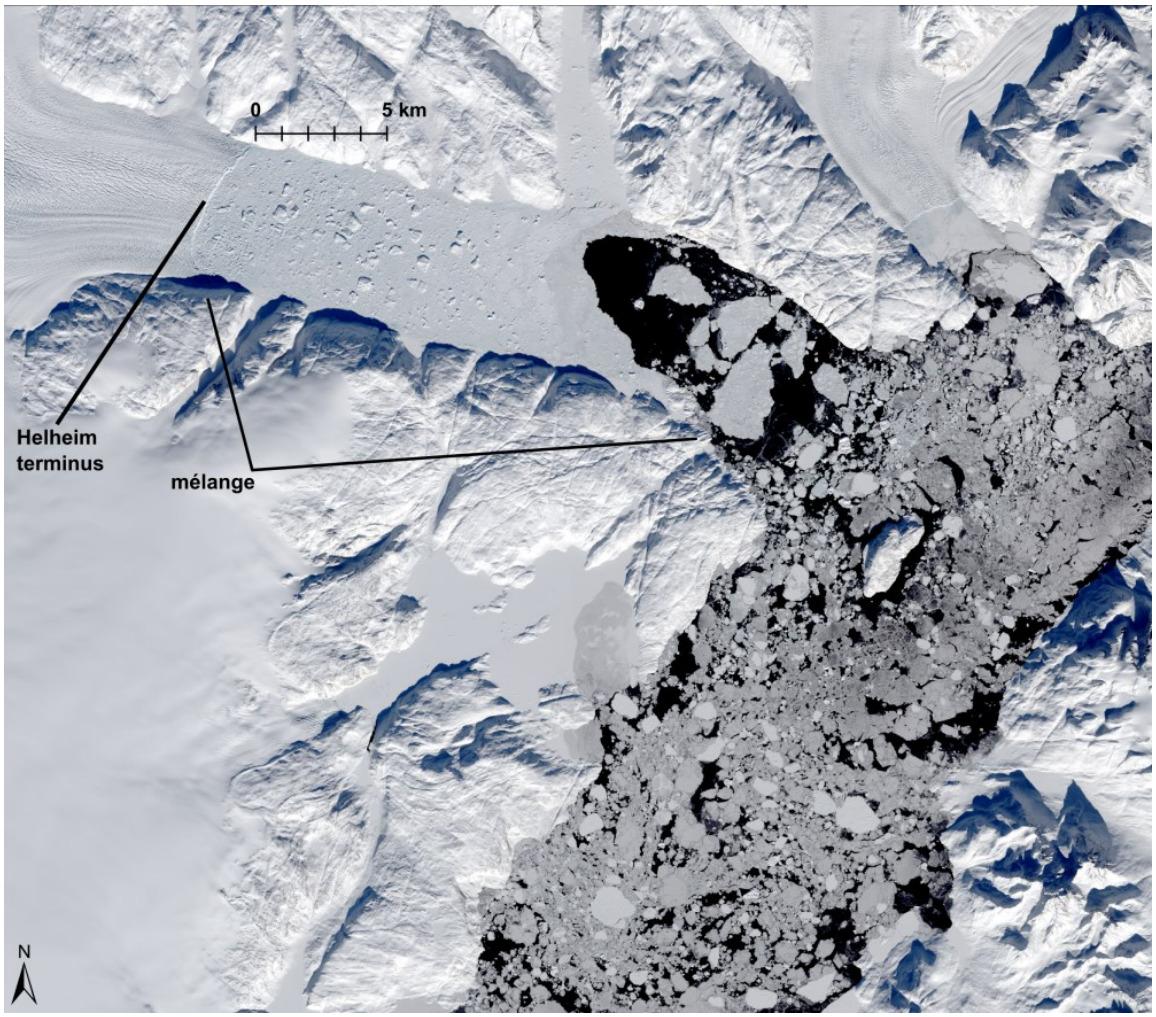

Figure 6. Landsat 8 OLI scene of the Helheim/Fenris glacier system and the head of Sermilik fjord, pan-sharpened to 15 m resolution. Image acquired 20-Mar-2013. Source: Landsat 8 / USGS.

2.3. Results

Static maps of iceberg tracks from time of deployment to loss of transmission provide a qualitative first inspection of iceberg motion through three distinct regions: the ice mélange, main fjord, and continental shelf (Figure 7).

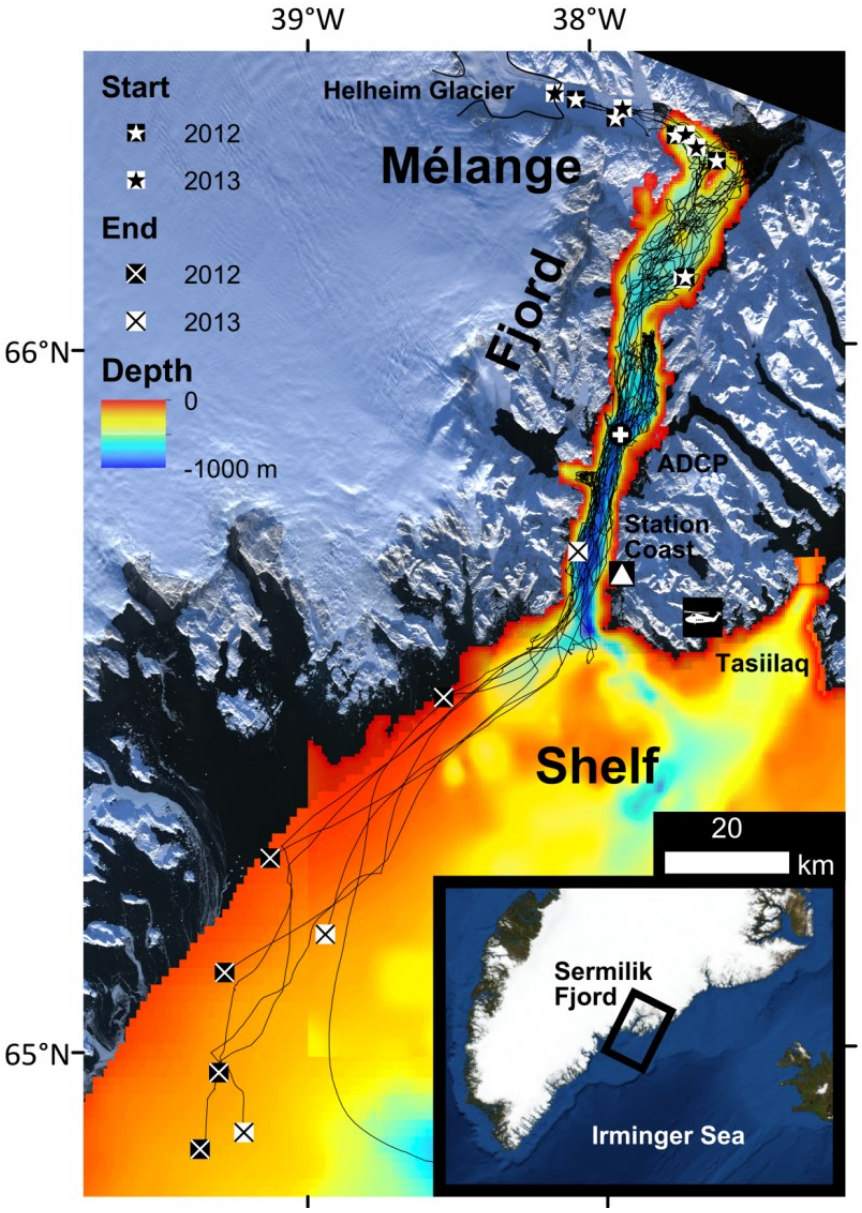

Figure 7. Map of Sermilik fjord with bathymetry and iceberg tracks from the 2012 and 2013 seasons, highlighting the three major circulation regions (Mélange, Fjord, and Shelf), Helheim Glacier, and the locations of the DMI weather station (Station Coast) and the moored ADCP. The base image is a 15m pan-sharpened Landsat 8 scene acquired 15 Nov 2013.

For each iceberg we calculate a residence time in the three regions using the GPS data (Table 2). For icebergs deployed in the mélange, residence times in the mélange averaged 81 ± 67 (mean ± st. dev.) days. These timescales do not necessarily represent the complete life cycle of a calved iceberg in the mélange, since each GPS unit was deployed at varying distances from the terminus. Icebergs spent 77 ± 49 (mean ± st. dev.) days in the ~80 km open region of Sermilik Fjord from latitude 66.25°N to 65.61°N, excluding records where the GPS unit stopped transmitting while in the fjord. On the shelf, the number of active transmission days was limited by how long each GPS continued transmitting until the iceberg presumably overturned.

Table 2. Data from all iceberg trackers up to 9-May-2014, with time spent in each region, total transmitting time and distance covered, iceberg shape classification (B = Blocky, T = Tabular), length estimates from field observations, calculated iceberg keel and height (above water) from 3:1 and 5:1 length ratios (Savage, 2001), and the keel depth from the most closely-correlated ADCP depth average for each iceberg. Note that iceberg UO8 was not included in the calculation of average fjord residence time, as it stopped transmitting while still inside the fjord.

	Name	Days in mélange	Days in fjord	Days in shelf until tx loss	Total tx time (days)	Total km traveled	Type	Length (m)	Height (3:1)	Keel (3:1)	Height (5:1)	Keel (5:1)	Depth (ADCP corr)	R_{best}
2012	**UO1**	-	49	3	52	251	B	500	167	149	100	89	60	0.95
	UO2	-	98	24	122	391	T	500	167	149	100	89	300	0.48
	UO3	-	75	10	87	399	T	500	167	149	100	89	75	0.8
	UO4	39	100	301	441	503	T	-	-	-	-	-	380	0.7
	UO5	16	43	11	70	382	T	-	-	-	-	-	60	0.75
2013	**UO6**	116	42	107+	264+	341	T	200	67	60	40	36	-	-
	UO8	4	~~12~~	-	15	290	T	-	-	-	-	-	-	-
	UO9	122	80	74+	264+	589	T	300	100	89	60	54	-	-
	UO10	-	191	58	227	751	T	-	-	-	-	-	-	-
	UO11	190	13	59+	264+	678	T	100	33	30	20	18	-	-

In the field, we estimated the width of several icebergs and assigned them a standard shape classification (Canadian Ice Service, 2005; Savage, 2001). Most icebergs were classified as “tabular” (Figure 8) with horizontal or flat tops and length/height ratios approaching 5:1. We also estimated each the total height of each iceberg(the sum of its above- and below-water heights) using width/height ratios of 3:1 and 5:1, within the range of observed large iceberg dimensions (Hotzel & Miller, 1983). Keel depths below water were calculated using the difference between freshwater ice and ambient seawater density.

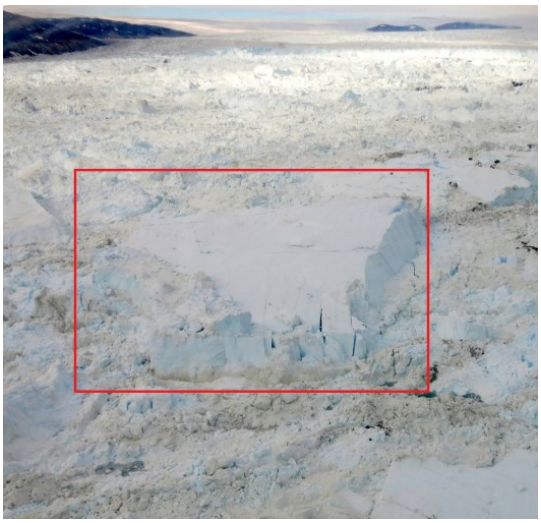

Figure 8. Iceberg UO11 (highlighted), classified as Tabular with an estimated width of 100 m.

2.3.1. Ice Mélange

In Sermilik Fjord, five GPS trackers were deployed in the ice mélange (2 in 2012, 3 in 2013). At low speeds, the GPS fix error, enhanced by poor satellite coverage and steep fjord walls, overwhelms the signal of net movement in the ice mélange, rendering velocity measurements accurate only on daily or longer timescales.

Icebergs in the ice mélange are pushed forward at speeds of 18-26 m d^{-1} (Figure 9), consistent with past observations of the range of terminus flow speeds of Helheim glacier (Enderlin & Howat, 2013). Step-like events, where the icebergs quickly move away from the glacier simultaneously (Figure 9), could be caused by either strong katabatic winds or a large calving event. In the center of the mélange, these step events last from 1-3 hours with speeds exceeding 0.3 m s^{-1} (averaged over the hour). Near where the mélange meets the more open water in the fjord, iceberg breakout is slower and more gradual, occurring over a period of 1-2 days (Figure 9).

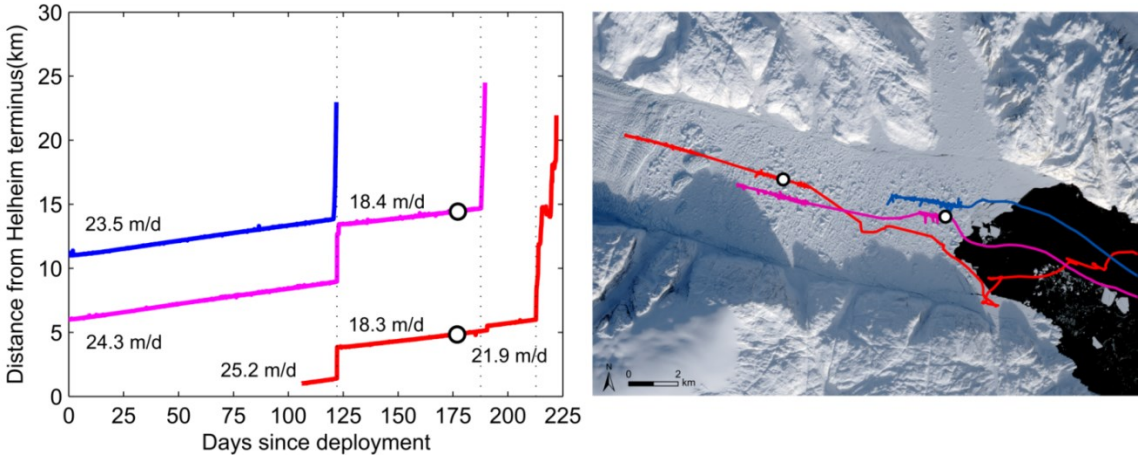

Figure 9. (Left): Iceberg distance and velocity in the mélange. Circles highlight iceberg positions at the time of the satellite image. Dashed vertical lines indicate the onset of "steps" in iceberg positions out of the mélange. (Right): Tracks in the ice mélange from 2013 icebergs UO6 (red), UO9 (blue), and UO11 (magenta), covering the period 18 Aug 2013 – 31 Mar 2014, and overlaid on a 15 m Landsat 8 image acquired on February 12th, 2014. The ice mélange edge extends approximately 15 km from the terminus of Helheim Glacier.

2.3.2. Fjord

Once the deep-keeled icebergs escape from the ice mélange, they enter the fjord and presumably begin to move with the upper layer of the water column. In the fjord, several circulation processes can influence velocity variability, and thus iceberg motion, including tides, local along-fjord winds, and the two-layer, intermediary flow driven by winds on the continental shelf (Harden et al., 2014; Jackson et al., 2014).

In the fjord region, iceberg motions show tidal variability at semi-diurnal frequencies and velocity magnitudes of 1-2 cm s^{-1} (For full timeseries for each iceberg, see Appendix B). These compare well with previously observed data (Sutherland et al., 2014). After filtering out oscillations shorter than 24 hours, the velocities appear to be dominated by relatively high-amplitude events with downfjord velocities exceeding 0.1 m s^{-1} on timescales ranging from 1-5 days and iceberg excursions averaging 5-20 km (Figure 10).

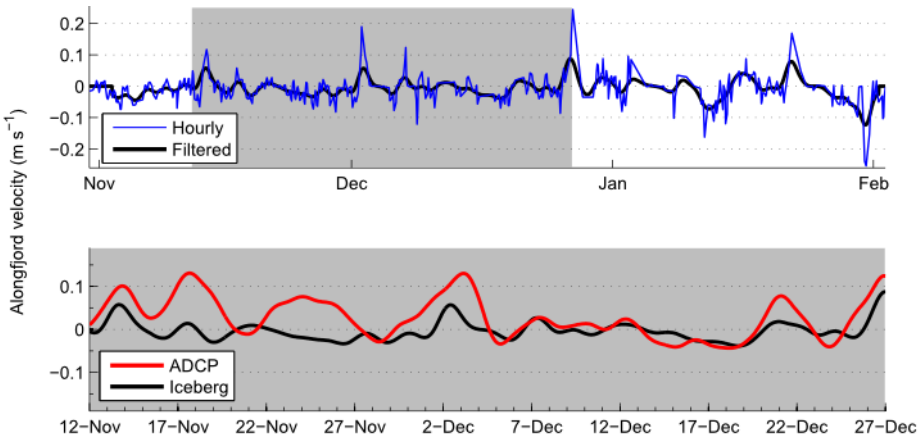

Figure 10. Along-fjord velocity data from 2012 iceberg tracker UO4, typical of the main fjord region. Positive values represent inward motion toward the glacier terminus; negative velocities represent outward motion toward the fjord mouth. Top: Raw and tidal-filtered iceberg velocity rotated to the fjord axis. Bottom: Comparison of iceberg and measured water column velocities from moored ADCP data. The ADCP data shown is the best-correlated depth average with iceberg UO4 (R = 0.7), from 50-380 m.

For each iceberg in the 2012 season, we also calculated the linear correlation coefficient (R) between each iceberg record and the range of cumulative depth averages from the top (54 m) bin ADCP record downward (to 384 m) (Figure 11), during the time period when each iceberg was located within 20 km of the ADCP mooring. We then interpreted the best-correlated depth average to be the most likely depth for each iceberg keel (Table 2).

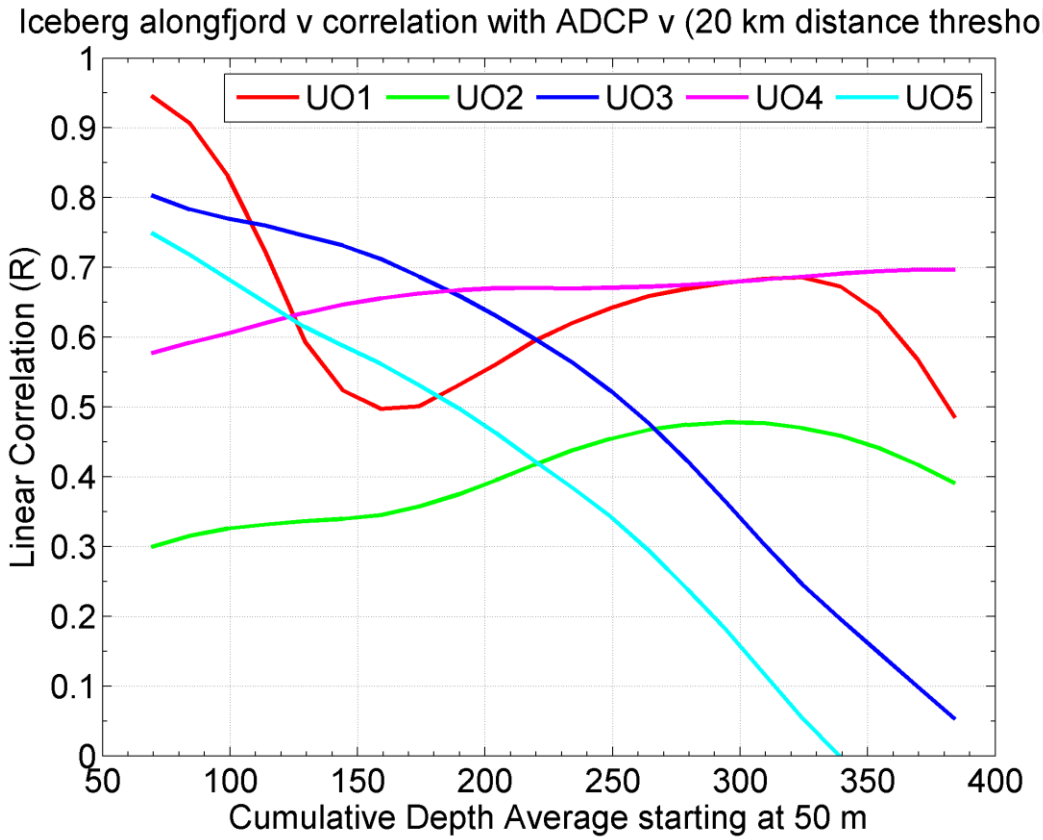

Figure 11. Correlation coefficient (R) for each 2012 iceberg's alongfjord velocity with the ADCP velocity at a range of depth averages.

2.3.3. Shelf

After the icebergs exit the fjord, they are carried parallel to the shelf by the EGCC at speeds of up to 1.5 m s^{-1} (Figure 12), consistent with hydrographic and ADCP observations of the equatorward core speed of the EGCC (Sutherland & Pickart, 2008). However, since the shelf below the EGCC only extends to depths of less than 350 m, iceberg keels often became grounded, leading to either immobilized icebergs, where the GPS units continued transmitting, or overturned icebergs where the GPS signal was lost (Figure 7 and Figure 12). Iceberg records on the shelf spanned from mid-August to mid-April, and most GPS units continued transmitting up to 100 days after exiting the fjord, with one unit continuing to transmit for over 300 days.

The frequent immobilization of icebergs on the shelf lead to a skewed distribution of iceberg speeds in this region (Figure 13). Speeds less than 0.1 m s^{-1} make up 87.7% of the total data values. If we calculate statistics only for speeds > 0.1 m s^{-1}, the mean speed of icebergs on the shelf is 0.34 ± 0.25 m s^{-1} (mean ± st. dev.). If this threshold is lowered to only 0.05 m s^{-1}, the mean ± st. dev. changes only slightly, to 0.31 ± 0.25 m s^{-1}.

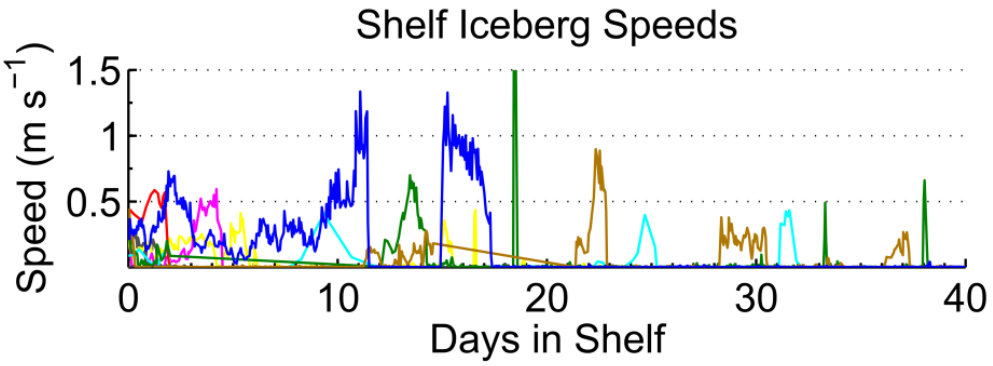

Figure 12. Speeds of 9 icebergs in the shelf region (1 tracker stopped transmitting while still in the fjord). Icebergs that do not overturn within ~40 days are considered immobilized, and their GPS units can continue transmitting for several months (Table 2).

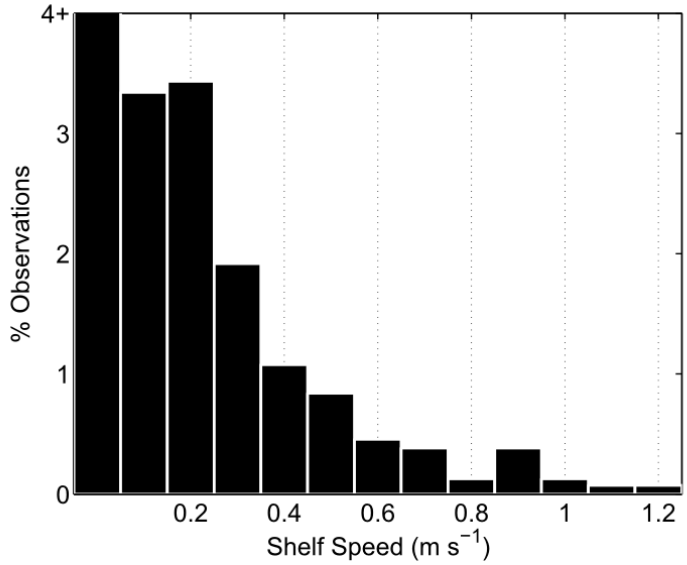

Figure 13. Histogram of iceberg speeds on the shelf, in 0.1 m s^{-1} bins. Speeds < 0.1 m s^{-1} make up 87.7% of observations, and speeds > 0.1 m s^{-1} make up the remaining 12.3%.

2.4. Discussion

Iceberg GPS trackers provided useful data on the velocities and timing of iceberg motion throughout the fjord. The motion of icebergs in Sermilik Fjord is controlled by several atmospheric and oceanographic mechanisms that operate in each of the three regions.

2.4.1. Ice Mélange

Though iceberg motion in the ice mélange is dominated by steady outward flow, the step changes in velocity, where icebergs move several km out from the terminus on timescales of several hours, are a crucial mechanism for pushing entrained ice out into the open region of the fjord.

After each iceberg velocity step change in the mélange, the icebergs in the mélange slow to once again presumably match the glacier flow speed. Flow speeds before and after an event are often different – these step-wise changes in Helheim's flow velocity have been documented (Nettles et al., 2008) and are attributed to the large calving events observed with satellite imagery and broadband seismometers. Since our data show that no single wind event is responsible for these step changes (Figure 14), we attribute the steps in the ice mélange velocity primarily to calving events. This hypothesis can be tested once a record of calving is constructed for Helheim Glacier.

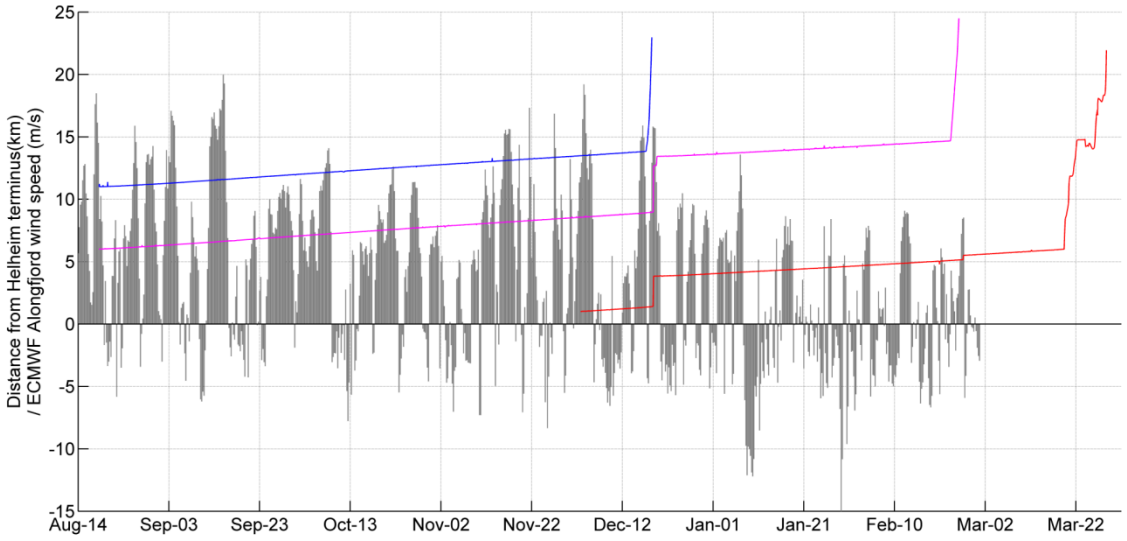

Figure 14. Iceberg positions in the ice mélange with alongfjord winds derived from the ECMWF-Interim product. Here, the ECMWF record displayed ends at 28 Feb 2013.

These iceberg trackers represent the first *in situ*, Lagrangian instruments for examining the dynamics of the ice mélange with high spatial and temporal resolution. A small array of trackers can provide information on the extent and two-dimensional velocity structure of the ice mélange with much finer time resolution than visible or InSAR satellite imagery, thus refining physical calculations of mélange forces on the

glacier terminus and subsequent calving (Amundson et al., 2010). During the time period where three trackers are president in the mélange, our data show a slight along-mélange velocity shear of $du/dx = -0.13$ m d^{-1} per kilometer of distance away from the glacier suggesting that the mélange may undergo compression along its length.

2.4.2. Fjord

In the fjord region, we interpret high-magnitude in-fjord and out-fjord circulation events as resulting from the two-layer, intermediary flow driven by winds along the shelf. Previous work has found this intermediary flow mechanism to dominate circulation in Sermilik fjord, at frequencies matching those found in our data (Jackson et al., 2014).

However, when compared with the lowpass filtered ADCP record in Sermilik Fjord (Figure 10), the lowpass filtered iceberg velocities are noticeably smaller, with velocity differences occasionally exceeding 0.5 m s^{-1}, or over an order of magnitude. Though these velocity differences could be caused by a fast-flowing surface water layer (<50 m depth) not captured in the ADCP record, the observed differences almost always exceed prior direct observations and estimates of the surface layer velocity in Sermilik Fjord (Sutherland & Straneo, 2012). Based on our previous work (Figure 2) with a reasonable range of wind and water velocities found in our results, we attribute this difference primarily to the effect of water drag, with a lesser contribution by air drag. However, there is good agreement in the timing of in- or out-fjord accelerations between the two datasets.

Four individual icebergs from the 2012 season show coincident responses to both katabatic and barrier wind events (Figure 15). For a barrier wind, the expected response

of the fjord waters is a delayed but strong up-fjord flow in the upper layer followed by a deceleration and strong down-fjord flow of the upper layer after the wind relaxes and the along-fjord isopycnal tilt flattens (Jackson et al., 2014). Each of the four icebergs shown exhibits an up-fjord acceleration near the peak of a barrier wind event, followed by a relaxation and a down-fjord acceleration of a similar magnitude. Katabatic along-fjord winds in the out-fjord direction are also represented by coincident down-fjord accelerations in all of the iceberg records, though the amplitudes of these along-fjord velocity pulses are smaller than those forced by the intermediary circulation.

In Sermilik Fjord, the period of the coincident iceberg response to a shelf wind event is 1-3 days, matching other observations of seiche behavior in fjords (Arneborg & Liljebladh, 2001; Jackson et al., 2014; Sutherland & Straneo, 2012). Notably, many barrier wind events are preceded 1-2 days earlier by katabatic wind events (Figure 15). Klein and Heinemann (2002) suggest the linkage between these events is due to katabatic winds enhancing or even driving the synoptic mesocyclone in the Irminger Sea. Additionally, these winds modulate sea ice concentrations at the mouth of Sermilik Fjord (Oltmanns et al., 2014), potentially affecting the residence time of icebergs inside the fjord by physically limiting their movement past the mouth.

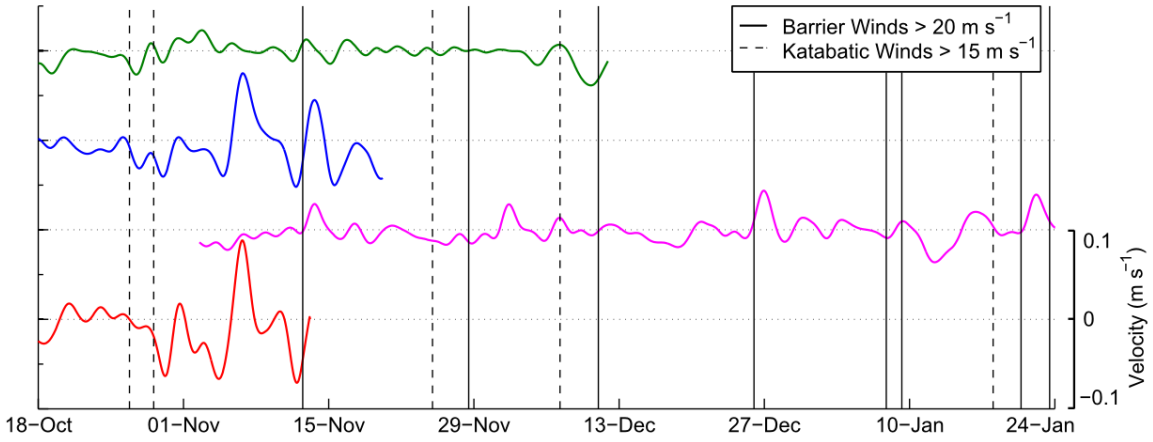

Figure 15. Along-fjord velocities of four 2012 icebergs, with vertical bars representing along-shelf barrier winds and along-fjord katabatic winds.

To examine the response of icebergs to each of the wind event types, we constructed composites (Figure 16) of along-shelf winds with peaks > 20 m s^{-1}, (including their speeds 24 h before and 96 h after the peak), along-fjord winds > 10 m s^{-1} (24 hours before and after their peak), and the along-fjord velocities of icebergs that were transmitting during these wind events. The chosen wind peak speed thresholds, though arbitrary, are consistent with values chosen for previous composite records in SE Greenland (Harden et al., 2011; Oltmanns et al., 2014).

Composites of the iceberg response to barrier wind events match the timescales found in responses to each wind event shown in selected examples from the ADCP velocity record (Figure 16). The peak in-fjord flow of the upper 200 m occurs between 24-30 h after the peak wind is measured, while the peak out-fjord flow occurs from 68-72 h after the peak wind. Again, the velocity magnitude appears diminished in the iceberg motion, due to the previously-mentioned water and air drag forces.

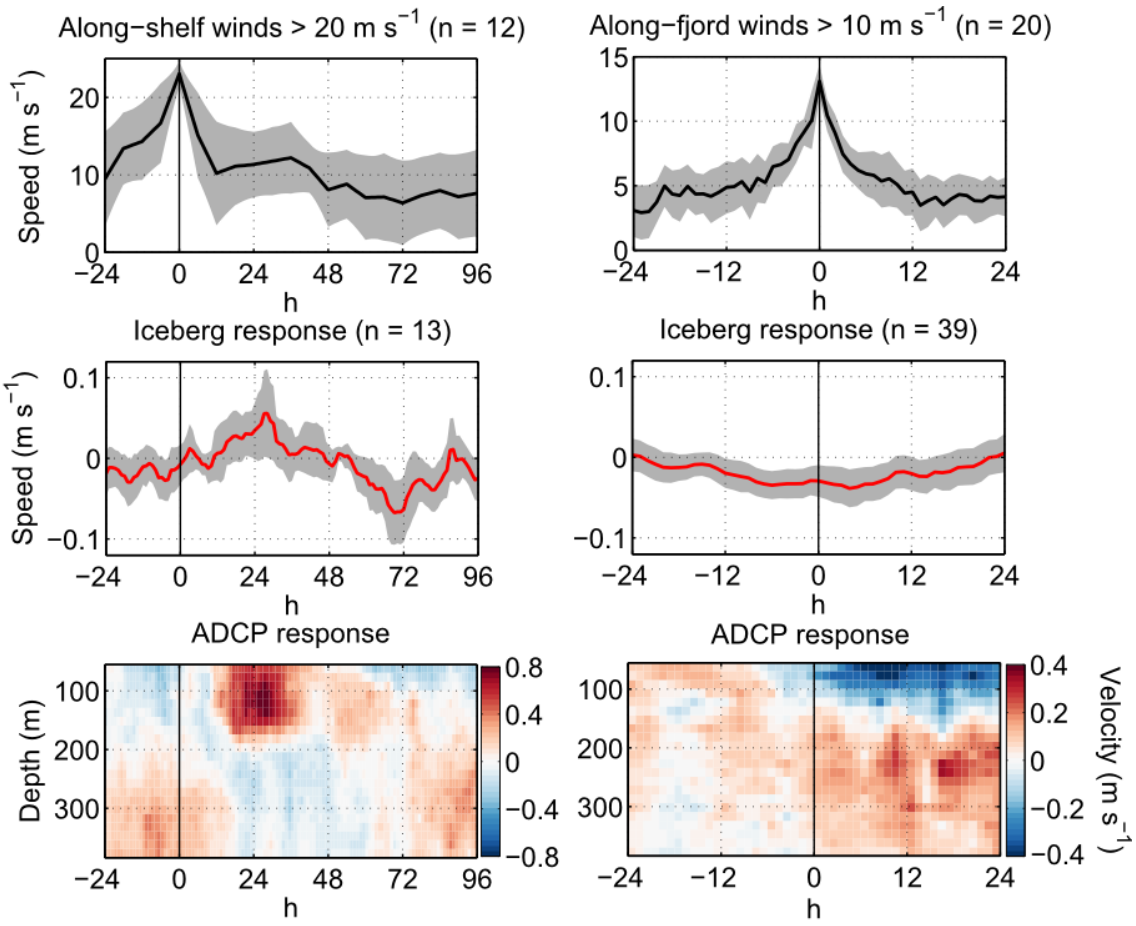

Figure 16. Composites of along-shelf and along-fjord wind events (top row) and the composite response of iceberg trackers in the fjord (middle row). Grey error bars represent the 95% confidence interval of the mean. Representative ADCP profiles (bottom row) taken at the time of one of each type of wind event show examples of the full water column response.

Down-fjord katabatic winds normally last under 48 hours (Oltmanns et al., 2014) but also result in a significant iceberg response, by both pushing on the iceberg surface above water and by accelerating the upper water column. This results in a down-fjord acceleration of icebergs. We assume that the iceberg response to along-fjord winds is stronger with a shallower keel depth – in this case, through the reduced contribution of vertical velocity shear and drag forces. For very deep-keeled icebergs, we expect the iceberg response to be slowed by increased velocity shear with depth, as strong along-

fjord winds have been shown to strengthen the two-layer flow in other glacial fjords, increasing the rate of inflow of deep water (Moffat, 2014).

Gridded contours of the mean circulation scheme in the upper water of Sermilik Fjord show both latitudinal and longitudinal variations in velocity (Figure 17a). North of 66°N, iceberg speeds are slower, implying a longer residence time in the wide upper basin. Icebergs are often diverted or slowed at the submarine ridge at 66°N. South of 66°N, where the fjord narrows and deepens, speeds increase and residence times decrease. Velocity variance also steeply increases south of this threshold (Figure 17b), and we interpret this southern region as an area where fjord-shelf circulation mechanisms, including both intermediary circulation and tides, are more strongly felt. Once the icebergs come within 5 km of the mouth, they quickly flush out to the shelf.

Plots of the iceberg tracks (Figure 7) help inform the patterns visible in the gridded vector plots. At the top of the main fjord branch, near 66.3°N, icebergs often recirculate around the island before re-entering the main fjord. Icebergs also avoid flowing over the shallow submarine ridge at 66°N, which we interpret as a combination of bathymetric funneling of the deep fjord waters and a simple physical barrier to deep-keeled iceberg motion. Both the vector plots and the iceberg tracks display a rightward preference (moving from the fjord towards the mouth) south of 66°N, suggesting that rotational effects are felt in this region.

The 2013 (Year 2) icebergs experienced similar mean residence times but greater residence time variance in the fjord (81 ± 67 days mean ± st. dev.) compared to the 2012 icebergs (73 ± 24 days mean ± st. dev.). The Year 2 icebergs were deployed approximately 1 month earlier in the year than the Year 1 icebergs, encompassing more

of the warm summer season where Sermilik Fjord remains free of sea ice and is not blocked at the mouth by Arctic sea ice (Figure 5). In particular, the larger variance in residence times found in the Year 2 icebergs is exacerbated by iceberg UO10 (Table 2), which spent several months grounded on shallow bathymetry near the fjord wall.

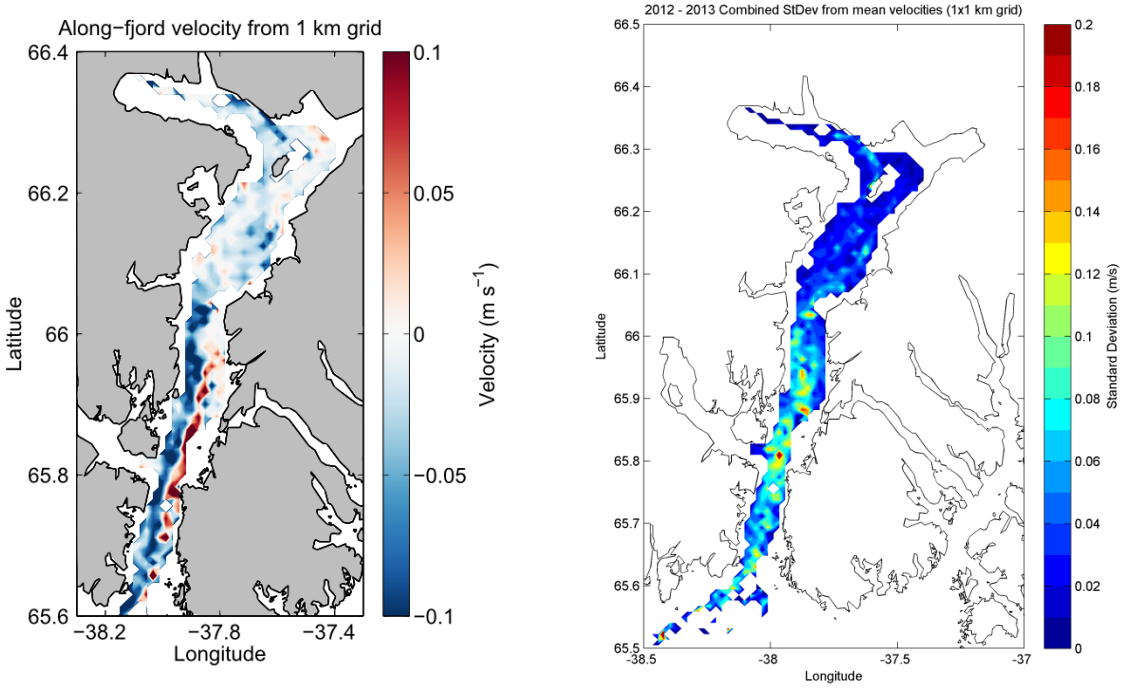

Figure 17. Gridded mean along-fjord iceberg velocities (left) and standard deviation of velocity (right) from the combined 2012-2013 GPS tracks.

2.4.3. Shelf

All five of the 2012 icebergs eventually stopped transmitting in a 1000 km^2 region 100-200 km south-west of Sermilik Fjord, between November 2012 and April 2013. Presumably, this is a region of shallow water where the icebergs become stuck, leading them to break apart or overturn. However, all of the icebergs were able to flow through the channel SW of the mouth of the fjord without becoming stuck, suggesting that this channel may be even more well-defined than shown in the bathymetry gridded from seal

dive data (Sutherland et al., 2013). Of the three 2013 icebergs that reached the shelf, two stopped transmitting in this area, while one continued southward. Since the SE Greenland shelf is a site of thick (> 1 m) sea ice growth in the winter months, sea ice may have also had a role in immobilizing the icebergs.

Iceberg UO11 (Figure 18) was an anomaly. It made a sharp south-eastward turn after leaving the fjord in March 2014 and continued to travel southward along the coast at speeds between 0.2-1.4 m s^{-1} for over 11 days, before becoming stuck in thick Arctic sea ice or grounded on the shallow shelf near 64°N. After two days, it re-mobilized and then became stuck in thick ice two days later near 62.5°N (Figure 19). Throughout its journey, iceberg UO11 traveled over 500 km along the southeast Greenland coast in the EGCC. Iceberg tracks on the shelf provide a winter-time compliment to the drifter deployments carried out by Bacon et al. (2002) in August-December 1997. The new observations match both the previously observed spatial structure of the EGCC, as well as the locations of regions exceeding speeds of 1 m s^{-1} (Bacon et al., 2014; Sutherland & Pickart, 2008), where the EGCC accelerates southward as the shelf narrows.

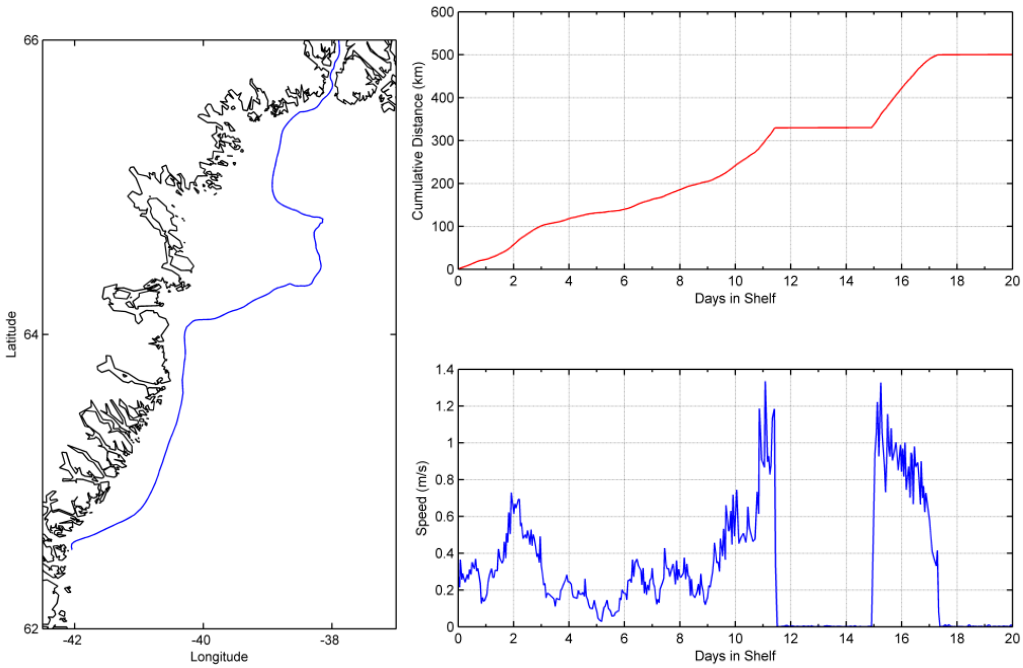

Figure 18. The path of Iceberg UO11 along the SE Greenland coast (left), cumulative distance traveled (top right), and speed (bottom right).

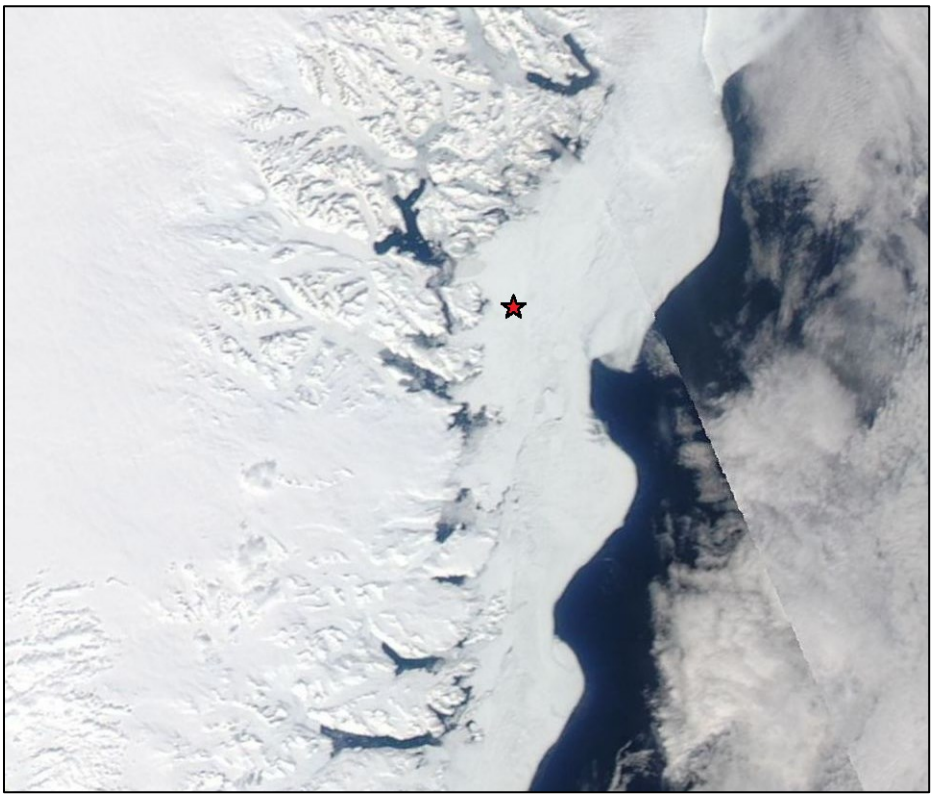

Figure 19. MODIS AQUA image acquired on 25-Apr-2014, with the location of the immobilized iceberg UO11 (red star) on that date.

CHAPTER III

ICEBERG MELT

3.1. Introduction

The GrIS's contributions to sea level rise can come from liquid meltwater flux from submarine melting or surface runoff, and from solid ice flux, through iceberg calving from tidewater glaciers. Despite their ubiquitous presence, the effect of icebergs on the horizontal distribution of freshwater and vertical stratification is unknown in Greenland's fjords. Icebergs melt at rates dependent on local temperature and salinity differences, as well as the wave energy incident on the sides and the keel depth of the iceberg. This melt can locally affect the density structure of the surrounding water (Huppert & Turner, 1980; Morison & Goldberg, 2012). The amount of melt produced by icebergs in a given fjord depends on the residence time of the icebergs in the fjord, which is controlled primarily by the large-scale circulation and geometry of the fjord. Icebergs can distribute their freshwater directly into the fjord and into coastal waters after exiting the fjord, where they can potentially impact buoyancy-driven flows on the continental shelf.

Each of the circulation processes mentioned above can influence the residence time of icebergs in Sermilik Fjord. However, to address how much freshwater is being deposited in the fjord, we also require information on 1) the number and size distribution of icebergs in Sermilik fjord, and 2) the melting characteristics of these icebergs.

Several authors have modeled and refined the shapes (Barker, Sayed, & Carrieres, 2004; McKenna, 2005), strength and temperature properties (Jones, 2006), and thermodynamics (Bigg, Wadley, Stevens, & Johnson, 1997; Silva, Bigg, & Nicholls,

2006) of floating icebergs. Hotzel and Miller (1983) and Savage (2001) compiled statistics on iceberg dimensions, mass, and volume from data recorded by the International Ice Patrol (IIP) and by oil companies working on the Grand Banks near Nova Scotia, and found that the average length to total height ratios of icebergs is about 3:1, with values ranging from 0.5:1 to 50:1. We expect tabular icebergs, such as those tracked in this study, to have a larger ratio, on the order of 5:1 (Table 2). Shipboard observations of icebergs in one east Greenland fjord have been used to construct empirical histograms of the sizes and numbers of icebergs found in the inner fjord, mid-fjord, and coastal regimes (Dowdeswell et al., 1992). These observations showed a roughly log-normal distribution of iceberg sizes, with the largest number of icebergs in the sub-100 m width class, decaying to lower frequencies with each larger width, due in part to the generation of smaller icebergs from the breakup of larger ones.

Lab experiments performed with melting ice chunks in cold, salinity-stratified water (Huppert & Josberger, 1980; Huppert & Turner, 1980; Huppert, 1980) have shown that the structure of melting along the vertical faces of icebergs combines complex double-diffusive and turbulent boundary layer processes. Silva et al. (2006) calculated melt rates for modeled Antarctic icebergs, using parameterizations with ambient water temperature and salinity, motion of water across the submerged keel, and wave erosion at the water surface. This combined literature provides useful tools for estimating the freshwater flux in Sermilik Fjord contributed by floating icebergs.

3.2. Iceberg Size Distributions

Calculations of the total meltwater flux by floating icebergs in a fjord first require an estimate of the total submerged surface area of those icebergs. This surface area estimate is dependent not only on the total amount of floating ice, but also on the distribution of iceberg sizes and the number of icebergs in each size class.

Using MODIS satellite imagery from 18-Sep-2012 (Figure 20), we identified all individual icebergs with a diameter > 500 m, or twice the size of a single pixel. For iceberg sizes above 500 m, we quantified their diameters in 250 m intervals, including 750 m and 1000 m sizes. There were no icebergs found with diameters > 1000 m.

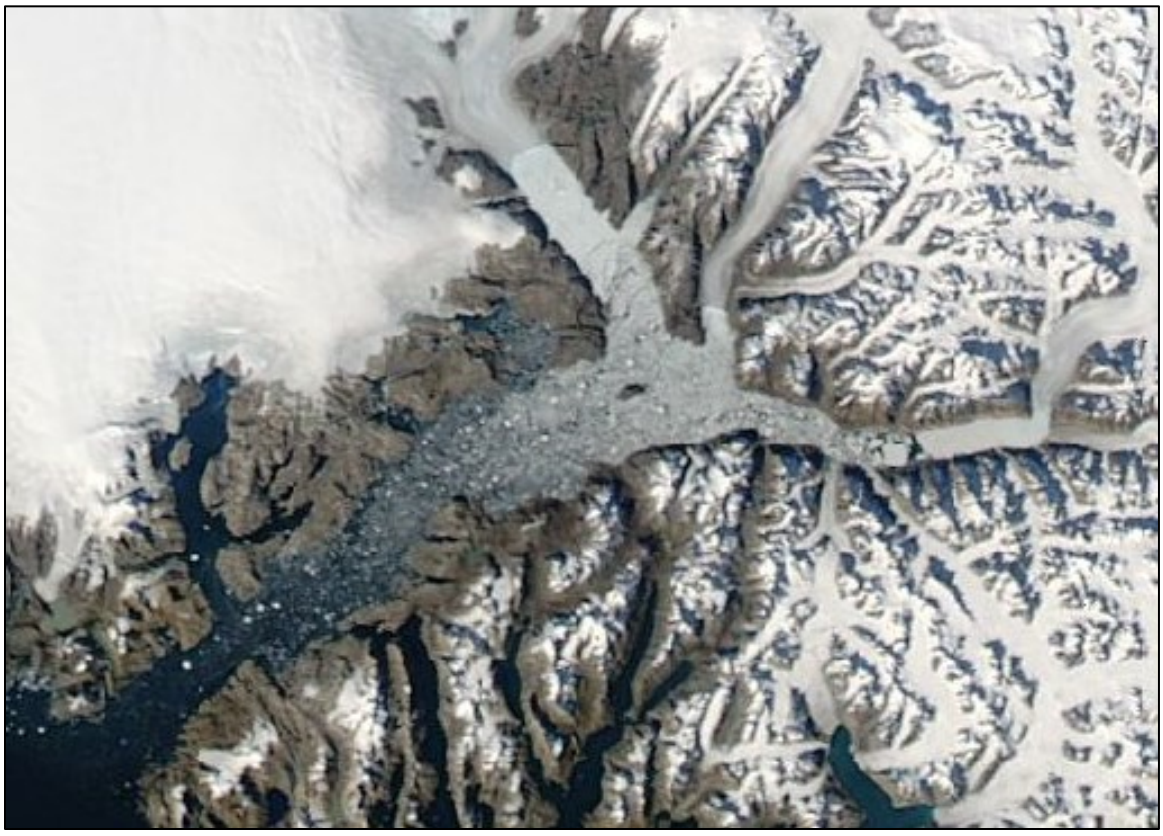

Figure 20. The MODIS AQUA image used for calculating an iceberg size distribution in Sermilik Fjord. Image acquired 18-Sep-2012.

We then used the empirically-derived iceberg size histograms from Dowdeswell et al. (1992) to extrapolate the possible numbers of icebergs smaller than 250 m in Sermilik Fjord (Figure 21). Because the shape of the size histograms in their study varied depending on the fjord, location in the fjord, and natural sampling variability in iceberg numbers due to changes in calving rates, winds, and circulation, we also extrapolated "small" and "big" histograms in addition to the mean histogram, representing iceberg size frequencies skewed towards larger numbers of small (< 100 m) and large (> 400 m) icebergs, respectively. Finally, we calculated the estimated below-water surface area of an iceberg in each size class, using the iceberg size calculations from Savage (2001) and Morison and Goldberg (2012).

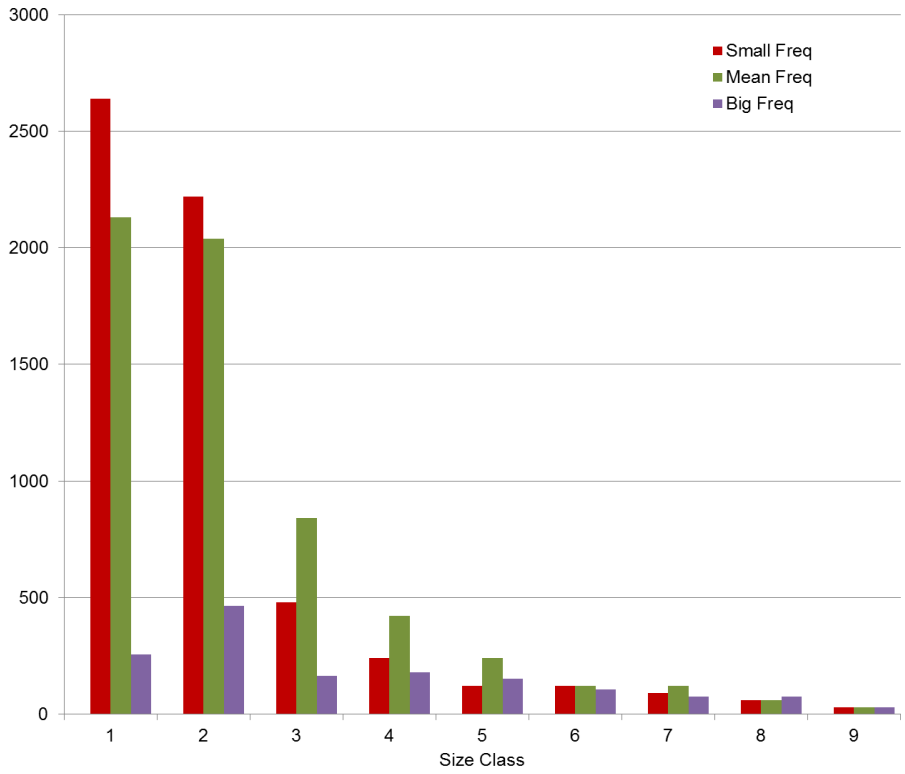

Figure 21. The three extrapolated iceberg size distributions for Sermilik Fjord. For the size classes, Size Class 1 = 100 m diameter and smaller, 2 = 100-200 m, 3 = 200-300 m, etc.

3.3. Melt Rates

Using the turbulent heat transfer melt rate parameterizations from Silva et al. (2006) (Eqns. 4-7, Table 3), which relies on water movement past the submerged ice surface, we calculated values for melt rates for a given far-field water temperature range and relative water velocity range across the bottom and sides of the submerged surface area of the icebergs (Figure 22),

$$T_B = aS_B + b + cp_B \quad (4)$$

$$|u|\gamma_T(T_\infty - T_B) = -M_T \frac{L + \Delta T c_i}{c_w} \quad (5)$$

$$|u|\gamma_S(S_\infty - S_B) = -M_T S_B \quad (6)$$

$$T_{sh} = T_\infty - (aS_\infty + b + cp_B), \quad (7)$$

holding salinity constant at 32 psu, and defining the temperature difference between the core and skin of the iceberg as 20°C. The calculated melt rates are far less sensitive to these two values than to the ambient water temperature and velocity. Note that we did not calculate the contribution of wave erosion to iceberg melt (Gladstone et al., 2001),

$$M_W = \frac{1}{12} S_S[1 - \cos(C^3\pi)](T_W + 2), \quad (8)$$

where S_S is the sea state on the Beaufort scale, and C is the fractional sea ice concentration, which can dampen the wave erosion. Savage (2001) estimated melt rate contributions by wave erosion to icebergs in the open ocean and found that wave erosion accounted for over 50% of total volume loss, with turbulent heat transfer contributing

only 11-25%. Here, we examine only the turbulent heat transfer terms, acknowledging that wave erosion, wind convection, solar radiation, and iceberg breakup serve as important, dynamic processes of iceberg meltwater flux.

Table 3. Melt rate parameters and variables used in Eqns. 4-8.

Parameter	Symbol	Units	Value
Salinity coefficient of freezing equation	a	°C psu^{-1}	-5.73×10^{-2}
Constant coefficient of freezing equation	b	°C	8.32×10^{-2}
Pressure coefficient of freezing equation	c	°C dbar^{-1}	-7.61×10^{-4}
Fractional sea ice concentration	C		
Specific heat capacity of ice	c_i	J kg^{-1} °C^{-1}	2010
Specific heat capacity of water	c_w	J kg^{-1} °C^{-1}	4000
Latent heat of fusion of ice	L	J kg^{-1}	3.35×10^5
Turbulent melt rate	M_T	m s^{-1}	
Wave erosion melt rate	M_W	m d^{-1}	
Pressure at the iceberg base	p_B	dbar	100
Beaufort sea state	S_S		
Salinity at the iceberg base	S_B	psu	
Far-field salinity	S_∞	psu	32
Temperature at the iceberg base	T_B	°C	
Far-field temperature	T_∞	°C	-2 to 10
Water speed relative to iceberg surface	u	m s^{-1}	0 to 0.5
Salt transfer coefficient	γ_S		2.2×10^{-5}
Heat transfer coefficient	γ_T		6×10^{-4}
Temperature difference between ice skin and core	ΔT	°C	-20

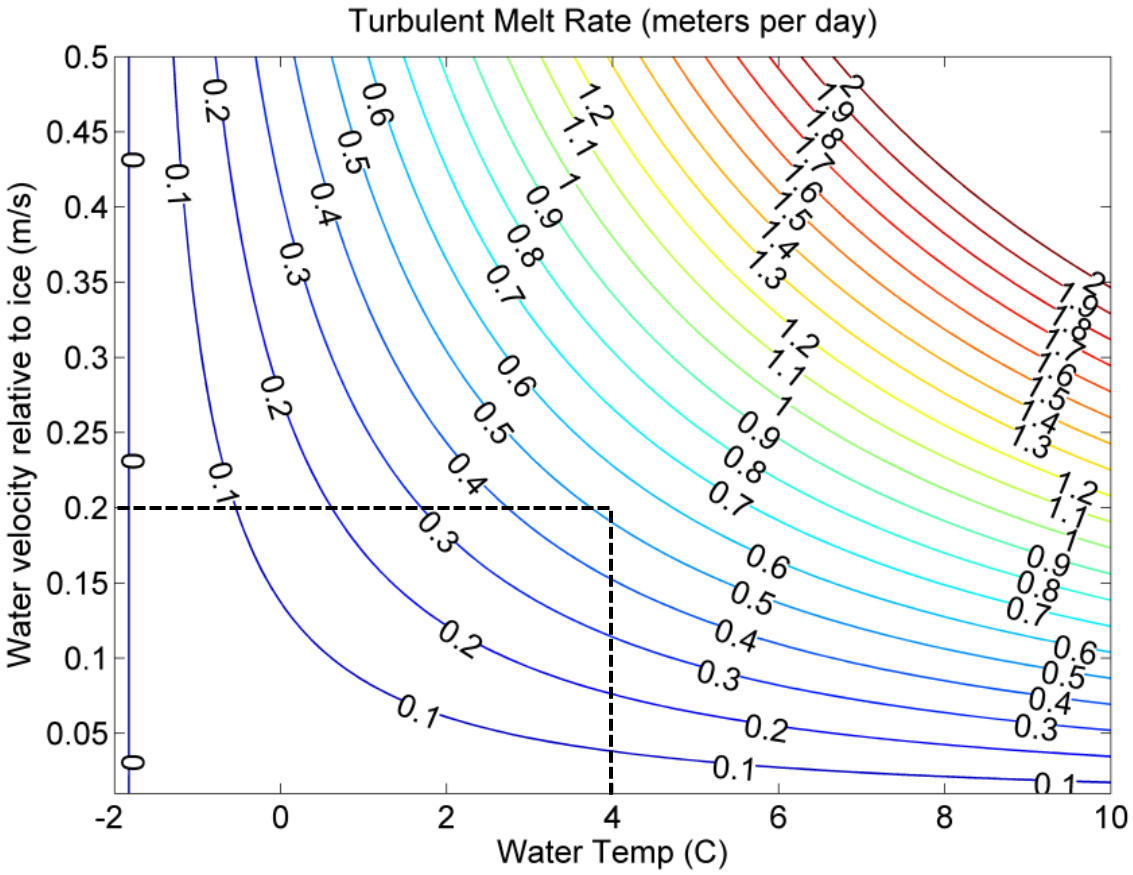

Figure 22. Melt rate contour plot (m per day) using the turbulent melt rate parameterization in Silva et al. (2006). Values underneath the dashed box indicate conditions typically found in Sermilik Fjord.

3.4. Meltwater Flux Estimates

Using the iceberg size distributions (and their below-water surface areas) and the turbulent heat flux melt rate parameterization above (Eqns. 4-7), we then calculated total iceberg meltwater flux in Sermilik Fjord (Table 4), neglecting wave erosion, wind convection, and solar radiation. Because depth-averaged water temperature in Sermilik Fjord rarely exceeds 4°C (Straneo et al., 2010) and the relative velocities between icebergs and water in our work rarely exceeded 0.2 m s^{-1}, for more than a few days (Appendix E), we did not calculate fluxes for melt rates higher than 0.4 m d^{-1}.

Table 4. (Left) Estimated daily melt flux by icebergs into Sermilik Fjord, for the three constructed iceberg size distributions (small, mean, and big). (Right) Daily melt flux multiplied by the 77-day average iceberg residence time.

Melt rate ($m\ d^{-1}$)	Total melt flux ($\times 10^6\ m^3\ d^{-1}$)			Melt amount for 77 days (km^3)		
	Small	**Mean**	**Big**	**Small**	**Mean**	**Big**
0.05	88	107	53	7	8	4
0.1	176	214	105	14	16	8
0.2	353	429	210	27	33	16
0.3	529	643	315	41	49	24
0.4	706	857	420	54	66	32

3.5. Discussion

Our melt rate estimates for Sermilik Fjord (Table 4) result in an iceberg melt flux ranging from 4-66 km^3 totaled over the average iceberg residence time in one year. In comparison, the modeled mean ice discharge from Helheim, Midgård, and Fenris glaciers into Sermilik Fjord for an entire year is 34 $km^3\ y^{-1}$, and the discharge from other sources (terrestrial runoff, precipitation, subglacial geothermal melting, and subglacial frictional melting) equals 6.5 $km^3\ y^{-1}$ (Mernild et al., 2010). From our calculations, an average melt rate of only 0.2 m d^{-1} over the average iceberg residence time would be needed to equal the entire year's total ice discharge, meaning that 100% of all ice discharged into Sermilik Fjord would melt before it could exit the fjord.

However, we can confidently constrain our estimates of iceberg melt rate and flux to the lower range. Our GPS data (Figure 7) confirm that almost all large (> 100 m length) icebergs eventually exit the fjord without fully melting, or melting enough to catastrophically overturn. Even for a very high melt rate of 0.4 m d^{-1}, a large iceberg would only melt 30.8 m of its submerged radius during the observed average residence

time in the fjord. Additionally, by excluding the wave erosion, wind convection, and solar radiation melt terms mentioned above, we can further reduce our estimates of melt by turbulent heat transfer.

In an additional constraint to the lower melt flux range, the small icebergs most vulnerable to melting away entirely extend only within the colder (-1-0 °C) PW layer, from 0-200 m, where the vertical velocity shear and drag forces are low, compared to the larger, deeper-keeled icebergs that extend more than 200 m in depth.

These calculations also exclude the melt contribution of the ice mélange, which contains a higher concentration of smaller and thus more easily-melted ice, but which is also closer to the very cold subglacial meltwater plume. So far, the relative contributions of these two competing factors remain unconstrained, and it is unclear if iceberg melt fluxes within the ice mélange are significant compared to those in the main fjord.

Our results show that iceberg melt may nonetheless be a significant source of freshwater to Sermilik fjord. For deep-keeled icebergs, meltwater is produced at depth, and often reaches a level of neutral density below the surface due to entrainment of ambient water (Holland & Jenkins, 1999). Iceberg melt also has the potential to increase density stratification in the fjord far from the glacier terminus and the influence of the fresh glacial outflow plume. Though numerous studies have examined stratification and buoyancy in Sermilik and other fjords (Straneo et al., 2010; Sutherland et al., 2014), none have yet attempted to quantify the relative contributions of glacial and iceberg meltwater to the total freshwater distribution.

In terms of ice discharge, four of the five most productive glaciers in Greenland are located on the SE Greenland coast, and together account for nearly 30% of the total

ice discharge of all outlet glaciers from the GrIS (Enderlin et al., 2014). Because of this, the contributions of icebergs melting on the continental shelf may be crucial in supplying freshwater to the EGCC system, maintaining or enhancing the cross-shelf density gradient that drives geostrophic flow in the EGCC.

CHAPTER IV

CHALLENGES AND LIMITATIONS

The GPS trackers used here were set to an hourly transmission interval to optimize the tradeoff of resolution vs. battery life and cost per transmission. Currently the finest available transmission interval for a SmartOne GPS unit is 35 minutes. Higher temporal resolution is needed to better examine mélange dynamics on the timescale of large calving events. Previous work with broadband seismometers deployed near Jakobshavn Isbrae in West Greenland has shown that changes in the mélange structure and force balance can occur in minutes (Amundson et al., 2010). Tracking iceberg motions at high temporal resolution throughout their evolution in the ice mélange may be a crucial new tool in the lingering question of ice mélange dynamics and the mélange's influence on glacier flow and calving at the terminus.

Better bathymetry products are needed to more adequately understand certain regions of iceberg motion, especially on the continental shelf. If an iceberg becomes grounded, high-resolution bathymetry at that point acts as a measure of the iceberg's keel depth. High-resolution bathymetry can also be used to spot iceberg keel plow marks on the ocean floor, showing the directions of past and present iceberg motion.

Steep fjord walls, poor weather conditions, and cold temperatures reduced the ability of the GPS trackers to obtain and transmit a successful fix each hour. Thus, resolution was often below-hourly, and we identified gaps in the GPS record lasting several days. To fill in these gaps, we used linear interpolation, which provided sensible average positions and velocities, but eliminated any signal of velocity variability that each iceberg no doubt experienced over the missing time intervals.

Overturning icebergs acted as the final, inescapable end to GPS transmissions, especially in the shelf region. Though future designs for the GPS deployment tripods will incorporate a lower profile, higher weight, and increased traction on the ice, a full iceberg overturning or breakup will inevitably destroy any iceberg-mounted instrumentation.

CHAPTER V

CONCLUSIONS

Low-cost, expendable GPS units deployed on iceberg "drifters" have proven their utility in successfully diagnosing fjord circulation on tidal to synoptic timescales. These drifters are currently the only high-resolution instrumentation capable of safely collecting *in situ* observations of ice mélange velocity. Analysis of drifter tracks within Sermilik Fjord confirms the links between winds, fjord-shelf water exchange, and the timescales and geographic thresholds of upper water circulation in the fjord.

Iceberg residence times in Sermilik Fjord average 77 ± 49 (mean ± st. dev.) days after exiting the ice mélange, with velocity variability on tidal and synoptic timescales. Analysis of this velocity variability confirms earlier hypotheses that shelf wind-driven, two-layer flow is the dominant circulation mechanism in Sermilik Fjord. Perhaps the most important conclusion from this work is that the timing and scale of these events can be observed with no ship presence or other in situ oceanographic instrumentation; less than a day of helicopter time deploying GPS trackers, and freely available, coarse resolution weather data products are the only tools needed to monitor circulation in any large Arctic fjord remaining relatively free of sea ice throughout the study period. These data can also provide insights to spatial patterns of circulation and recirculation in the fjord which cannot be observed by moored instruments, satellite or aerial imagery, or limited ship time.

These drifters also provided new measurements of the speeds and structure of the East Greenland Coastal Current in winter. These measurements aid estimates in

quantifying the EGCC's role as an important freshwater pathway in the subpolar North Atlantic.

Ultimately, these data provide useful information on residence times and volume fluxes used to calculate heat transport and melt rates by warm Atlantic Water to the terminus of Helheim Glacier and the other glaciers in Sermilik Fjord. Furthermore, these residence times, when combined with existing temperature and salinity profiles in Sermilik Fjord, constrain calculations of the freshwater melt fluxes from floating icebergs. As ice discharge from the GrIS accelerates, the importance of the freshwater contribution to ocean temperature, salinity, and stratification by melting icebergs may also be increasing.

APPENDIX A

SETTING/OVERVIEW

Here, we show several maps of the raw GPS tracks from the 2012 deployment year, including satellite imagery and bathymetry in the Sermilik Fjord region.

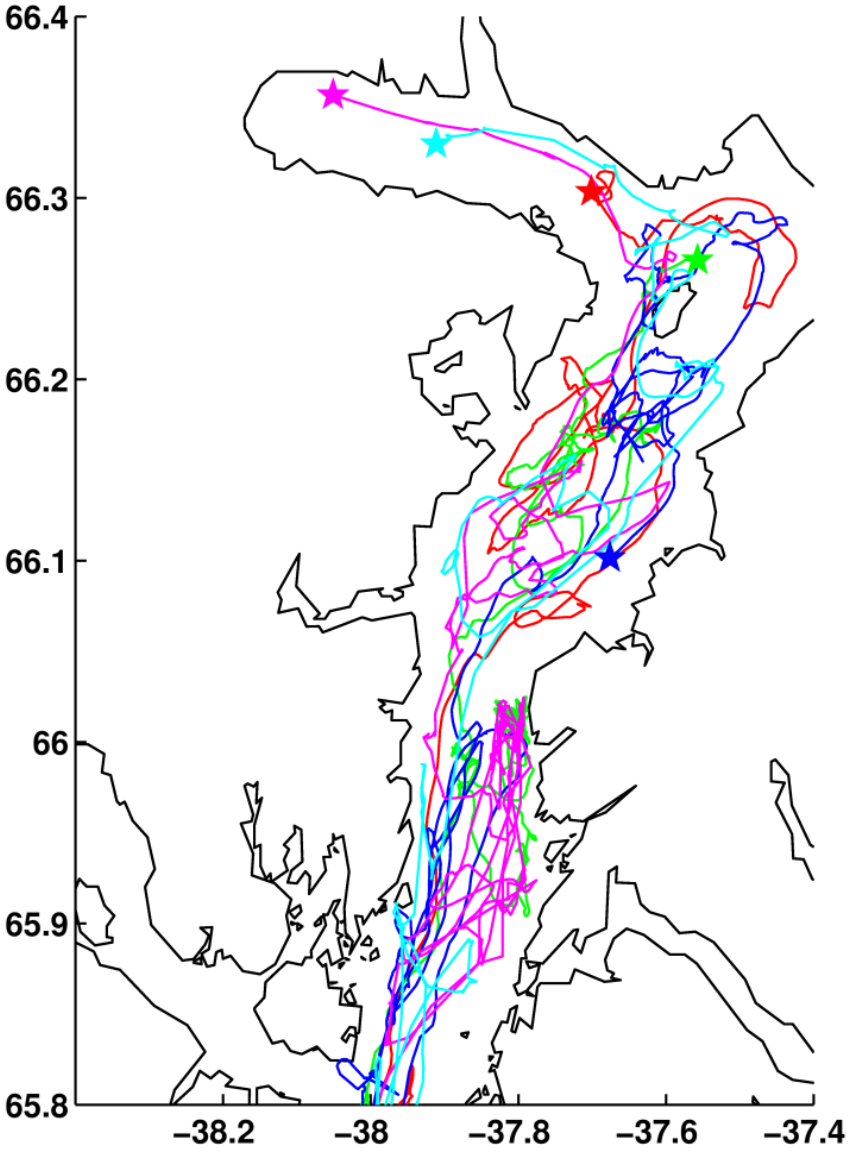

Figure 23. The 2012 series of trackers, zoomed into the upper fjord region.

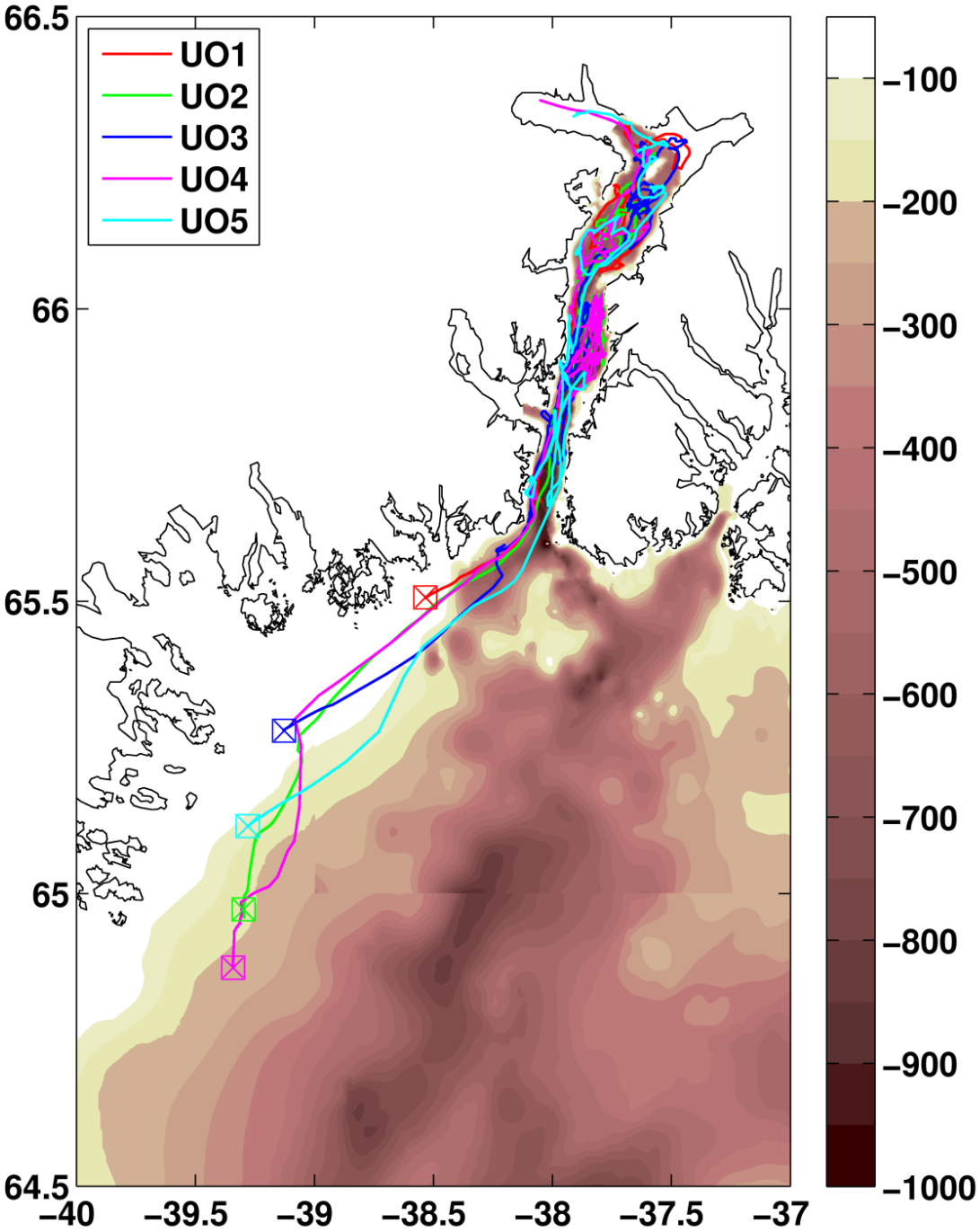

Figure 24. Map of the 2012 series of drifters overlaid on shelf bathymetry combined from GEBCO and seal tracks (source). After icebergs exit the fjord, they travel with the EGCC and are pushed shoreward by downwelling-favorable winds.

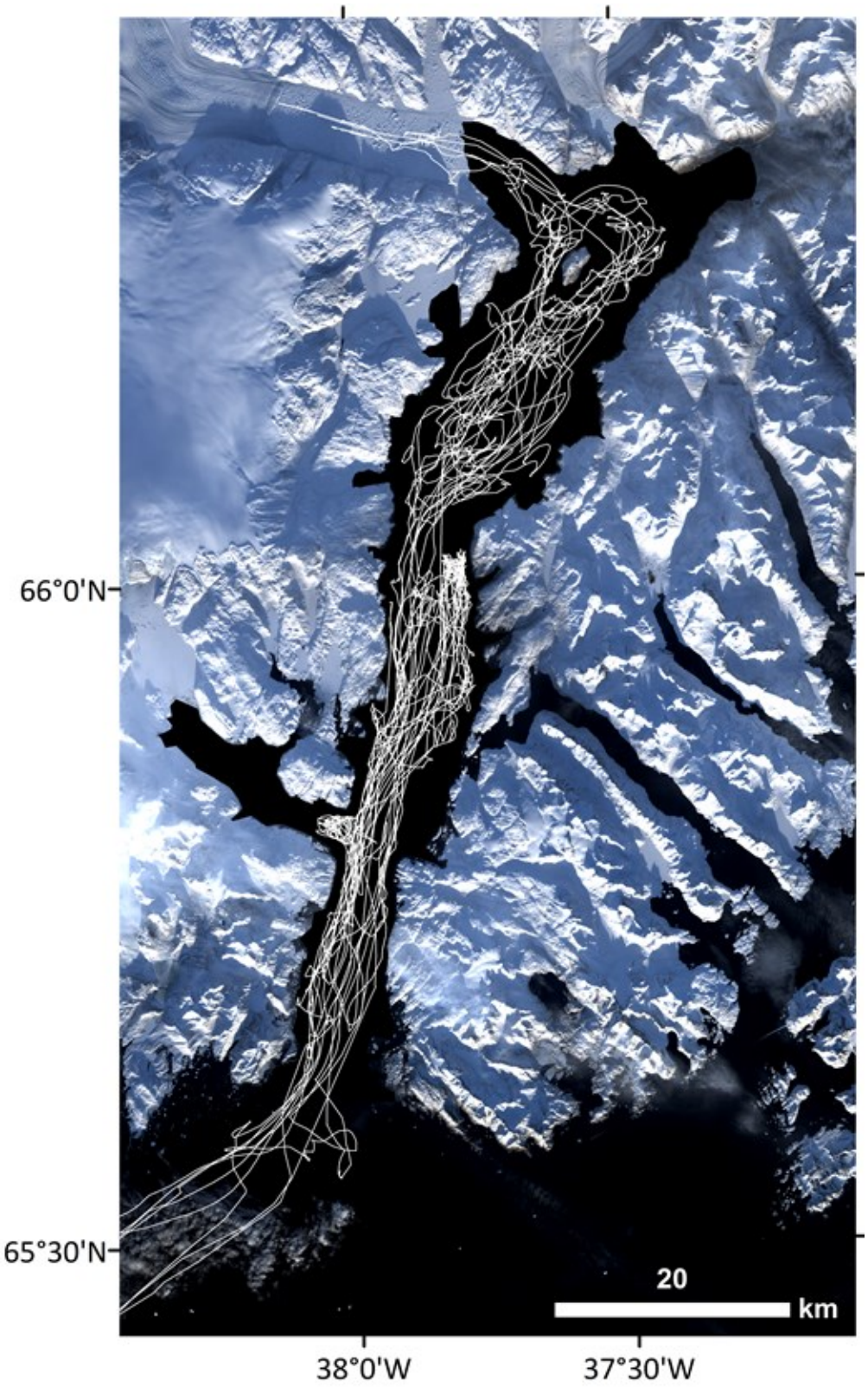

Figure 25. Complete map of all 2012 and 2013 drifter tracks overlaid on Landsat-8 imagery.

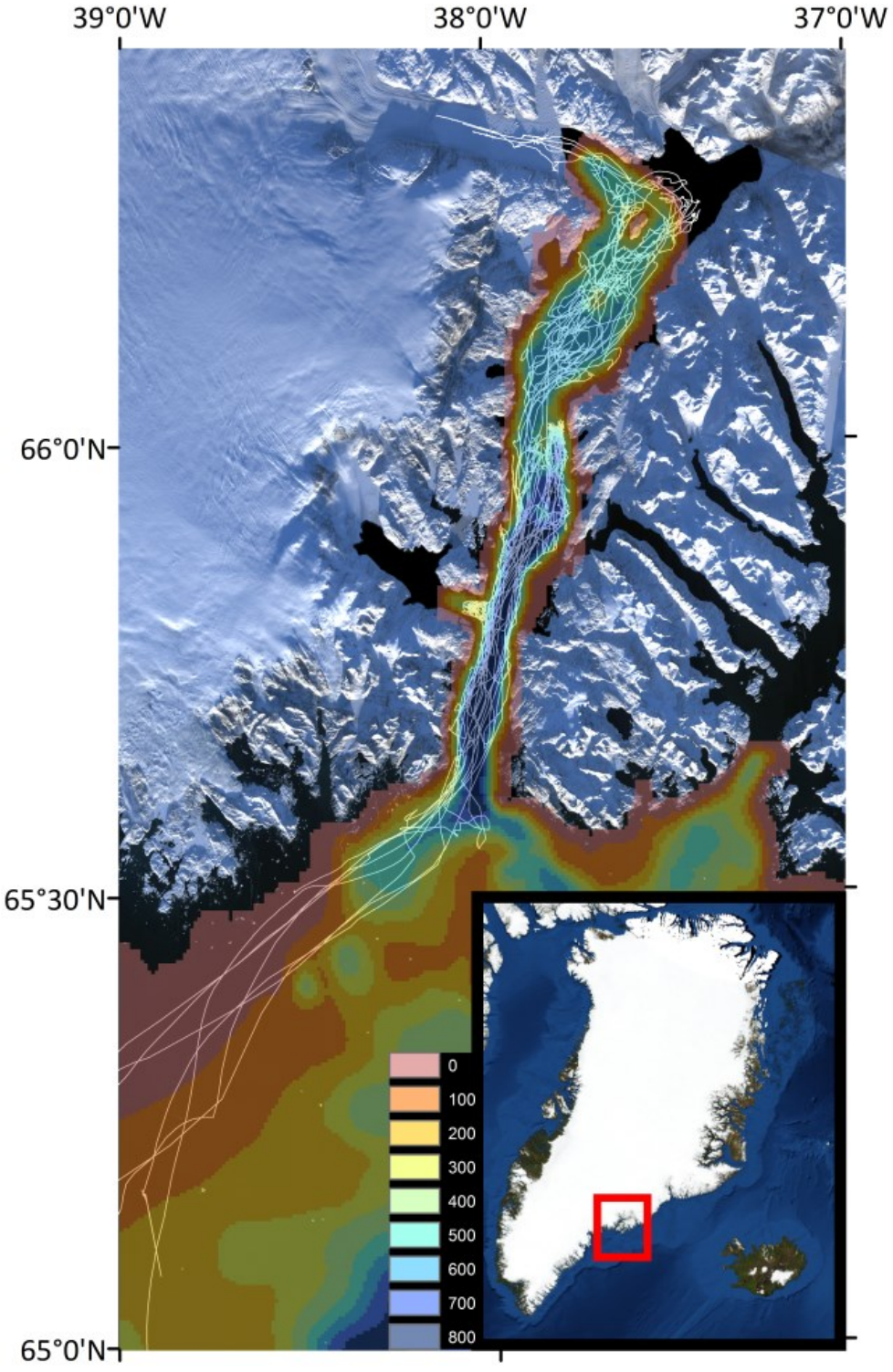

Figure 26. Complete map of all 2012 and 2013 drifter tracks overlaid on Landsat-8 imagery, including gridded GEBCO, gridded single-beam, and seal dive-derived bathymetry.

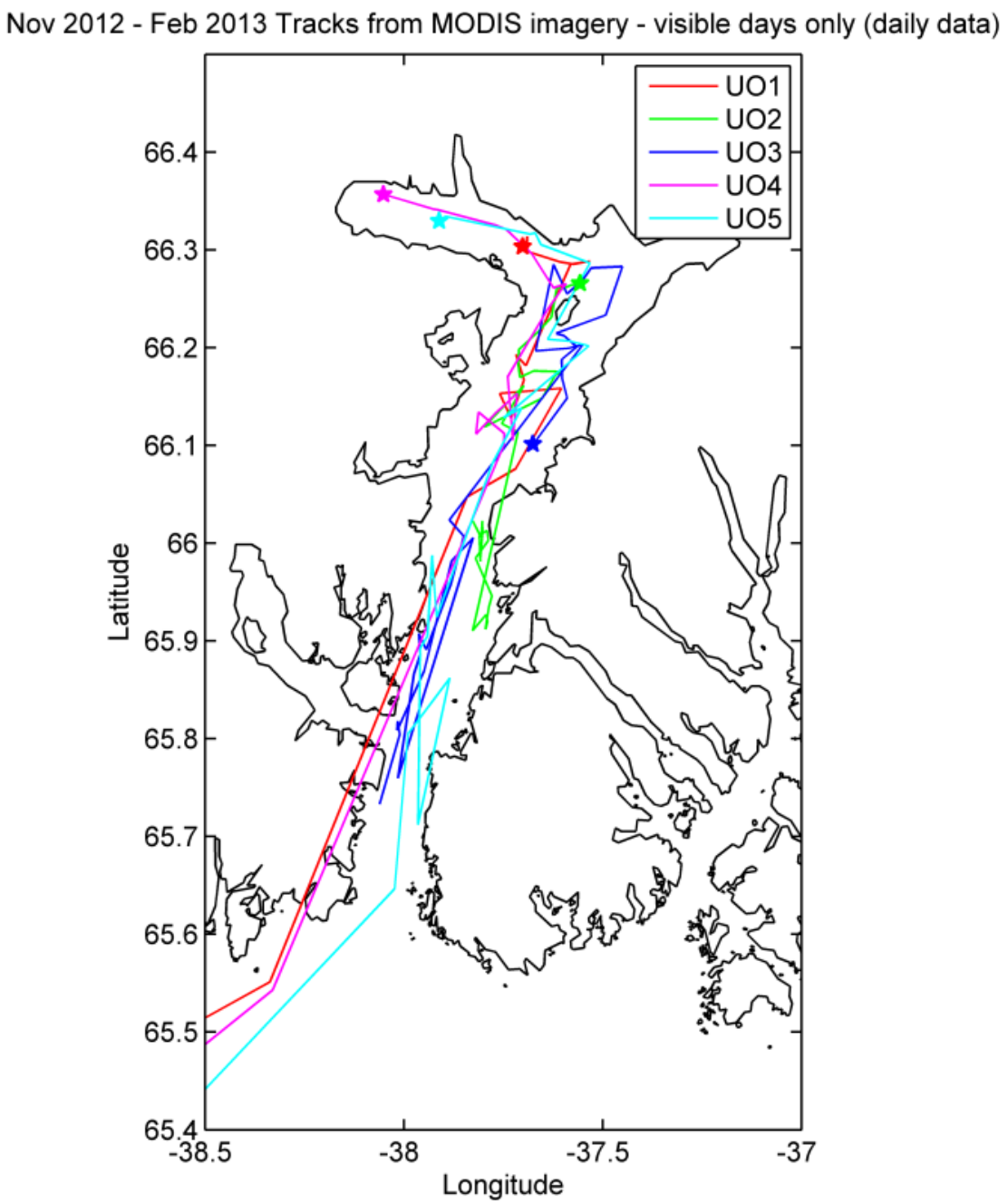

Figure 27. Iceberg drifters have an extremely significant spatial and temporal resolution advantage over feature tracking with satellite imagery. Here we show the paths of the five 2012 icebergs if iceberg locations were sampled only on dates with available, cloud-free MODIS imagery.

APPENDIX B

FJORD DYNAMICS

The raw iceberg tracker position and velocity data from 2012 and 2013 were used to analyze the circulation in Sermilik Fjord.

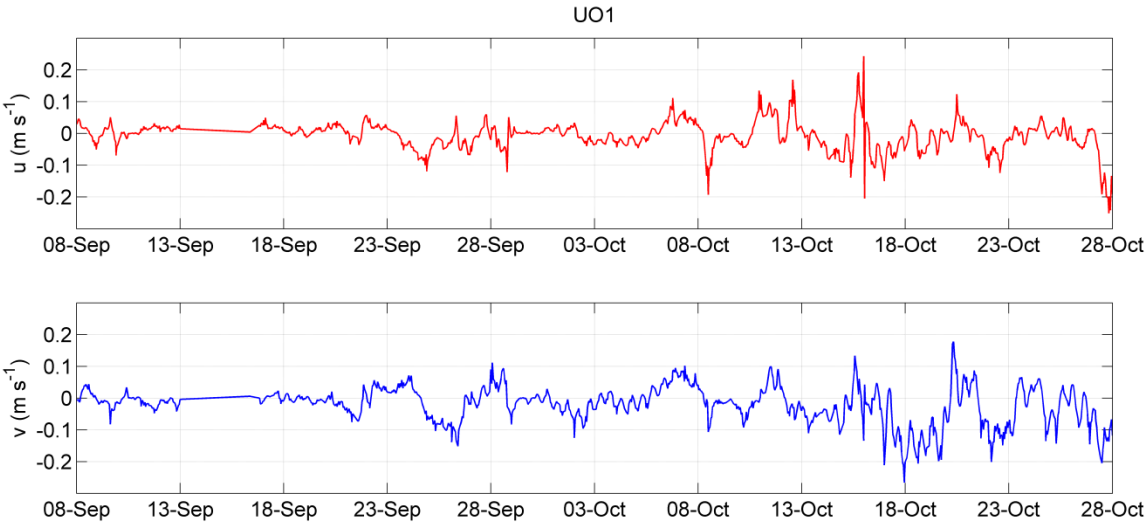

Figure 28. Raw *u* and *v* for 2012 iceberg UO1.

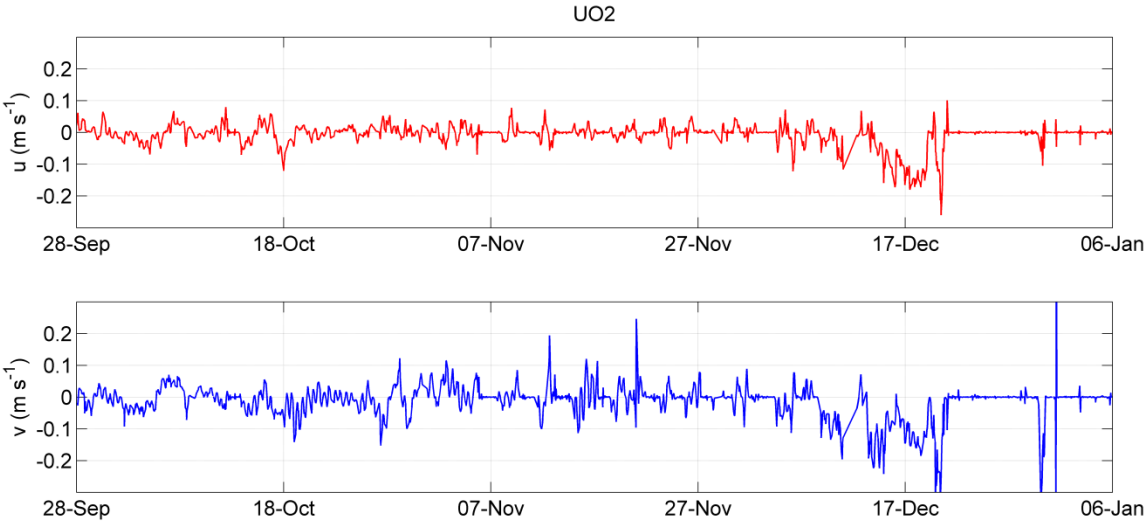

Figure 29. Raw *u* and *v* for 2012 iceberg UO2.

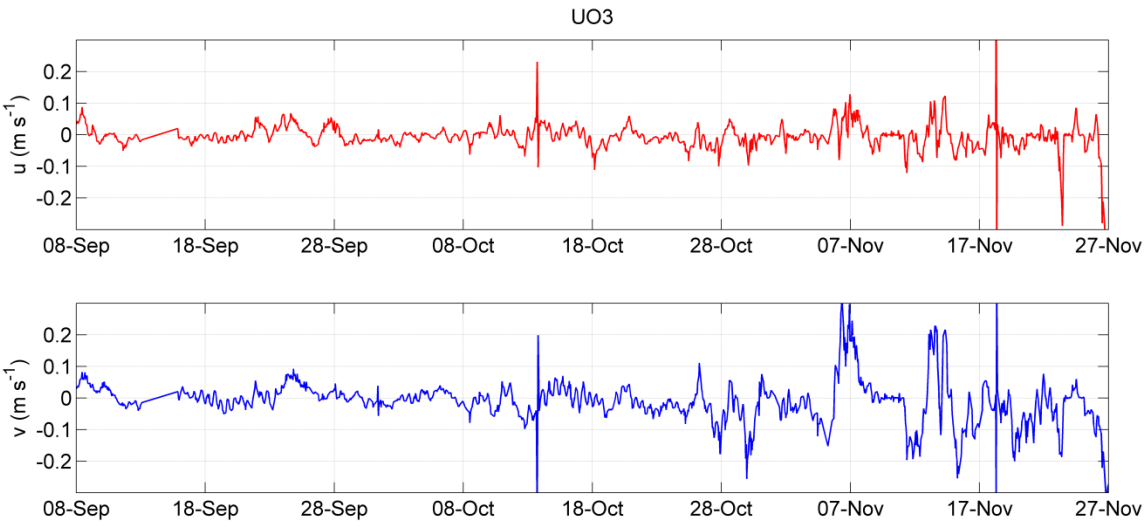

Figure 30. Raw *u* and *v* for 2012 iceberg UO3.

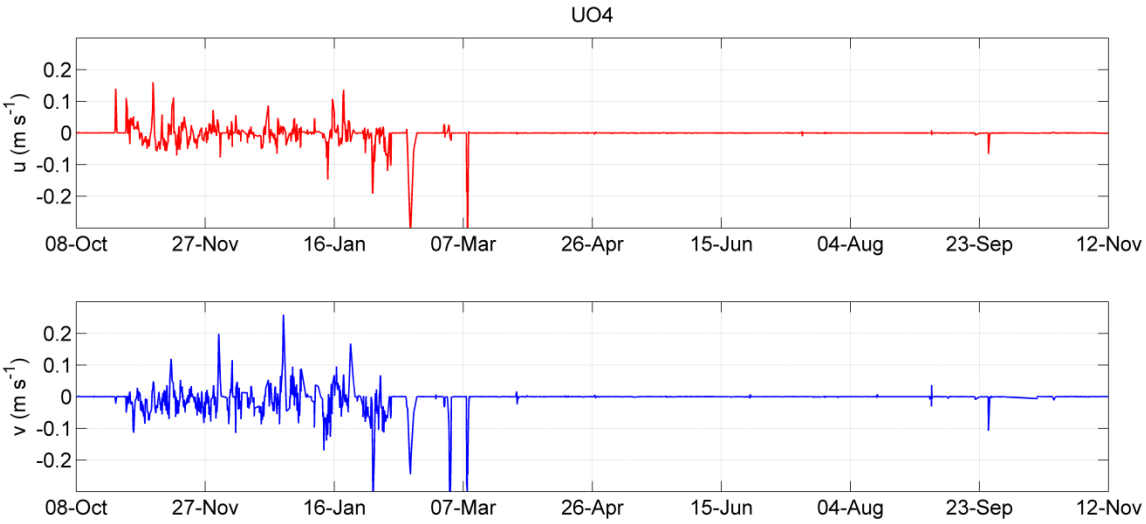

Figure 31. Raw *u* and *v* for 2012 iceberg UO4.

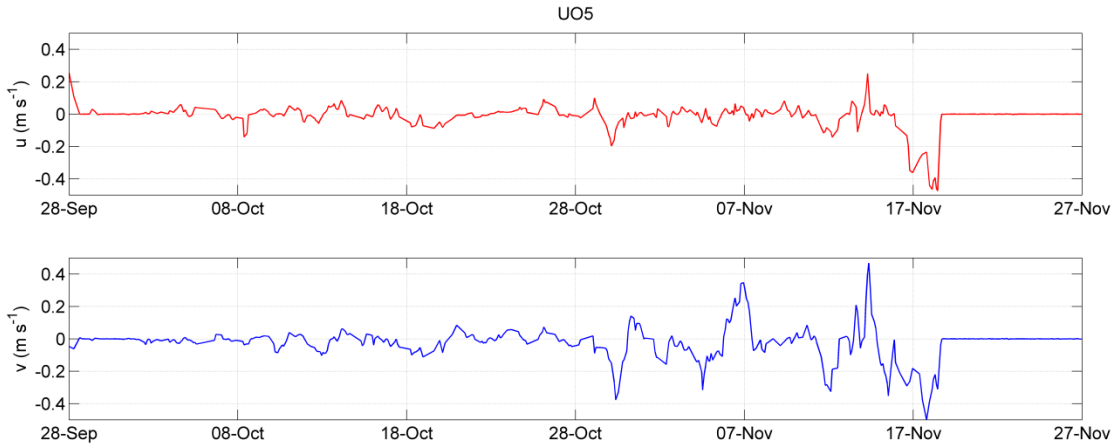

Figure 32. Raw *u* and *v* for 2012 iceberg UO5.

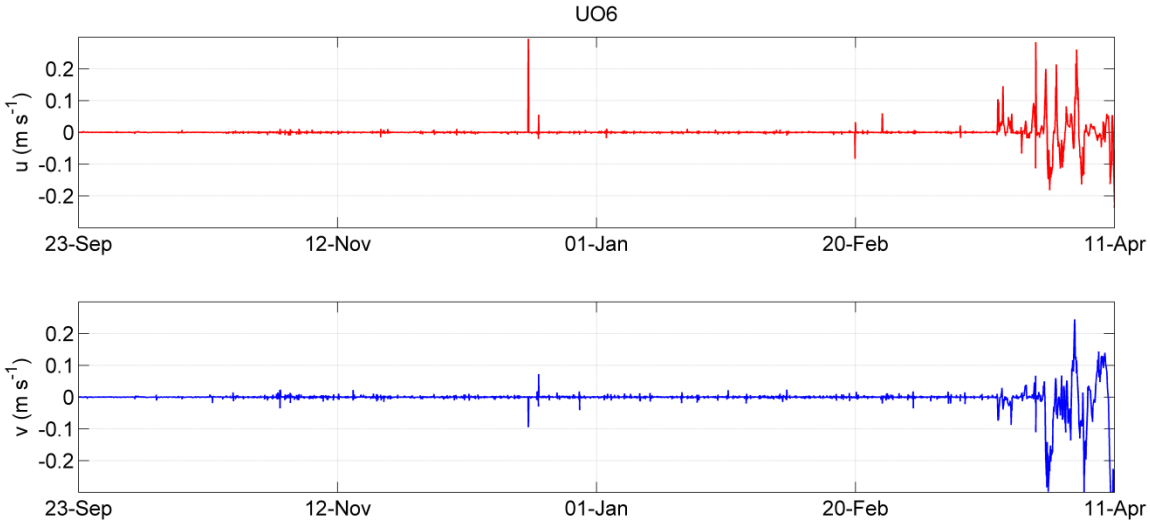

Figure 33. Raw *u* and *v* for 2013 iceberg UO6.

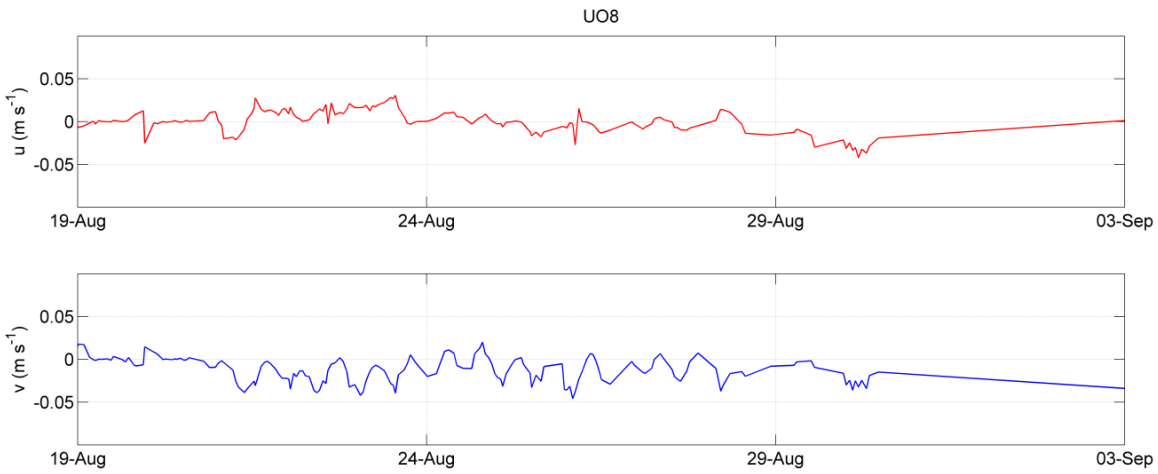

Figure 34. Raw *u* and *v* for 2013 iceberg UO8.

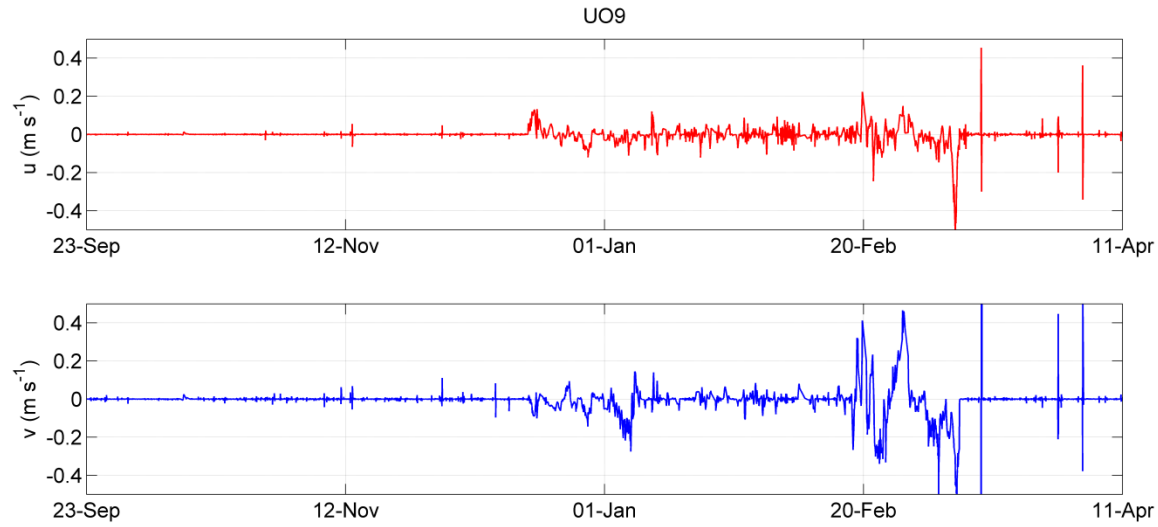

Figure 35. Raw *u* and *v* for 2013 iceberg UO9.

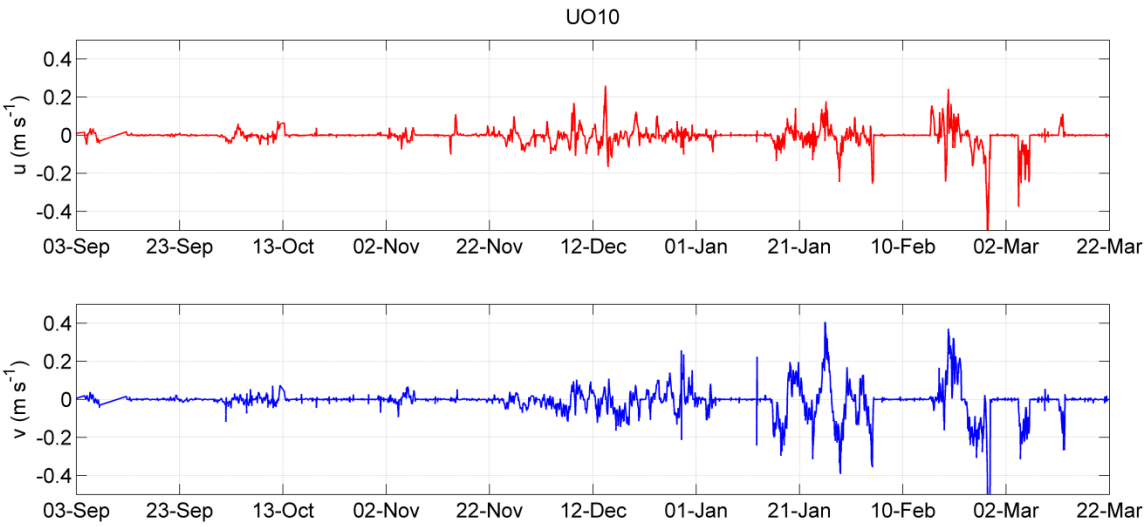

Figure 36. Raw *u* and *v* for 2013 iceberg UO10.

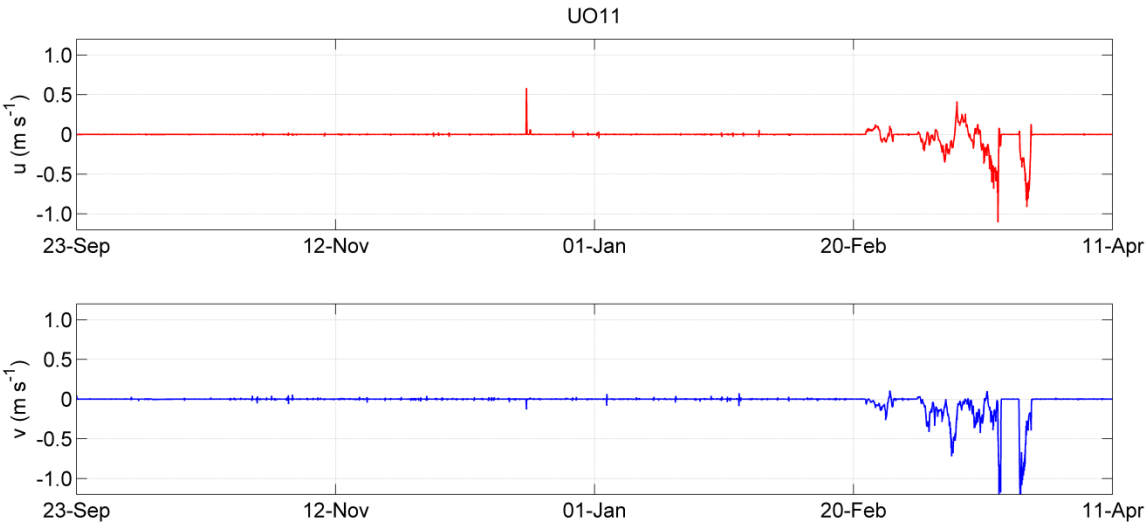

Figure 37. Raw *u* and *v* for 2013 iceberg UO11.

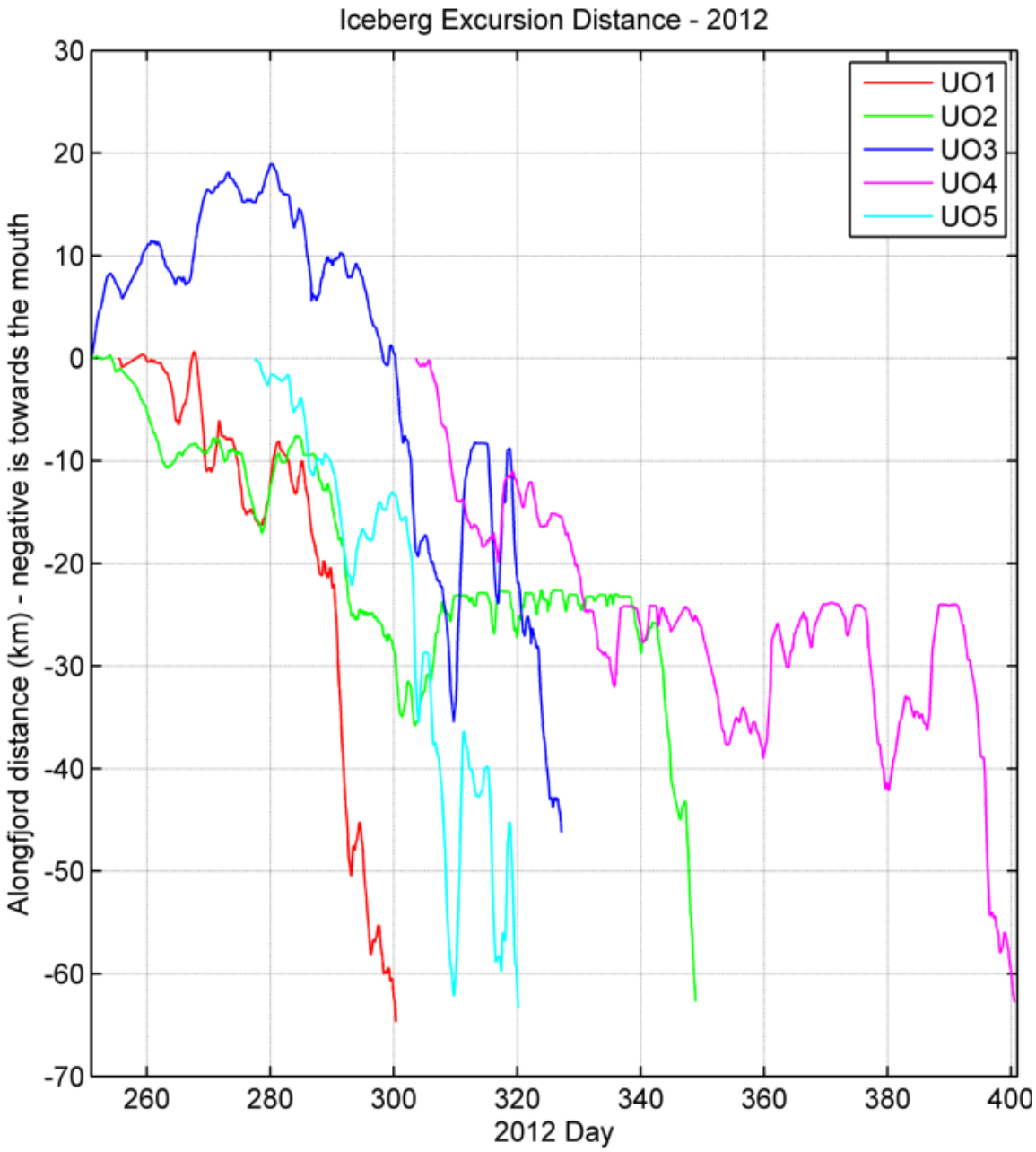

Figure 38. Excursions of the 2012 icebergs in the fjord can exceed over 40 km over a period of a few days.

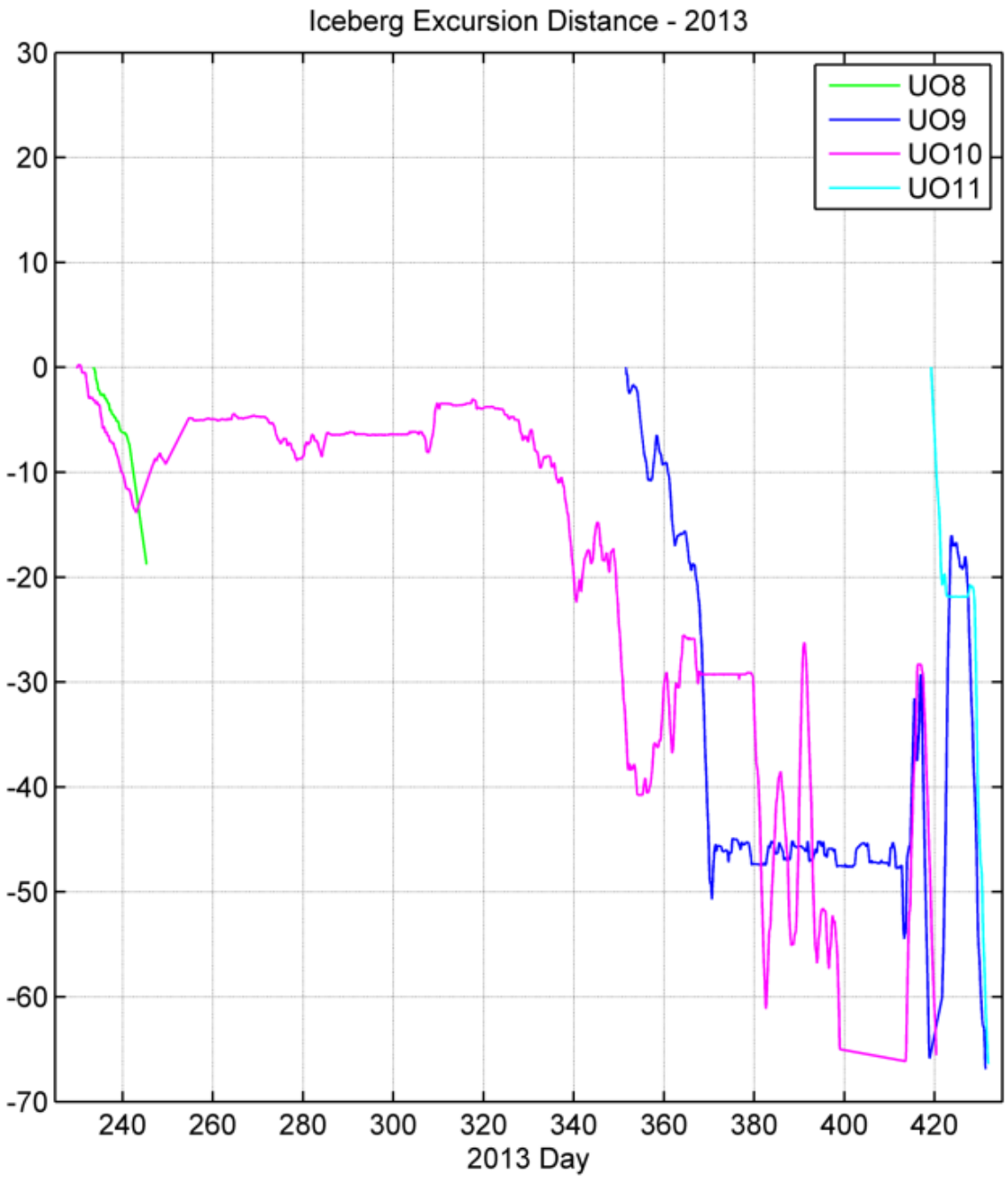

Figure 39. Excursions of the 2013 icebergs in the fjord can exceed over 40 km over a period of a few days. Note that iceberg UO8 (green) did not exit the fjord before transmission ceased.

APPENDIX C

SHELF DYNAMICS

Iceberg position and velocity data from the SE Greenland continental shelf were combined with bathymetry and satellite imagery to present a regional view of the interactions between icebergs and the EGCC.

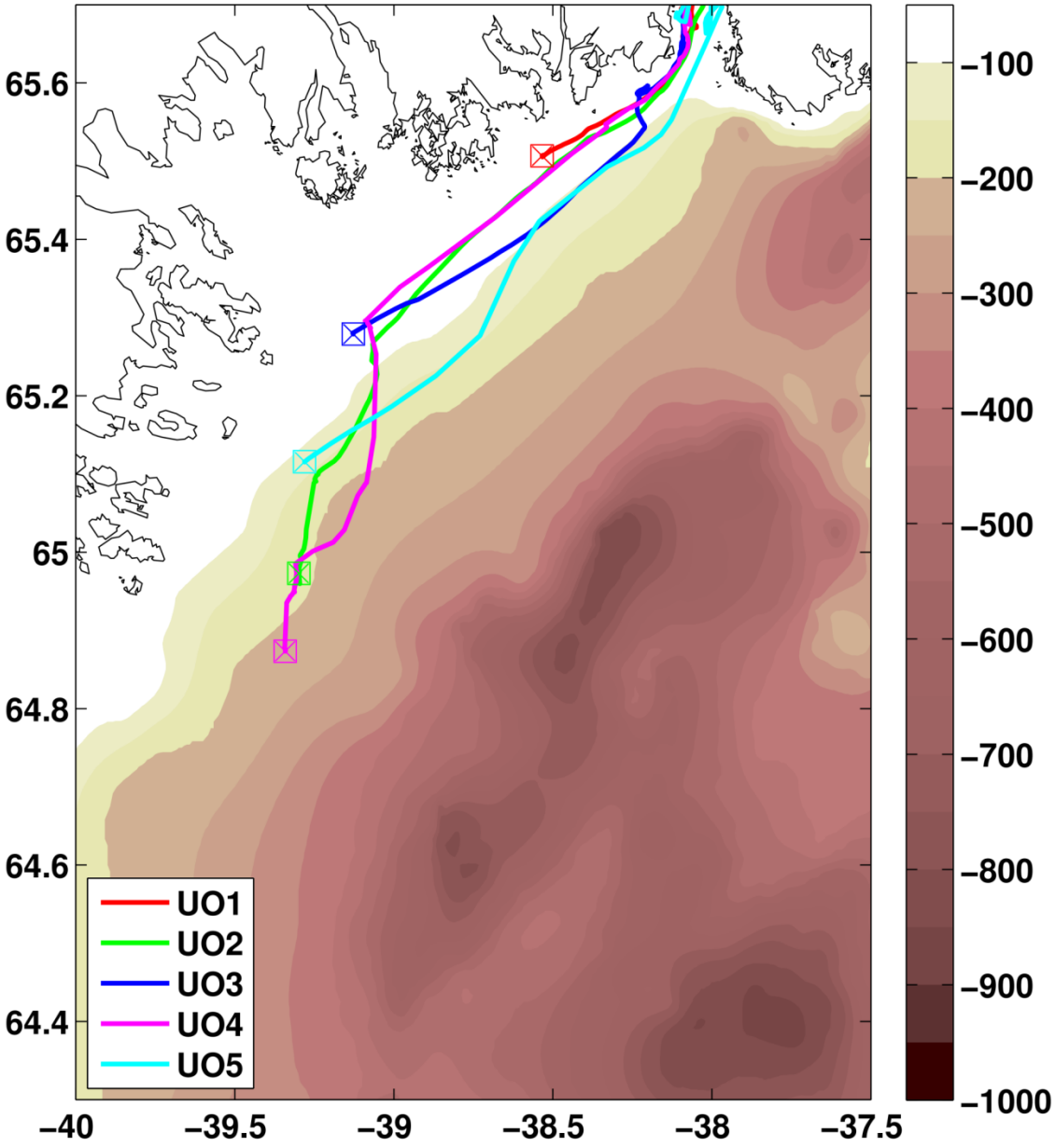

Figure 40. Composite of shelf bathymetry from GEBCO and tagged seal data (Sutherland et al., 2013) After icebergs exit the fjord, they travel with the EGCC with a slight shoreward velocity component forced by downwelling-favorable winds.

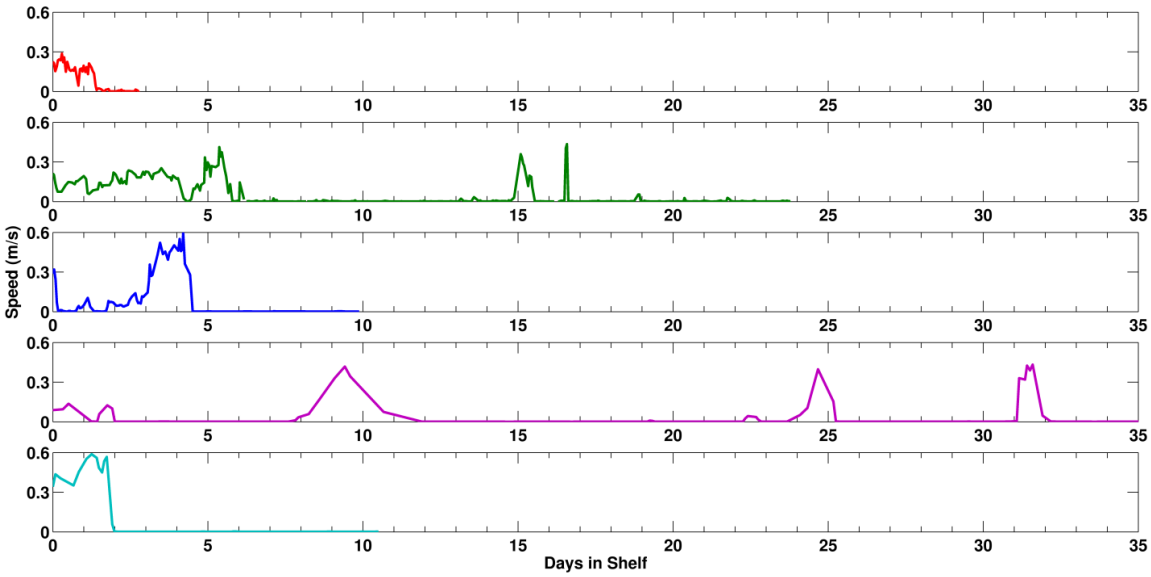

Figure 41. Speeds of the five 2012 icebergs in the shelf. Once icebergs escape the fjord, they move southwestward at much higher speeds than in the fjord and mélange regions, with velocities suggesting entrainment in the East Greenland Coastal Current. Periods of no motion are assumed to indicate grounding of the iceberg on shallow shelf bathymetry (see Fig. 2). The data end when communication with the GPS unit is lost, most likely due to iceberg breakup or capsizing.

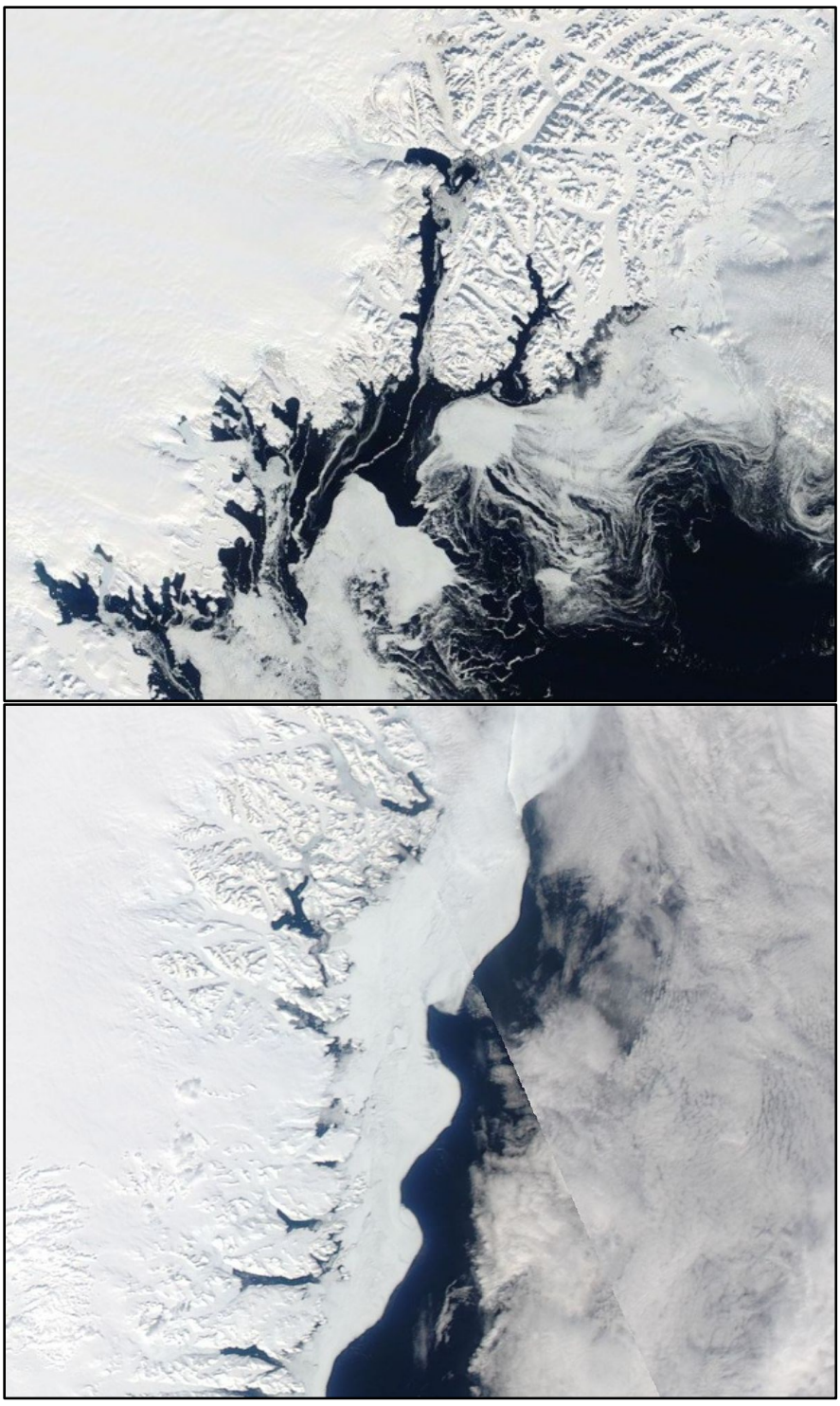

Figure 42. (Top) MODIS imagery from the Sermilik Fjord region during the UO11 shelf excursion (March 17th) shows the high concentration of sea ice in the EGCC. (Bottom) MODIS image from 500 km south, acquired April 25th, 2014, in the region where UO11 was trapped in thick sea ice and shallow bathymetry for a second time.

APPENDIX D

WHOLE-REGION PATTERNS

Gridded products constructed from the 2012 and 2013 iceberg tracks helped diagnose spatial patterns of upper water circulation and recirculation in Sermilik Fjord.

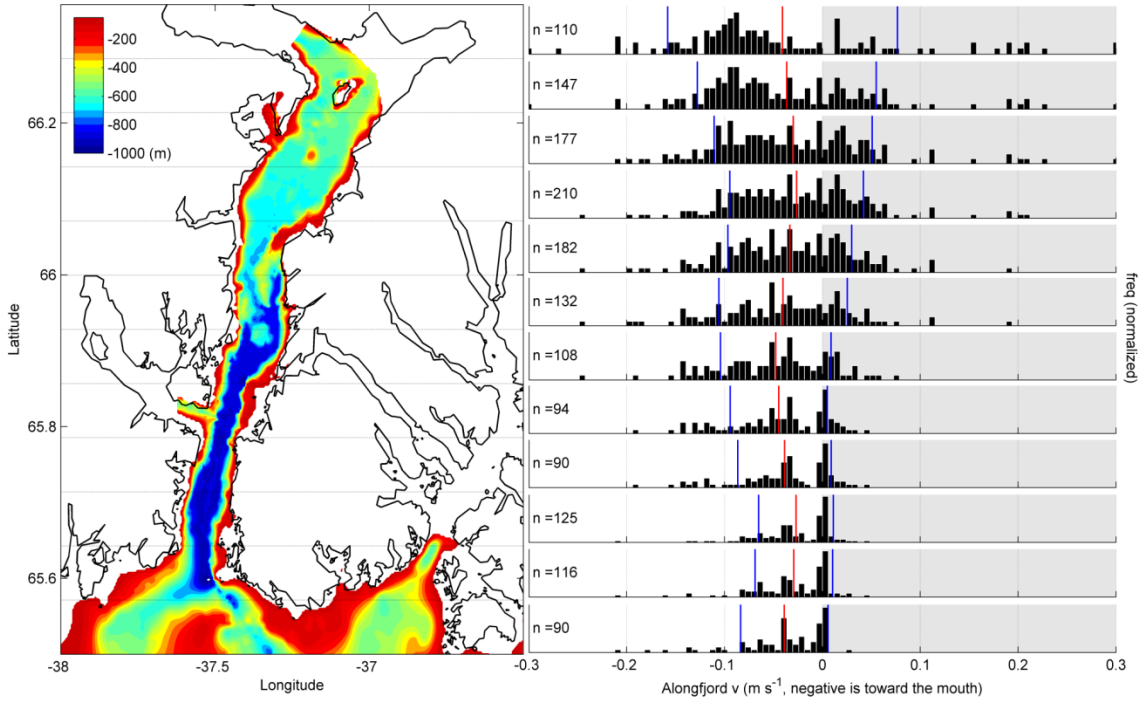

Figure 43. (Left) Bathymetry in Sermilik Fjord. (Right) Histograms of alongfjord velocity from the entire 2012-2013 iceberg record, sorted into 8 km latitude bins. Red bars represent the mean alongfjord velocity (negative is toward the mouth), and blue bars represent +/- 1 standard deviation from the mean. As icebergs move outward, the variation in their mean velocity decreases, reducing the likelihood that an iceberg will turn and move back up the fjord.

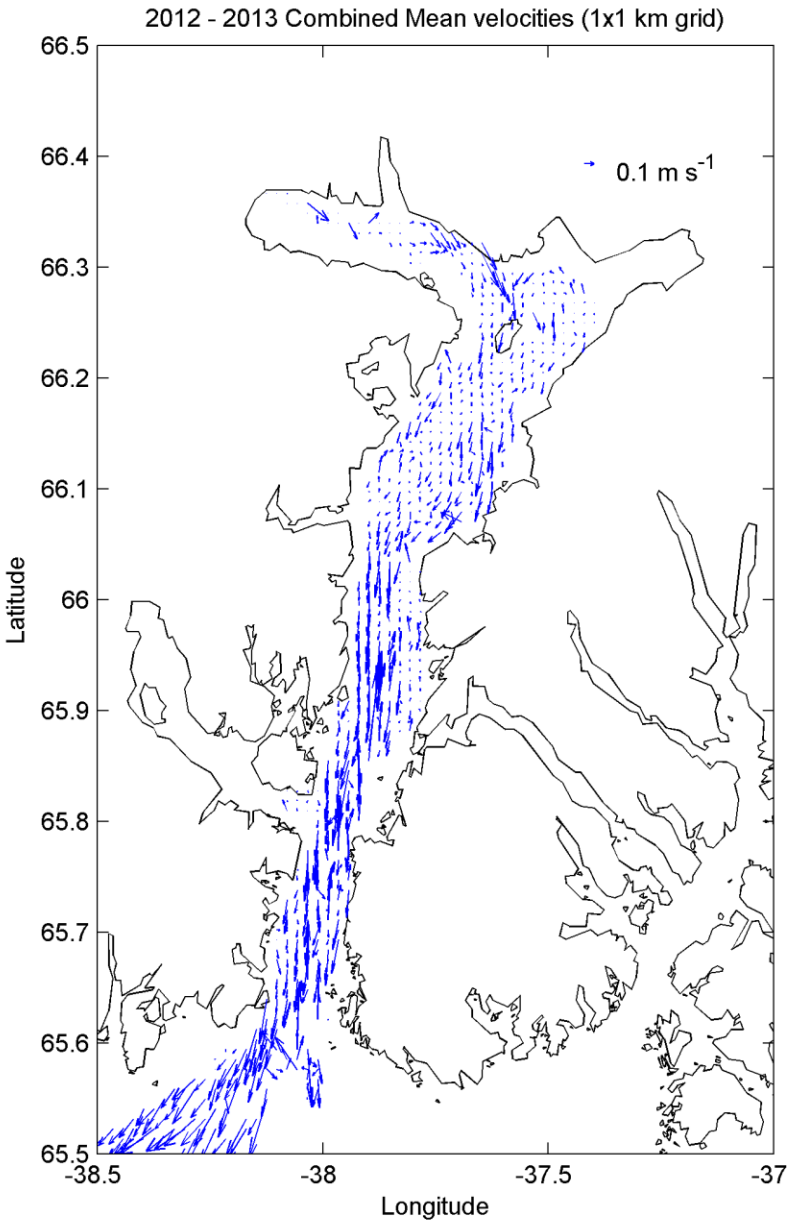

Figure 44. Mean schematic of the general iceberg circulation throughout Sermilik Fjord extracted from drifter velocities through a 1x1 km mesh grid. Near the glacier, mean velocities are slow as icebergs jostle through the rigid, granular ice mélange. Once they break free, icebergs generally move towards the mouth along the west (right, facing outward) side of the fjord. Occasionally, icebergs will travel to the east of Amagak Island (66.25 N, 37.6 W) where they often become trapped in ice mélange from both Midgård and Fenris glaciers.

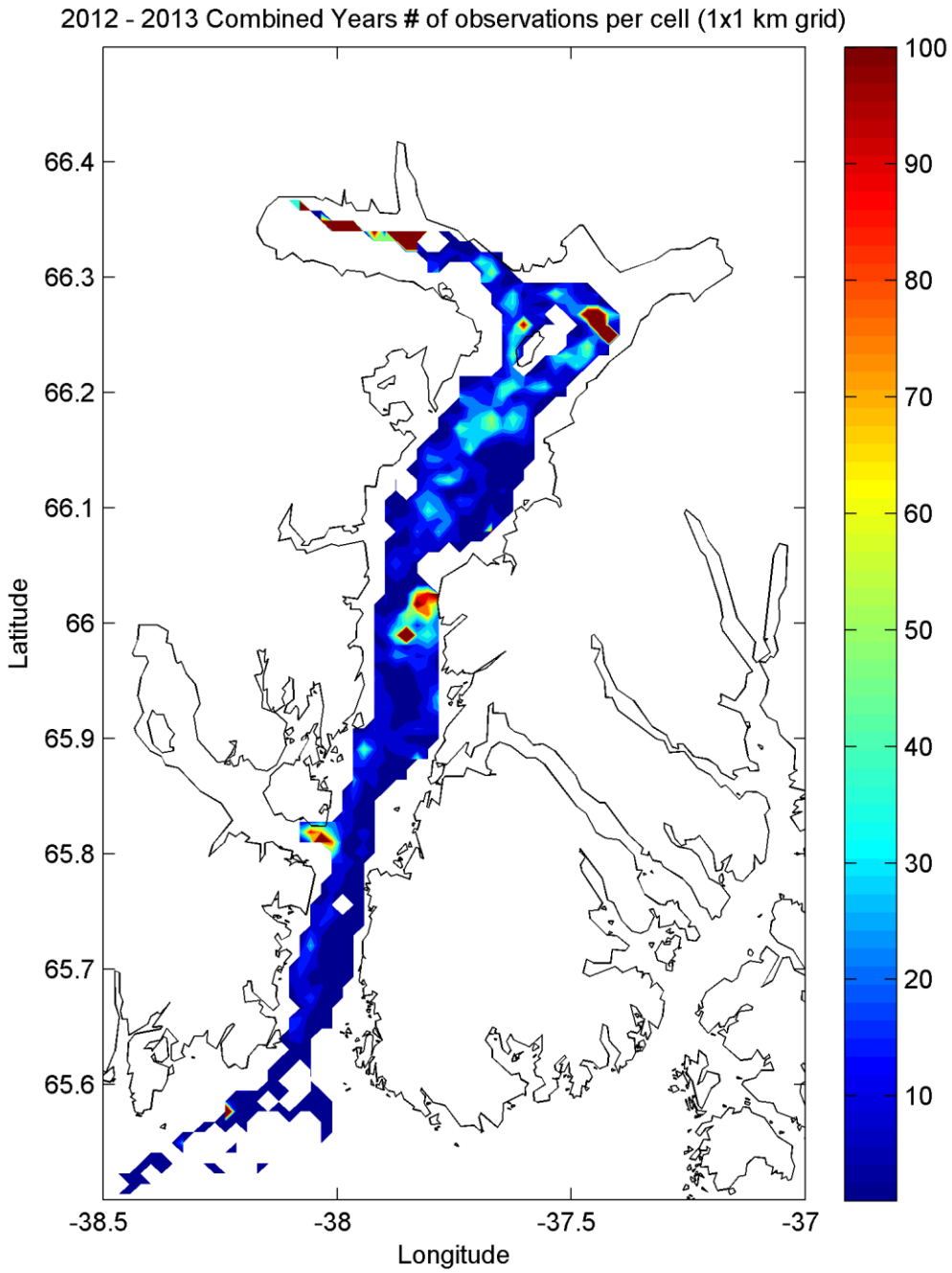

Figure 45. The number of drifter track points in each 1x1 km grid cell provide useful qualitative information on the spatial patterns of iceberg residence time in the fjord. Grid cells in the ice mélange contain hundreds of data points; cells in the upper fjord, where recirculation is common, contain dozens. Once icebergs pass the 66N threshold, velocities increase and icebergs either move quickly with the tides or exit the fjord.

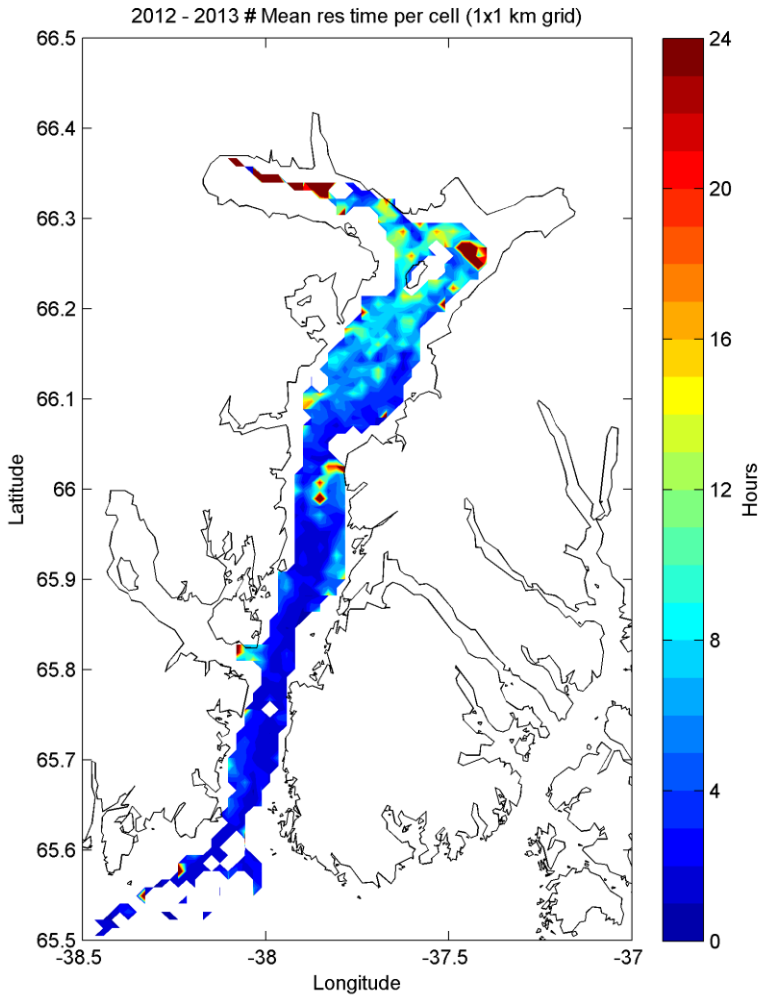

Figure 46. Gridded residence time through each cell, defined as the 1km cell size divided by the mean iceberg speed through the cell, shows two distinct regions. In the upper fjord, icebergs recirculate and are slow to move out of the fjord, often spending 12 or more hours traveling 1km (a speed of 0.02 m/s, on the same order as the tides). The residence time plot also reveals areas where icebergs often become stuck, either due to ice mélange from Helheim, Fenris, and Midgård glaciers, or from a bathymetric high in the eastern portion of the fjord at 66 N or in the inlet at 65.8 N.

By comparing the residence time grid with the standard deviation grid, we can determine whether a given region tends to "trap" icebergs or if it is simply a site where icebergs tend to travel through quickly in any direction. Icebergs in the ice mélange regions and at the 66 N bathymetric high have long residence times and low standard deviations; their speeds are consistently low. In the lower fjord, areas of low (under 4 hours) residence time and high (> 0.1 m/s) standard deviation reaffirm that icebergs are traveling both upfjord and downfjord at high speeds.

APPENDIX E

ADCP RECORD

Data from a moored ADCP, deployed by Woods Hole Oceanographic Institution, aided in the comparison between iceberg velocities, water velocities, and winds in Sermilik Fjord.

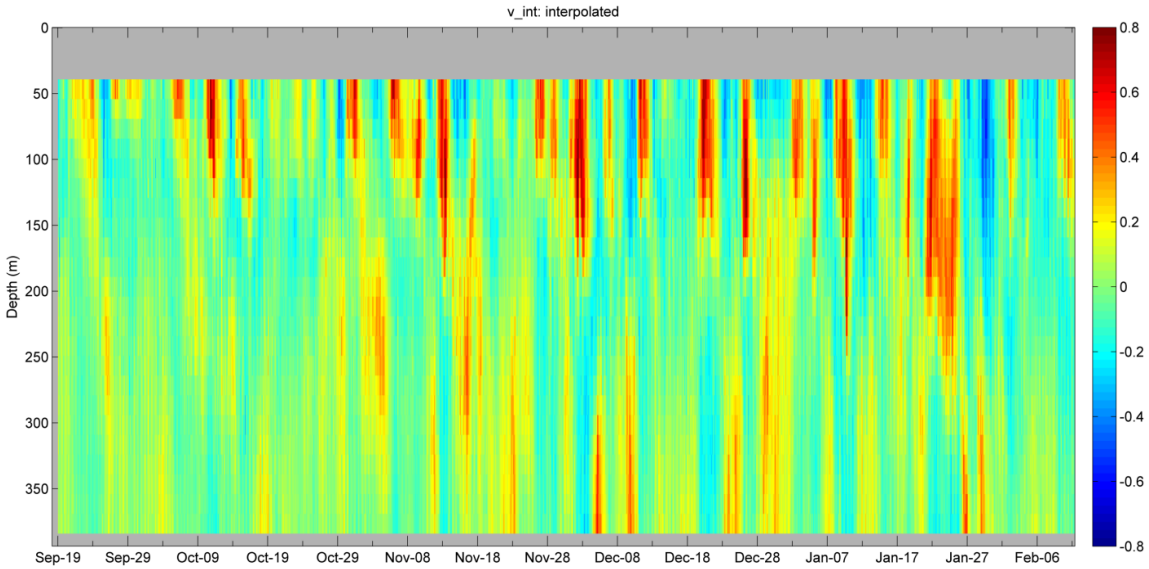

Figure 47. The full ADCP velocity record recovered from the September 2012 – February 2013 season. Data represent alongfjord velocity about the 31.5 degree fjord axis. The velocity convention represents the standard for this study: positive is towards the glacier; negative is towards the mouth. Data was quality-controlled and eliminated measurements from the top 54 m of the water column.

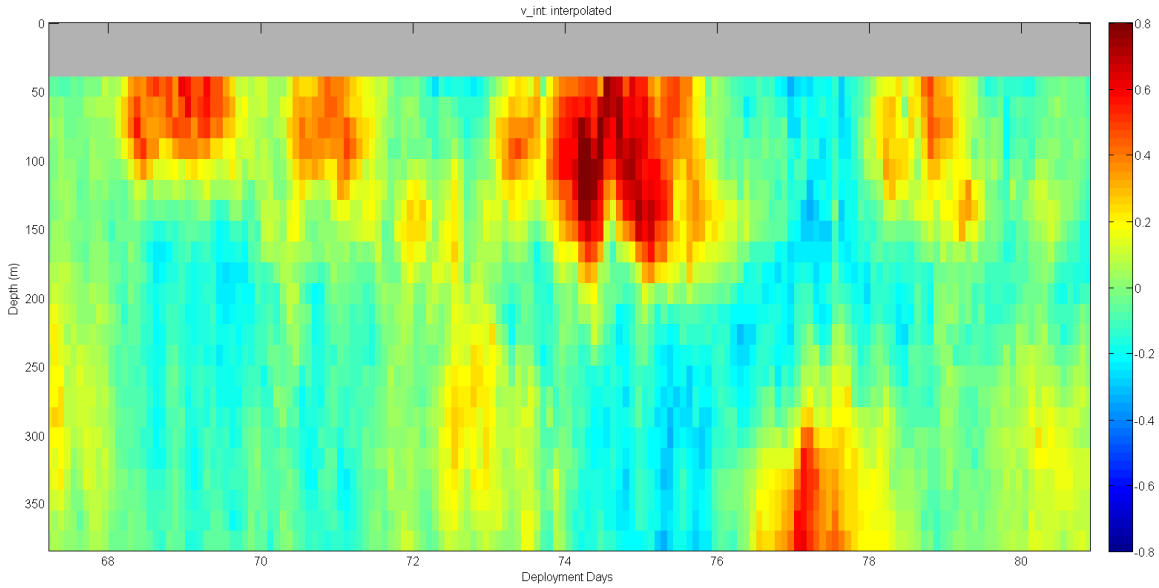

Figure 48. ADCP data from November 2012 zoomed to show the timescales and two-layer structure of circulation in the fjord. Strong out-fjord pulses in the upper (~200 m) layer are matched with in-fjord return flow in the lower layer.

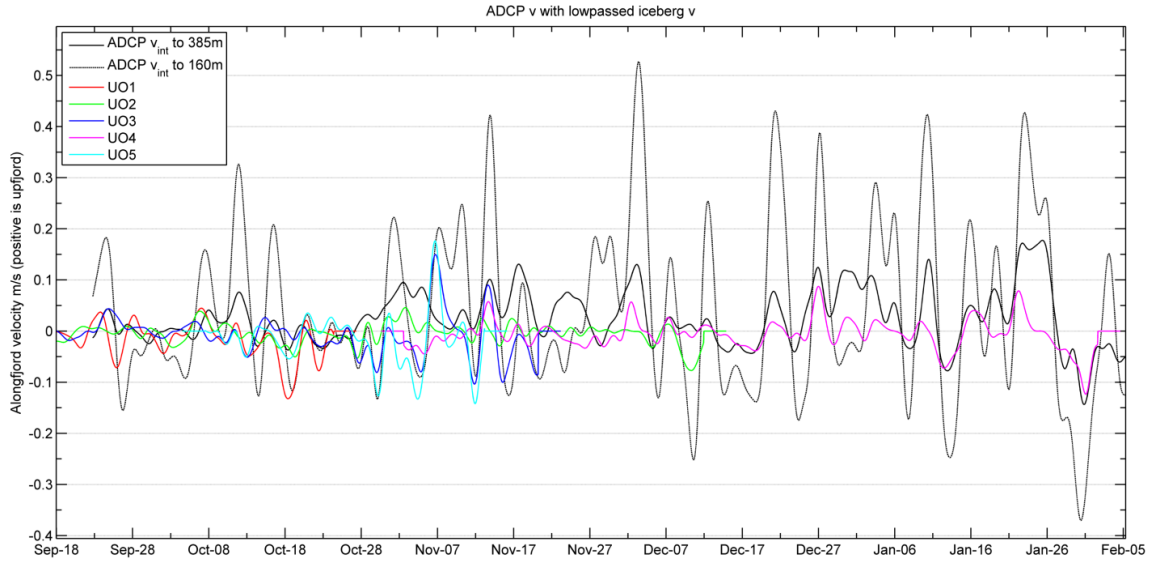

Figure 49. 2012 Iceberg alongfjord velocity with alongfjord current velocity from the upper layer (54-160 m) and whole-column (54-385 m) depth averages from the ADCP record. Because the upper and lower layers are often moving in opposite directions, the amplitude of full-column velocity pulses is necessarily reduced compared to those in just the upper layer.

APPENDIX F

WINDS AND INTERMEDIARY CIRCULATION

Large-scale cyclonic winds in the Irminger Sea drive intermediary circulation in Sermilik Fjord, which acts as the dominant mechanism for fjord-shelf water exchange and iceberg flushing.

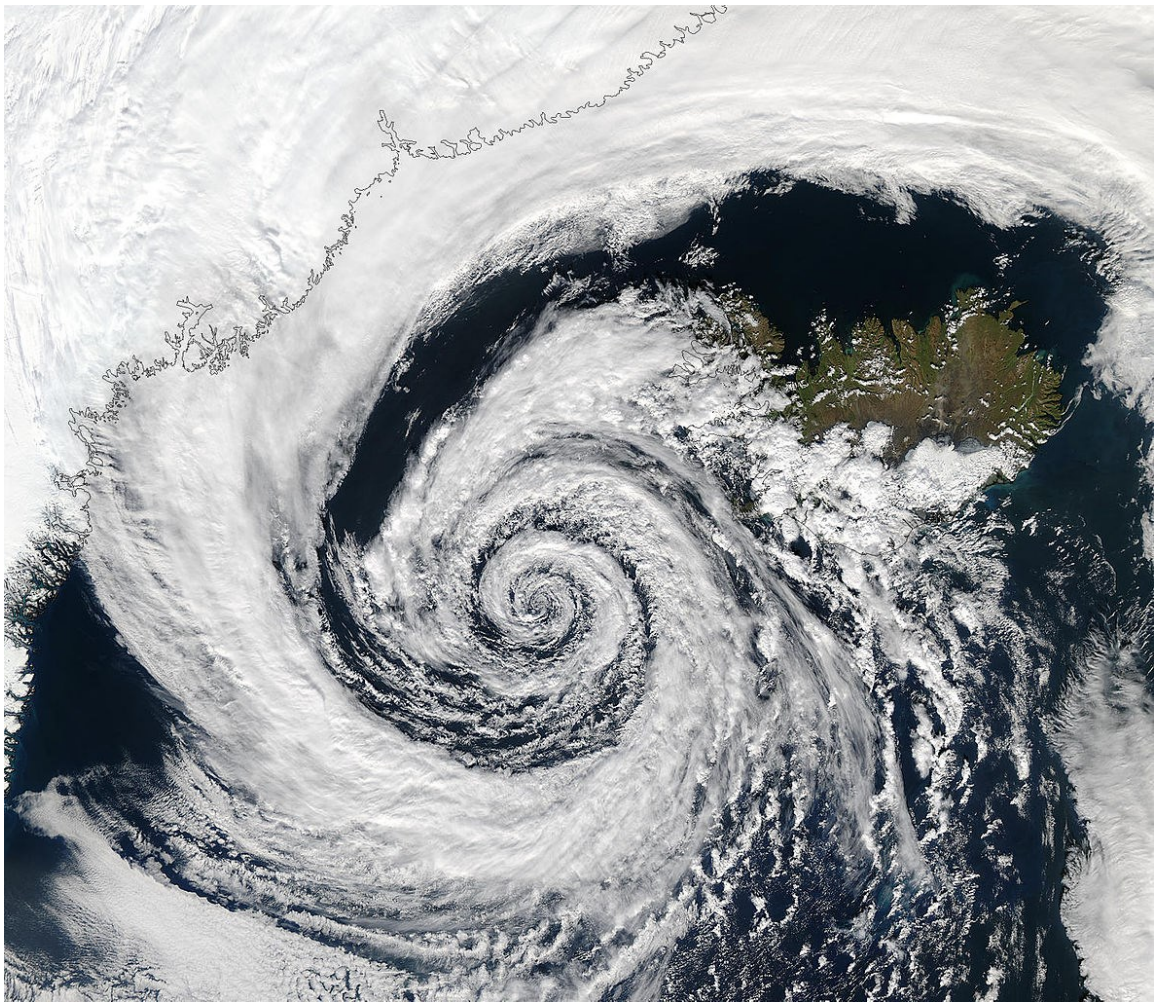

Figure 50. MODIS Terra (1km resolution) image of a strong cyclonic Icelandic low in September 2003. http://rapidfire.sci.gsfc.nasa.gov/gallery/?2003247-0904/Iceland.A2003247.1410.1km.jpg

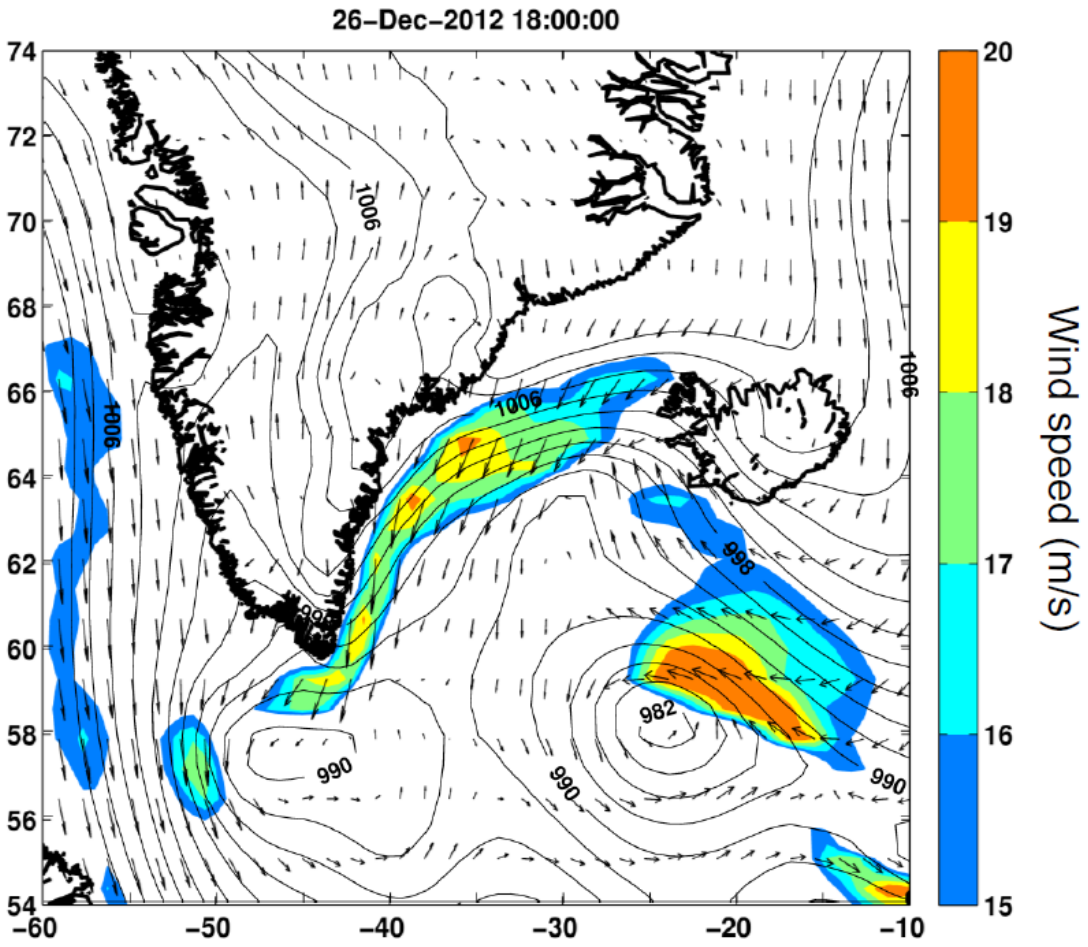

Figure 51. Barrier wind event shown in ECMWF-Interim climate reanalysis data, Iceland and Southern Greenland, on 26 Dec 2012. Strong, northeasterly barrier wind events occur along the East Greenland coast during the winter months, when the cyclonic Icelandic Low is compressed and amplified by the steep topography of SE Greenland. These wind events can exceed speeds of 20 m s^{-1} (40 kt), and can occur as often as weekly and can last several days.

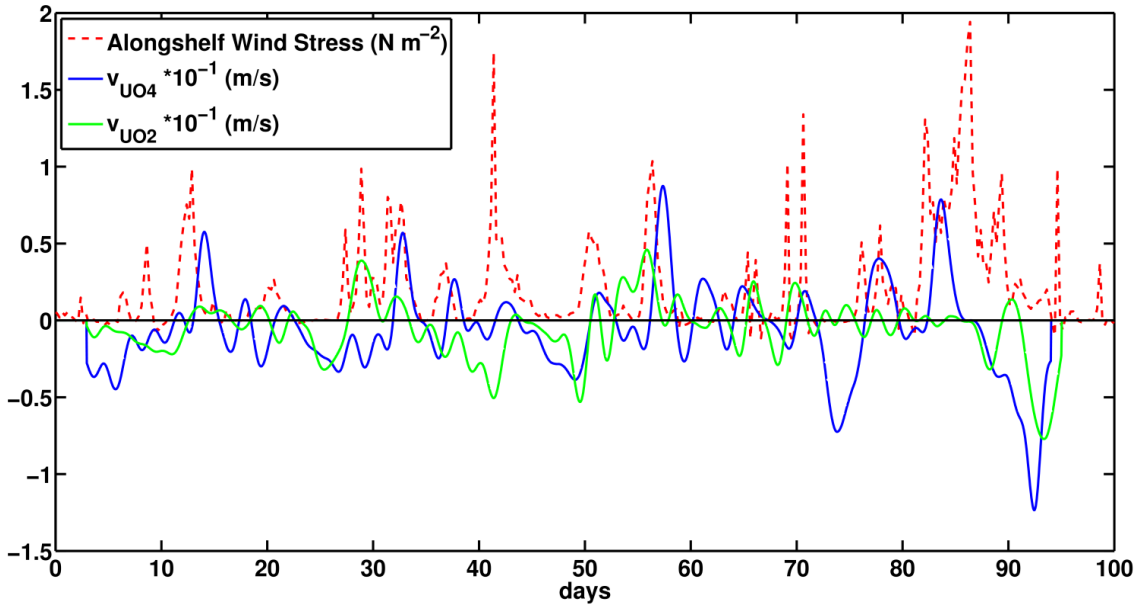

Figure 52. Example plot of alongshelf wind stress in the southwestward direction with iceberg velocity along the fjord axis. We expect alongshelf wind pulses to drive the upper layer and icebergs up the fjord, followed by a vigorous outflow as the winds relax.

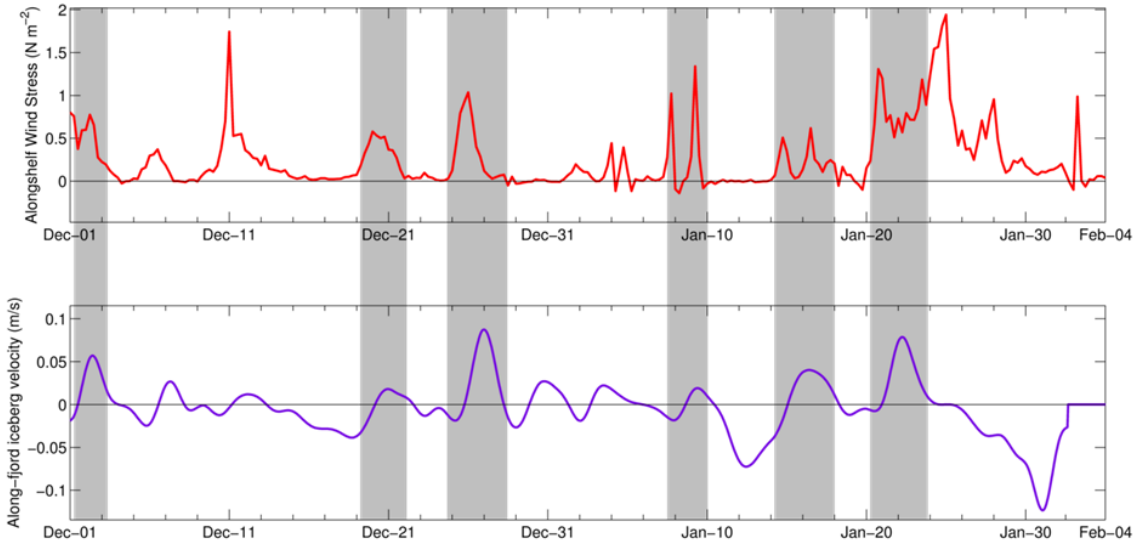

Figure 53. (Top) During the winter, barrier wind events (gray bars) along the SE Greenland shelf drive a two-layer, intermediary circulation (ref). (bottom) In a typical event, the downwelling-favorable winds induce an iceberg velocity into the fjord at speeds of up to 10 cm s^{-1}, in line with the expected response of the upper Polar Water layer. As the winds relax, the iceberg velocity flow switches direction to out-fjord.

REFERENCES CITED

Amundson, J. M., Fahnestock, M. A., Truffer, M., Brown, J., Lüthi, M. P., & Motyka, R. J. (2010). Ice mélange dynamics and implications for terminus stability, Jakobshavn Isbræ, Greenland. *Journal of Geophysical Research*, *115*(F1), 1–12. doi:10.1029/2009JF001405

Andersen, M. L., Larsen, T. B., Nettles, M., Elósegui, P., van As, D., Hamilton, G. S., … Dahl-Jensen, D. (2010). Spatial and temporal melt variability at Helheim Glacier, East Greenland, and its effect on ice dynamics. *Journal of Geophysical Research*, *115*(F4), 1–18. doi:10.1029/2010JF001760

Andresen, C. S., Straneo, F., & Ribergaard, M. H. (2011). Rapid response of Helheim Glacier in Greenland to climate variability over the past century - Supplementary information. *Nature Geoscience*, *4*(12), 1–16. doi:10.1038/NGEO1349

Andresen, C. S., Straneo, F., Ribergaard, M. H., Bjørk, A. A., Andersen, T. J., Kuijpers, A., … Ahlstrøm, A. P. (2011). Rapid response of Helheim Glacier in Greenland to climate variability over the past century. *Nature Geoscience*, *5*(1), 37–41. doi:10.1038/ngeo1349

Arneborg, L., & Liljebladh, B. (2001). The internal seiches in Gullmar Fjord. Part I: dynamics. *Journal of Physical Oceanography*, *31*(9), 2549–2566.

Aure, J., Ert, J. M., & Stigebrandt, A. (1997). Observations of Inshore Water Exchange Forced by a Fluctuating Offshore Density Field, *33*(97).

Azetsu-Scott, K., & Tan, F. C. (1997). Oxygen isotope studies from Iceland to an East Greenland Fjord: Behaviour of glacial meltwater plume. *Marine Chemistry*, *56*(3), 129–251.

Bacon, S., Marshall, A., Holliday, N. P., Aksenov, Y., & Dye, S. R. (2014). Seasonal variability of the East Greenland Coastal Current. *Journal of Geophysical Research: Oceans*, *In Press*.

Bacon, S., Reverdin, G., Rigor, I. G., & Snaith, H. M. (2002). A freshwater jet on the east Greenland shelf. *Journal of Geophysical …*, *107*(C7), 5.1 – 5.16.

Barker, A., Sayed, M., & Carrieres, T. (2004). Determination of Iceberg Draft, Mass and Cross-Sectional Areas. In *Proceedings of The Fourteenth (2004) International Offshore and Polar Engineering Conference*.

Bigg, G. R., Wadley, M. R., Stevens, D. P., & Johnson, J. A. (1996). Prediction of iceberg trajectories for the North Atlantic and Arctic Oceans. *Geophysical Research Letters*, *23*(24), 3587–3590.

Bigg, G. R., Wadley, M. R., Stevens, D. P., & Johnson, J. A. (1997). Modelling the dynamics and thermodynamics of icebergs. *Cold Regions Science and Technology*, *26*(2), 113–135. doi:10.1016/S0165-232X(97)00012-8

Bigg, G. R., Wei, H. L., Wilton, D. J., Zhao, Y., Billings, S. A., Hanna, E., & Kadirkamanathan, V. (2014). A century of variation in the dependence of Greenland iceberg calving on ice sheet surface mass balance and regional climate change. *Proceedings of the Royal Society A: Mathematical, Physical and Engineering Science*, *470*(2166), 20130662. doi:10.1098/rspa.2013.0662

Canadian Ice Service. (2005). *Manual of Standard Procedures for Observing and Reporting Ice Conditions* (Revised Ni., p. 146). Ottawa: Environment Canada.

Christoffersen, P., O'Leary, M., Van Angelen, J. H., & Van Den Broeke, M. (2012). Partitioning effects from ocean and atmosphere on the calving stability of Kangerdlugssuaq Glacier, East Greenland. *Annals of Glaciology*, *53*(60), 249–256. doi:10.3189/2012AoG60A087

Cottier, F. R., Nilsen, F., Skogseth, R., Tverberg, V., Skardhamar, J., & Svendsen, H. (2010). Arctic fjords: a review of the oceanographic environment and dominant physical processes. *Geological Society, London, Special Publications*, *344*, 35–50. doi:10.1144/SP344.4

Dowdeswell, J. A., Whittington, R. J., & Hodgkins, R. (1992). The sizes, frequencies, and freeboards of East Greenland icebergs observed using ship radar and sextant. *Journal of Geophysical Research*, *97*, 3515–3528.

Enderlin, E. M., & Howat, I. M. (2013). Submarine melt rate estimates for floating termini of Greenland outlet glaciers (2000–2010). *Journal of Glaciology*, *59*(213), 67–75. doi:10.3189/2013JoG12J049

Enderlin, E. M., Howat, I. M., Jeong, S., Noh, M. J., Angelen, J. H., & Broeke, M. R. (2014). An Improved Mass Budget for the Greenland Ice Sheet. *Geophysical Research Letters*, *41*(3), 866–872. doi:10.1002/2013GL059010.Received

Gladstone, R. M., Bigg, G. R., & Nicholls, K. W. (2001). Iceberg trajectory modeling and meltwater injection. *Journal of Geophysical Research*, *106*(C9), 19903–19915. doi:10.1029/2000JC000347

Hansen, B., & Østerhus, S. (2000). North Atlantic–Nordic Seas exchanges. *Progress In Oceanography*, *45*(2), 109–208. doi:10.1016/S0079-6611(99)00052-X

Harden, B. E., Renfrew, I. A., & Petersen, G. N. (2011). A Climatology of Wintertime Barrier Winds off Southeast Greenland. *Journal of Climate*, *24*(17), 4701–4717. doi:10.1175/2011JCLI4113.1

Harden, B. E., Straneo, F., & Sutherland, D. A. (2014). Moored observations of synoptic and seasonal variability in the East Greenland Coastal Current. *Journal of Geophysical Research: Oceans*, (Submitted).

Holland, D. M., & Jenkins, A. (1999). Modeling thermodynamic ice-ocean interactions at the base of an ice shelf. *Journal of Physical Oceanography*, *29*(1987), 1787–1800.

Holland, D. M., Thomas, R. H., de Young, B., Ribergaard, M. H., & Lyberth, B. (2008). Acceleration of Jakobshavn Isbræ triggered by warm subsurface ocean waters. *Nature Geoscience*, *1*(10), 659–664. doi:10.1038/ngeo316

Hotzel, S., & Miller, J. (1983). Icebergs: their physical dimensions and the presentation and application of measured data. *Annals of Glaciology*, *4*, 116–123.

Howat, I. M., & Eddy, A. (2011). Multi-decadal retreat of Greenland's marine-terminating glaciers. *Journal of Glaciology*, *57*(203), 389–396.

Howat, I. M., Joughin, I., & Scambos, T. A. (2007). Rapid Changes in Ice Discharge from Greenland Outlet Glaciers. *Science*, *315*(March), 1559–1561.

Howat, I. M., Joughin, I., Tulaczyk, S., & Gogineni, S. (2005). Rapid retreat and acceleration of Helheim Glacier, east Greenland. *Geophysical Research Letters*, *32*(22), L22502. doi:10.1029/2005GL024737

Huppert, H. E. (1980). The physical processes involved in the melting of icebergs. *Annals of Glaciology*, *1*, 97–101.

Huppert, H. E., & Josberger, E. (1980). The melting of ice in cold stratified water. *Journal of Physical Oceanography*, *10*, 953–960.

Huppert, H. E., & Turner, J. (1980). Ice blocks melting into a salinity gradient. *Journal of Fluid Mechanics*, *100*(2), 367–384.

Jackson, R. H., Straneo, F., & Sutherland, D. A. (2013). Shelf-forced fjord circulation and heat transport at the terminus of a major outlet glacier. In *Understanding the Response of Greenland's Marine Terminating Glaciers to Oceanic and Atmospheric Forcing*. Beverly, MA.

Jackson, R. H., Straneo, F., & Sutherland, D. A. (2014). Ocean temperature at Helheim Glacier controlled by shelf-driven flow in non-summer months. *Nature Geoscience*, *In Press*.

Johnson, H. L., Münchow, A., Falkner, K. K., & Melling, H. (2011). Ocean circulation and properties in Petermann Fjord, Greenland. *Journal of Geophysical Research*, *116*(C1), 1–18. doi:10.1029/2010JC006519

Jones, S. J. (2006). *Comparison of the strength of iceberg and other freshwater ice and the effect of temperature*. St. John's, NL.

Joughin, I., Alley, R. B., & Holland, D. M. (2012). Ice-Sheet Response to Oceanic Forcing. *Science*, *338*(November), 1172–1176.

Joughin, I., Howat, I. M., Fahnestock, M. A., Smith, B. E., Krabill, W., Alley, R. B., … Truffer, M. (2008). Continued evolution of Jakobshavn Isbrae following its rapid speedup. *Journal of Geophysical Research*, *113*(F4), F04006. doi:10.1029/2008JF001023

Klein, T., & Heinemann, G. (2002). Interaction of katabatic winds and mesocyclones near the eastern coast of Greenland. *Meteorological Applications*, *9*(4), 407–422. doi:10.1017/S1350482702004036

Klinck, J. M., O'Brien, J. J., & Svendsen, H. (1981). A simple model of fjord and coastal circulation interaction. *Journal of Physical Oceanography*, *11*, 1612–1626.

Kubat, I., Sayed, M., Savage, S. B., Carrieres, T., & Crocker, G. B. (2007). An Operational Iceberg Deterioration Model. *Proceedings of the Seventeenth International Offshore and Polar Engineering Conference*, 652–657.

MacAyeal, D. R., Freed-Brown, J., Zhang, W. W., & Amundson, J. M. (2012). The influence of ice melange on fjord seiches. *Annals of Glaciology*, *53*(60), 45–49. doi:10.3189/2012/AoG60A027

McKenna, R. (2005). *Refinement of iceberg shape characterization for risk to grand banks installations*. *Proceedings of the 18th International Conference on Port and Ocean Engineering under Arctic Conditions* (Vol. 2, pp. 555–564).

Mernild, S. H., Hansen, B. U., Jakobsen, B. H., & Hasholt, B. (2008). Climatic conditions at the Mittivakkat Glacier catchment (1994–2006), Ammassalik Island, SE Greenland, and in a 109-year perspective (1898–2006). *Danish Journal of Geography*, *108*(1), 51–72.

Mernild, S. H., Howat, I. M., Ahn, Y., Liston, G. E., Steffen, K., Jakobsen, B. H., … van As, D. (2010). Freshwater flux to Sermilik Fjord, SE Greenland. *The Cryosphere*, *4*(4), 453–465. doi:10.5194/tc-4-453-2010

Moffat, C. (2014). Wind-driven modulation of warm water supply to a proglacial fjord, Jorge Montt Glacier, Patagonia. *Geophysical Research Letters*, *In Press*. doi:10.1002/2014GL060071

Moon, T., Joughin, I., Smith, B. E., & Howat, I. M. (2012). 21st-Century Evolution of Greenland Outlet Glacier Velocities. *Science*, *336*(6081), 576–578. doi:10.1126/science.1219985

Morison, J., & Goldberg, D. (2012). A brief study of the force balance between a small iceberg, the ocean, sea ice, and atmosphere in the Weddell Sea. *Cold Regions Science and Technology*, *76-77*, 69–76. doi:10.1016/j.coldregions.2011.10.014

Mortensen, J., Bendtsen, J., Motyka, R. J., Lennert, K., Truffer, M., Fahnestock, M. A., & Rysgaard, S. (2013). On the seasonal freshwater stratification in the proximity of fast-flowing tidewater outlet glaciers in a sub-Arctic sill fjord. *Journal of Geophysical Research: Oceans*, *118*(3), 1–14. doi:10.1002/jgrc.20134

Mortensen, J., Lennert, K., Bendtsen, J., & Rysgaard, S. (2011). Heat sources for glacial melt in a sub-Arctic fjord (Godthåbsfjord) in contact with the Greenland Ice Sheet. *Journal of Geophysical Research*, *116*(C1), 1–13. doi:10.1029/2010JC006528

Murray, T., Scharrer, K., James, T. D., Dye, S. R., Hanna, E., Booth, A. D., … Huybrechts, P. (2010). Ocean regulation hypothesis for glacier dynamics in southeast Greenland and implications for ice sheet mass changes. *Journal of Geophysical Research*, *115*(F3), 1–15. doi:10.1029/2009JF001522

Nettles, M., Larsen, T. B., Elósegui, P., Hamilton, G. S., Stearns, L. A., Ahlstrøm, A. P., … Forsberg, R. (2008). Step-wise changes in glacier flow speed coincide with calving and glacial earthquakes at Helheim Glacier, Greenland. *Geophysical Research Letters*, *35*(24), L24503. doi:10.1029/2008GL036127

Newell, J. (1993). Exceptionally large icebergs and ice islands in eastern Canadian waters: a review of sightings from 1900 to present. *Arctic*, *46*(3), 205–211.

Nick, F. M., Vieli, A., Andersen, M. L., Joughin, I., Payne, A. J., Edwards, T. L., … Van De Wal, R. S. W. (2013). Future sea-level rise from Greenland's main outlet glaciers in a warming climate. *Nature*, *497*(7448), 235–238. doi:10.1038/nature12068

Oltmanns, M., Straneo, F., Moore, G. W. K., & Mernild, S. H. (2014). Strong Downslope Wind Events in Ammassalik, Southeast Greenland. *Journal of Climate*, *27*(3), 977–993. doi:10.1175/JCLI-D-13-00067.1

Pickart, R. S., Torres, D. J., & Fratantoni, P. S. (2005). The East Greenland Spill Jet. *Journal of Physical Oceanography*, *35*, 1037–1053.

Reeh, N., Thomsen, H. H., Higgins, A. K., & Weidick, A. (2001). Sea ice and the stability of north and northeast Greenland floating glaciers. *Annals of Glaciology*, *33*(1), 474–480. doi:10.3189/172756401781818554

Rignot, E., Fenty, I., Menemenlis, D., & Xu, Y. (2012). Spreading of warm ocean waters around Greenland as a possible cause for glacier acceleration. *Annals of Glaciology*, *53*(60), 257–266. doi:10.3189/2012AoG60A136

Rignot, E., Koppes, M. N., & Velicogna, I. (2010). Rapid submarine melting of the calving faces of West Greenland glaciers. *Nature Geoscience*, *3*(3), 187–191. doi:10.1038/ngeo765

Savage, S. B. (2001). Aspects of Iceberg Deterioration and Drift. In N. J. Balmforth & A. Provezale (Eds.), *Geomorphological Fluid Mechanics* (pp. 279–318). Berlin: Springer Berlin Heidelberg. doi:10.1007/3-540-45670-8_12

Schild, K. M., & Hamilton, G. S. (2013). Seasonal variations of outlet glacier terminus position in Greenland. *Journal of Glaciology*, *59*(216), 759–770. doi:10.3189/2013JoG12J238

Schjøth, F., Andresen, C. S., Straneo, F., Murray, T., Scharrer, K., & Korablev, A. (2012). Campaign to map the bathymetry of a major Greenland fjord. *Eos Trans. AGU*, *93*(14).

Sciascia, R., Straneo, F., Cenedese, C., & Heimbach, P. (2013). Seasonal variability of submarine melt rate and circulation in an East Greenland fjord. *Journal of Geophysical Research: Oceans*, *118*(5), 2492–2506. doi:10.1002/jgrc.20142

Serreze, M. C., Barrett, A. P., Slater, A. G., Woodgate, R. A., Aagaard, K., Lammers, R. B., … Lee, C. M. (2006). The large-scale freshwater cycle of the Arctic. *Journal of Geophysical Research*, *111*(C11), 1–19. doi:10.1029/2005JC003424

Shepherd, A., Ivins, E. R., A, G., Barletta, V. R., Bentley, M. J., Bettadpur, S., … Zwally, H. J. (2012). A reconciled estimate of ice-sheet mass balance. *Science*, *338*(6111), 1183–9. doi:10.1126/science.1228102

Silva, T. A. M., Bigg, G. R., & Nicholls, K. W. (2006). Contribution of giant icebergs to the Southern Ocean freshwater flux. *Journal of Geophysical Research*, *111*(C3), C03004. doi:10.1029/2004JC002843

Stearns, L. A., & Hamilton, G. S. (2007). Rapid volume loss from two East Greenland outlet glaciers quantified using repeat stereo satellite imagery. *Geophysical Research Letters*, *34*(5), 1–5. doi:10.1029/2006GL028982

Stigebrandt, A. (1990). On the response of the horizontal mean vertical density distribution in a fjord to low-frequency density fluctuations in the coastal water. *Tellus*, *42A*(5), 605–614.

Stigebrandt, A. (2012). Hydrodynamics and Circulation of Fjords. In (L. Bengtsson, R. W. Herschy, & R. W. Fairbridge, Eds.)*Encyclopedia of Lakes and Reservoirs*. Dordrecht: Springer Netherlands. doi:10.1007/978-1-4020-4410-6

Straneo, F., Hamilton, G. S., Sutherland, D. A., Stearns, L. A., Davidson, F., Hammill, M. O., … Rosing-Asvid, A. (2010). Rapid circulation of warm subtropical waters in a major glacial fjord in East Greenland. *Nature Geoscience*, *3*(3), 182–186. doi:10.1038/ngeo764

Straneo, F., Sergienko, O., & Heimbach, P. (2012). *Understanding the Dynamic Response of Greenland's Marine Terminating Glaciers to Oceanic and Atmospheric Forcing* (p. 28).

Straneo, F., Sutherland, D. A., Holland, D. M., Gladish, C. V., Hamilton, G. S., Johnson, H. L., … Koppes, M. N. (2012). Characteristics of ocean waters reaching Greenland's glaciers. *Annals of Glaciology*, *53*(60), 202–210. doi:10.3189/2012AoG60A059

Sutherland, D. A., & Pickart, R. S. (2008). The East Greenland Coastal Current: Structure, variability, and forcing. *Progress In Oceanography*, *78*(1), 58–77. doi:10.1016/j.pocean.2007.09.006

Sutherland, D. A., & Straneo, F. (2012). Estimating ocean heat transports and submarine melt rates in Sermilik Fjord, Greenland, using lowered acoustic Doppler current profiler (LADCP) velocity profiles. *Annals of Glaciology*, *53*(60), 50–58. doi:10.3189/2012AoG60A050

Sutherland, D. A., Straneo, F., & Pickart, R. S. (2014). Characteristics and dynamics of two major Greenland glacial fjords. *Journal of Geophysical Research: Oceans*, *In Press*.

Sutherland, D. A., Straneo, F., Stenson, G. B., Davidson, F. J. M., Hammill, M. O., & Rosing-Asvid, A. (2013). Atlantic water variability on the SE Greenland continental shelf and its relationship to SST and bathymetry. *Journal of Geophysical Research*, *118*, 1–9. doi:10.1029/2012JC008354

Woodgate, R. A., Fahrbach, E., & Rohardt, G. (1999). Structure and transports of the East Greenland Current at 75 N from moored current meters. *Journal of Geophysical …*, *104*(C8), 18059–18072.

Xu, Y., Rignot, E., Fenty, I., Menemenlis, D., & Flexas, M. M. (2013). Subaqueous melting of Store Glacier, West Greenland from three-dimensional, high-resolution numerical modeling and ocean observations. *Geophysical Research Letters*, *40*, n/a–n/a. doi:10.1002/grl.50825